Water vapor permeability of hardened cement paste

Sørensen, Eigil V.; Radjy, Fariborz; Sellevold, Erik

Publication date:
1980

Document Version
Publisher's PDF, also known as Version of record

KKH

TECHNICAL REPORT 83/80

monologen vedr. 3H (p. 29)

WATER VAPOR PERMEABILITY OF HARDENED CEMENT PASTE

BY

EIGIL V. SØRENSEN

TECHNICAL UNIVERSITY OF DENMARK
DEPARTMENT OF CIVIL ENGINEERING
BUILDING MATERIALS LABORATORY

WATER VAPOUR PERMEABILITY OF HARDENED CEMENT PASTE

by

Eigil V. Sørensen

Building Materials Laboratory
Technical University of Denmark

PREFACE

The present thesis serves as partial fulfillment of the requirements for the degree of lic. techn. at the Technical University of Denmark. The experimental work reported herein was carried out at the Building Materials Laboratory.

I wish to gratefully acknowledge the inspiration, guidance and advice given me by my advisors, Dr. Fariborz Radjy and Dr. Erik Sellevold. I wish also to thank Professor Torben C. Hansen for his encouragement throughout my study.

The financial support of the Danish Government Fund for Scientific and Industrial Research, under grant no. 2532F, is gratefully acknowledged.

Finally, I wish to thank my wife, Birte, not least for her help in typing the manuscript.

Gistrup, December 1979

Eigil V. Sørensen

ABSTRACT

The central purpose of this project has been to generate systematic steady state water vapour permeability data for well defined specimens of hardened cement paste and to try to interpret the results in terms of the pore structure by applying developed principles of moisture transport in porous media.

The hardened cement pastes used include four types, specified by two water to cement ratios - 0.40 and 0.50 - and two curing procedures - room temperature curing, and steam curing at 97°C.

The specimens were characterized by pore structure analysis based on sorption isotherms as well as on mercury intrusion porosimetry.

Water vapour permeabilities of the hardened pastes were obtained from steady state measurements based on the cup method. Each measurement yields a mean permeability coefficient over the humidity range involved. It is shown how a series of cup experiments, covering a range of boundary humidities, forms the basis for deriving basic vapour pressure dependent permeabilities. Such permeability data were generated for the four specimen types. The experiments included both initially dry (adsorption) and initially resaturated specimens (desorption).

In general the water vapour permeabilities were found to be a function of both the humidity and the initial moisture content. For all specimen types, the adsorption permeabilities were remarkably constant up to a humidity of about 0.7, whereas the desorption permeabilities show a steady increase as a function of humidity. Since desorption permeabilities were considerably larger than the adsorption values the pastes exhibited a substantial "permeability hysteresis". The absolute values of permeability vary approximately by two orders of magnitude, from 10^{-4} to 10^{-2} g · m^{-1} · h^{-1} · torr^{-1}. The results are discussed in relation to literature reviews including both diffusion and permeability data.

Finally, the water vapour permeability results are analysed in terms of the pore structure, by applying developed principles of moisture transport to a simple model based on the mercury intrusion porosimetry data. Although this model could not fully explain the permeability behaviour of a system hardened cement paste-water, the model seems to be able to provide valuable qualitative information.

TABLE OF CONTENTS

INTRODUCTION

Permeability and strength are perhaps the two most important characterizing parameters for concrete. While the importance of strength as an engineering parameter for the design of a structure is self evident, permeability is the single most important characteristic relating to the durability of a concrete structure in its given environment. Is is for this reason that concrete mix design procedures recommend maximum water to cement ratios for various environments: the more corrosive the environment, the lower this maximum.

Yet, our theoretical understanding of moisture transport in concrete is limited, and even systematic experimental investigations are scarce. The greater part of the existing data are diffusion data, usually measured in the non-steady state by drying experiments, and data for permeability of hardened cement paste and concrete to liquid water.

Steady state measurements of water vapour transmission using the "cup" method have been done quite extensively over the years to characterize the water vapour permeability of building materials. However, each such characterization has been in terms of a mean transport coefficient specific to the actual experimental conditions.

The basic water vapour permeability coefficient as a function of relative vapour pressure can be derived from a series of specially designed cup experiments. Using this method, the purpose of the present work has been to generate systematic steady state water vapour permeability data for well defined specimens of hardened cement paste, and to try to interpret the results in terms of the pore structure by applying developed principles of moisture transport in porous media.

I. HARDENED CEMENT PASTE: CHEMICAL AND MICROSTRUCTURAL CHARACTERISTICS.

The purpose of this chapter is to give a very brief and to some extent simplified description of the material hardened cement paste, at various levels of "magnification", as an introduction to later discussions of properties in relation to (pore) structure.

I.1. Chemistry, crystal structure, and morphology

The unhydrated cement clinker contains four main phases: tricalcium silicate (C_3S)[x], β-dicalcium silicate (β-C_2S), tricalcium aluminate (C_3A), and a ferrite phase, often with approximate composition C_4AF (tetracalcium aluminate ferrite).

Paste hydration of portland cement leads eventually to several hydrated solid phases. The major phase is a calcium silicate hydrate gel (C-S-H gel) containing significant quantities of alumina, sulphate, and alkalies. The C-S-H gel is a poorly crystalline phase of colloidal dimensions which, together with a phase of well crystallized calcium hydroxide and some amorphous calcium hydroxide seems to be finally responsible for most of the physical and mechanical properties of hardened cement paste.

The hydration products, and the processes leading to their formation, are quite complex. Much of our present knowledge has been derived from a study of successively more complicated mixtures of the individual clinker phases. In the case of hydration of the C_3S and C_2S phases of clinker much of our understanding has evolved from studies of paste hydration of pure C_3S and C_2S. The stoichiometry of the C-S-H gel produced by hydration of the pure silicates, usually expressed in terms of the C/S and the H/S ratios, has been found to be a function of time (degree of hydration), water/solid ratio, and temperature (Hansen et al 1973).

The chemical environment of the C-S-H gel formed in pastes of portland cement is substantially different from that of the

x) The following symbols are used in cement chemistry: C = CaO, S = SiO_2, A = Al_2O_3, F = Fe_2O_3, H = H_2O

C-S-H gel produced by pastes of the pure silicates. The existence of sulphate, Fe^{3+}, and Al^{3+} ions promote gel substitution reactions, reactions which have been found to occur between C-S-H gels produced from pastes of C_3S and the ions mentioned, both during and after formation of the C-S-H gel (Copeland et al (1967)).

Gel substitution reactions appear to occur quite extensively in cement pastes steam cured at ≈ 100 °C(Taylor (1964)).
As is noted later, there is a considerable difference between the pore structure of hardened cement paste specimens that are heat treated and those that are simply cured at room temperature. These gel substitution reactions may, therefore, be quite relevant to transformations in the pore structure promoted by heat treatment.

The C-S-H gel, though poorly crystallized or near amorphous, has a structure, however ill defined. The crystal structure has some similarity to the naturally occurring mineral tobormorite, for what reason the gel has often been referred to as tobormorite gel. Well crystallized tobormorite is lamellar with a basal spacing of 9.3, 11.3 or 14.0 Å. The basic layer is a sandwich of a double Ca-O sheet between chains of dreierkette silica tetrahedra on top and bottom. In the channels existing between the ribs of the dreierkette, calcium ions and water molecules are placed in an indefinite fashion. The water molecules are believed to constitute the so-called interlayer water.

The morphology of the C-S-H gel can take several characteristic forms. Based on Scanning Electron Microscopy (SEM) studies, Diamond (1976) documents four types of particles of C-S-H gel (fig. I.1). The fibrous Type I particles represent a dominating morphology of C-S-H gel, especially at early ages. Type II morphology, described as a "reticular network", occurs in hardened cement paste contemporaneously or almost so with the Type I particles. As hydration proceeds, a morphology consisting of small, irregularly equant or flattened particles, designated as Type III, appears. Type IV C-S-H gel has a dimpled appearance, with either regular pores or close packed equant grains. Diamond notes that this habit is not common, and suggests that it represents an intermediate product in the early stage of hydration.

Mature cement paste has a microstructure in which C-S-H gel, mostly of type III, together with extensive deposits of calcium hydroxide are dominant. As hydration proceeds, calcium hydroxide deposits grow massive and invade and sometimes even encapsulate regions of the gel. An example of such material, recognized by parallel planes and smooth featureless surfaces, is seen in the upper left micrograph of type III gel in fig. I.1.

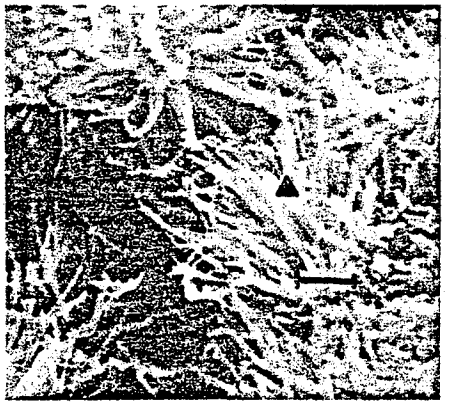

Type I

Type II

Type III

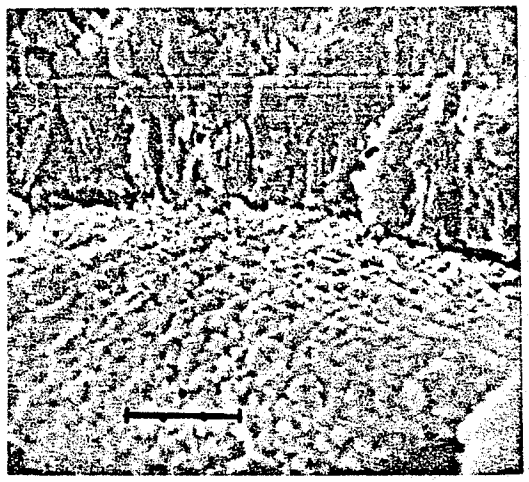

Type IV

Fig. I.1. SEM micrographs showing the four types of C-S-H gel structure. The linear scale indicator is 1 μm. (After Diamond (1976)).

I.2. Microstructure. State of water

Most mechanical and physical properties of hardened cement paste (hcp), and certainly a property such as permeability, are closely connected with its porosity, pore structure, and "moisture content". Assessment of these items is an interrelated problem, and is associated with the question of the state of water in this system.

Based on a comprehensive and systematic investigation of the properties of hcp, Powers and Brownyard (1948) proposed a model for the microstructure of hcp. This model is still widely used, although some modifications have been suggested. Very briefly, the Powers and Brownyard model visualizes the hardened paste as consisting of a primary binder phase, called the cement gel, with a characteristic porosity represented by very fine so-called gel pores (average radius about 15 Å). The cement gel envelops the so-called capillary pores, which on the average are much larger than the gel pores. In addition, the paste contains unhydrated cement grain residues in quantities depending on the degree of hydration. The various hydrates found by the reaction between the cement clinker and water, together with deposits of crystalline calcium hydroxide, constitute the solid part of the cement gel. Since the specific volume of the gel is greater than that of the original cement plus water, the initially water filled space between the cement grains is gradually deminished as hydration proceeds, i.e. the capillary porosity decreases, the capillary pores become smaller and in some cases the capillary pore system eventually looses its continuity. Hydration proceeds at an ever decreasing rate until complete hydration has been reached or until it stops due to space constraints or lack of water.

Ideally, the total water content of hcp may be divided into chemically combined water and physically bound water, the former being an integral part of the solid phase while the latter resides in the pore space, i.e. in the volume between solid "particles".

According to this division the chemically combined water includes hydrate water bound as hydroxyl groups or existing presumably in the molecular form as so-called interlayer water in the C-S-H gel and other hydrate phases, as well as hydroxyl groups in calcium hydroxide. The physically bound water is partly adsorbed on the gel particles and partly capillary condensed.

However, as noted by Powers and Brownyard (1948) in their classical work, there is a certain amount of overlap in the binding energy between different classes of water. As a consequence, the definition of the dry state has to be somewhat arbitrary. The following three states appear to be the ones most frequently referred to:

P-dry: The dry state defined by the water vapour pressure of a mixture of magnesium perchlorate di- and tetrahydrate, 8×10^{-3} torr at 23 °C. (Copeland and Bragg (1954)).

D-dry: The dry state defined by the water vapour pressure of ice at the dry ice temperature, 5×10^{-4} torr. (Copeland and Hayes (1953)).

Oven-dry: The state obtained by keeping the specimen in an (open) oven at 105 °C until it has reached constant weight.

The dry state divides the total water in the system into two groups: one nonevaporable, associated with the chemically bound water, and the other evaporable, associated with the physically bound water. The various drying procedures remove different amounts of water: when the content of nonevaporable water per gram of original cement is expressed as 100% for a P-dried paste, Copeland and Hayes (1953) found that it is about 92% by D-drying, and Powers and Brownyard (1948) report about 89% for oven-dried paste (with no attempt to control the water vapour pressure in the oven). As a consequence, a parameter such as porosity is a function of the choice of the dry state.

This problem has been extensively discussed in the literature, particularly regarding the role played by the interlayer water because there is a considerable overlap of binding energies be-

More recently Litvan (1976) measured the surface area of hcp by water vapour as well as nitrogen adsorption and found almost equal surface areas by the two methods when special techniques for drying the samples were applied. Typical features of the methods were replacement of the pore water by methyl alcohol which in turn was substituted by pentane, and drying was achieved by distillation either in vacuo or above the critical temperature, followed by a final D-drying. It was suggested that this very fast drying procedure avoided the collapse of the structure caused by the receding meniscus, indicating that the drying history to reach the final dry state may be decisive for microstructural changes taking place in the material during drying.

In order to perform BET surface area measurements the samples have to be in an initially dry condition. Winslow and Diamond (1974) measured the specific surface of hcp by a different method, small-angle X-ray scattering, which does not require that the specimens are dried prior to measurement. They found that the surface area of the paste in its normal saturated condition is much higher than previously thought, about 560 m^2/g of D-dried paste. Even partial dehydration was found to lower the measured surface area considerably. Equilibration at 50% humidity reduces the surface to X-rays by about half, with further substantial reduction accompanying more rigorous drying, such as P-drying, D-drying, and oven-drying. A further interesting point of this investigation is that the observed changes in surface area were fully reversible on resaturation.

Various other pieces of evidence indicate that the microstructure of hcp is sensitive to drying-rewetting treatments. In particular the first drying seems to produce some irreversible changes. Powers et al (1954) measured permeability of hcp to water under pressure and found that permeabilities for specimens which had been dried only down to 79% humidity were about seventy times those of virgin specimens. Helmuth and Turk (1967) found that the first shrinkage, i.e. the contraction caused by drying an initially saturated virgin specimen, down to a relative water vapour pressure of 11% is much greater than the subsequent swelling and shrinkage. The paste may be said to have

become stabilized by the first drying; thereafter only reversible shrinkage and swelling was observed.

In addition to the drying/rewetting history, the temperature history of hcp has a significant influence on its microstructure. We have already noted that the chemical composition of the hydrates have been found to vary with the curing temperature. The general influence of an increased curing temperature on the microstructure of hcp is to increase the porosity, produce a coarser (pore) structure, and decrease the surface area (Sellevold (1969), Odler (1976), Winslow and Diamond (1974)).

In the present work we have used two curing methods for the cement paste: isothermal curing at room temperature, and high temperature curing (97 ^{o}C). Hereby we obtain widely different pore structures from the same original mix. The microstructure of the hardened cement pastes was characterized in terms of porosity, internal surface area and pore size distribution.

P-drying was chosen to define the dry state, since, as we have seen, various pieces of evidence indicate that P-drying does not affect the microstructure of the material so severely as D-drying and oven-drying. The specimens were always P-dried prior to use. Since the material seems to become largely stabilized after the first drying, irreversible microstructural changes may be assumed to play a minor part during subsequent rewetting and drying. At the same time we should recall that the first drying may produce changes that increase the permeability, and that the exact details of the "moisture history" on the whole may affect the microstructure of the hardened paste.

The pore size distribution plays an important part in characterizing the specimens in this project. By reference to fig. I.1 and the description of the various morphological forms, it is evident that the main problem associated with pore structure analysis is to set up a realistic, and yet tractable, model of the pore structure. As a consequence, we are reduced to simple models with limited goals in our attempts to analyse moisture transport in this complicated system.

II MATERIALS CHARACTERIZATION

The purpose of this chapter is to describe the materials, experimental procedures, and results used to characterize the specimens of hardened cement paste in terms of porosity, internal surface area, and pore size distribution.

II.1. Materials

The cement used for all specimens was a Danish ordinary Portland cement with chemical and compound composition according to table II.1., and a specific surface area (Blaine) of 2740 cm^2/g. This cement corresponds approximately to an ASTM type I cement.

The mixing water used was destilled water.

Oxide composition		Computed compound composition (Bogue)		
SiO_2	21.7 %	Tricalcium silicate	(C_3S)	56.6%
Al_2O_3	5.0 %	Dicalcium silicate	(C_2S)	19.5%
Fe_2O_3	2.5 %	Tricalcium aluminate	(C_3A)	9.0%
CaO	65.5 %	Tetracalcium aluminate ferrite	(C_4AF)	7.6%
SO_3	2.8 %	Calcium sulphate		4.8%
MgO	1.3 %	Free CaO		0.6%
Ignition	1.0 %			
K_2O	0.68%			
Na_2O	0.36%			
Total Na_2O equ.	0.81%			

Table II.1. Chemical and compound composition of cement.

II.2. Specimen Production

The hardened cement paste specimens used in this project for measurements of moisture migration have to meet strong demands regarding homogeneity. Consequently, special care was taken to avoid inhomogeneities due to bleeding and due to the presence of air bubbles in the specimens.

II.2.1. Casting

Specimens were prepared with original water/cement ratios (w/c) equal to 0.40 and 0.50 (by weight).

In order to avoid air bubbles in the mix, the mixing water was degassed prior to use, and a mild vacuum was applied during mixing. The mixing schedule was: 2 minutes of mixing, 5 minutes rest, and then 2 minutes of remixing to overcome a possible false set.

After mixing, the paste was transferred to a vacuum hand mixer and evacuated during vigorous stirring. Hereafter the paste was poured into moulds through a bottom outlet of the hand mixer. The moulds used were 5 mm thick teflon tubes of inner diameter 20 mm, and 150 mm long. During filling, the tube was closed in one end by a rubber stopper. After filling, the paste was sealed in the tube by pressing a rubber stopper with a hypodermic needle into the open end of the tube, and removing the needle when the paste started to flow through (see fig. II.1.).

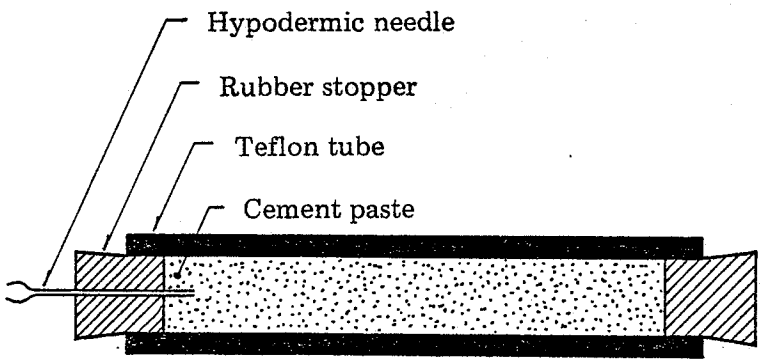

Fig. II.1.: Specimen casting principle

II.2.2. Curing

All specimens were given a common precuring at room temperature. Immediately after casting, the moulds were fixed to a slowly rotating cylinder, parallel to the rotation axis, and left rotating at room temperature for 1 day. This procedure was used to avoid bleeding in the fresh paste. After this the specimens were demoulded, and subsequently cured in two ways.

One part of the specimens from a batch were placed in glass test tubes (fig. II.2.2.) with water at the bottom. The test tubes were submerged in a thermostated water bath maintained at 97 °C, and sealed after a few minutes. For a period of 7 days the specimens were steam cured at atmospheric pressure in this way. Hereafter they were slowly cooled to room temperature and stored submerged in saturated lime water until use. The lime water was contained in closed bottles to avoid carbonation. This curing procedure will hereafter be referred to as "steam curing" or "S-curing".

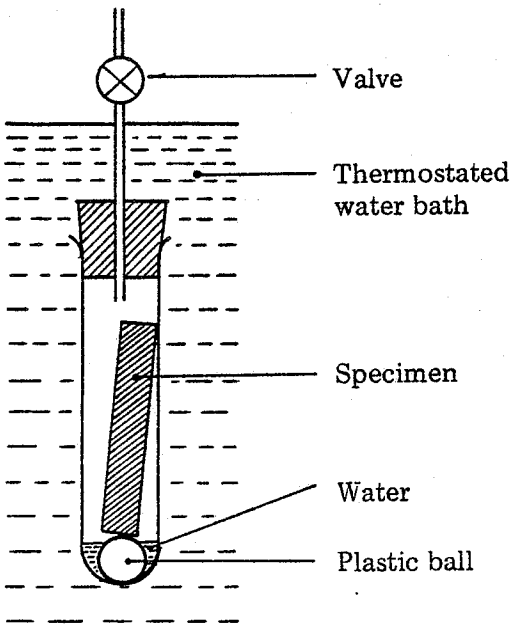

Fig. II.2. Steam curing of specimens

The remaining part of the specimens from a batch were continuously cured at room temperature submerged in saturated lime water in closed bottles until use. This method of curing will be referred to as "room temperature curing" or "RT-curing".

Table II.2. summarizes the 4 specimen types we shall be dealing with in the following.

II.3. Density and Porosity. Drying

II.3.1. Density measurement

The density of the hardened paste is most easily measured when

the specimens are in the saturated surface dry (SSD) condition.

Determination of the SSD weight of the sample involves the problem of finding a reliable procedure to establish the SSD state. Various experiments showed that good reproducibility was obtained by simply wiping the sample with a tissue and expose it to air until it was judged by visual inspection that the SSD state had been reached. The sample was then quickly put into a tared closed weighing bottle with water and weighed. In that way the SSD state was maintained during weighing. Once the SSD weight of the specimen was measured, its volume could be obtained using a pycnometer with water.

Homogenity of the cylindrical specimens was tested by measuring the SSD density of consecutive sections of a specimen. All specimens so tested showed to be homogeneous within the accuracy of measurement.

Measured densities of the 4 specimen types are listed in table II.2.

II.3.2. Porosity

II.3.2.1. Definition

Ideally the porosity of a specimen may be defined as the ratio of pore (or void) volume to the total bulk volume of the specimen. As was discussed in section I.2., however, any hcp specimen contains water more or less loosely bound. Division of the water into chemically combined water and adsorbed or capillary condensed water is somewhat arbitrary and depends on the specific drying method.

In this project we have chosen to define the porosity as the weight gained when a unit volume (or unit weight) of P-dried hcp is brought to the water saturated surface dry (SSD) condition.

We shall make two comments to this definition:

1. P-drying has been chosen to define the dry state. As we noted in section I.2., P-drying is the mildest one of the three standard drying methods. It presumably does not affect the microstructure of the material so severely as D-drying and oven-drying.

2. The definition of porosity is based on the water uptake by resaturation of a previously dried specimen. This is consistent with the fact that all specimens used in this project were P-dried prior to use, so that properties are measured during the first adsorption and the second desorption. As discussed in section I.2. drying is accompanied by various microstructural changes. Moreover, there is evidence which indicates that the paste may be said to have become largely stabilized after the first drying has taken place, at least regarding the shrinkage and swelling performance.

II.3.2.2. Drying

As we have already mentioned, P-drying was chosen to define the dry state. The P-dry state is reached by equilibrating the hcp at the water vapour pressure of a mixture of magnesium perchlorate dihydrate and magnesium perchlorate tetrahydrate, $\approx 8 \times 10^{-3}$ torr at 23 ^{o}C (see section I.2.).

Usually the water content of desiccant was determined both prior to use and after use by thermogravimetric analysis (TGA). Fig. II.3. shows a TGA trace-sample weight versus temperature - for a sample of magnesium perchlorate hydrate, together with the weights of the various hydrates calculated according to their molar weights.

In some cases the commercially available magnesium perchlorate hydrate had to be somewhat conditioned before use, in order to obtain the prescribed mixture of di- and tetrahydrate.

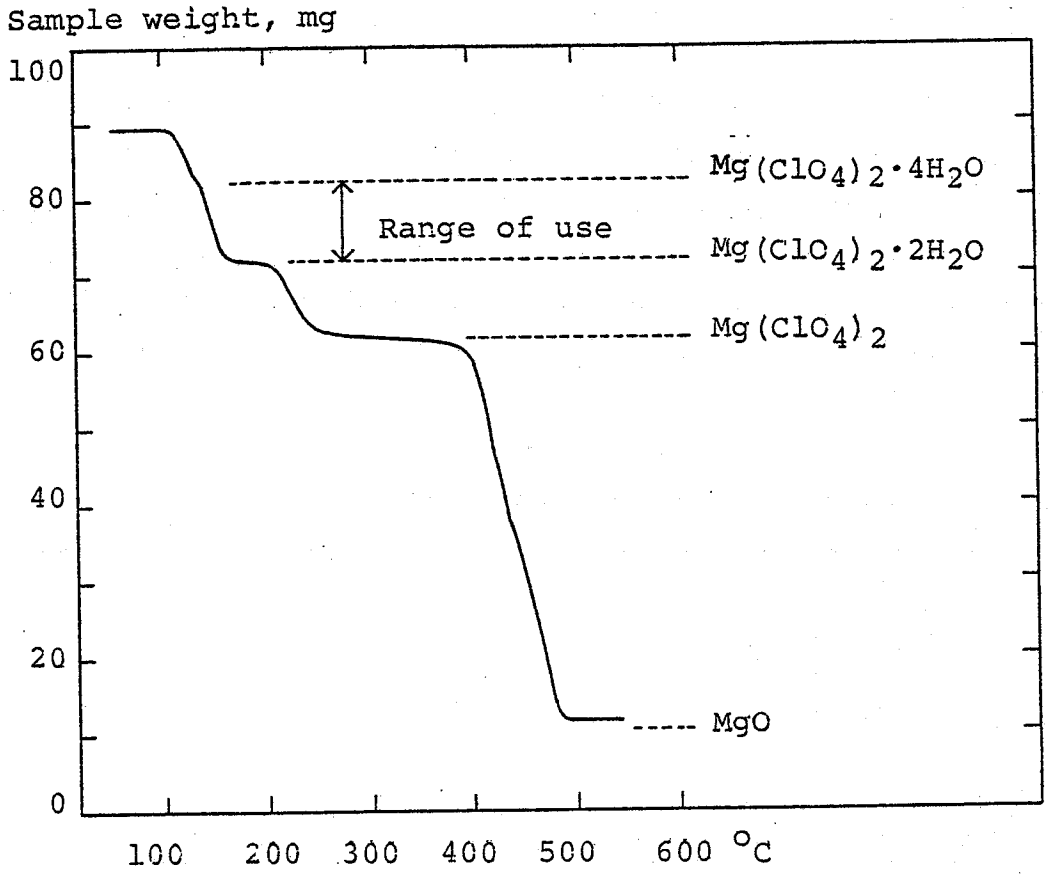

Fig. II.3. Record from thermogravimetric analysis of magnesium perchlorate hydrate. The weights of the hydrates indicated are computed according to their molar weights.

II.3.2.3. Experimental

The specimens used for porosity measurements were discs 20 mm in diameter and 1 mm thick (as used later on in the cup experiments).

Each disc was placed in a weighing bottle in a desiccator containing a mixture of magnesium perchorate dihydrate and tetrahydrate. During drying of the specimens, the disiccator was evacuated to a pressure about equal to the equilibrium water vapour pressure of the perchlorate, 8×10^{-3} torr. The progress

of drying was followed by occasional weighing. Some weighings done within 1 day of drying indicated that more than 90% of the weight loss had taken place. Generally the specimens were found to have reached constant weights, or at least rates of weight loss less than 0.1 mg/g dry material/day within a week.

After having reached the P-dry state, the discs were placed over water in a desiccator for some hours, and subsequently submerged and resaturated in vacuo for about 1 day. The porosity computed hereafter, ε_w, is expressed in cm^3/g dry material. By using the SSD density ρ_{SSD}, this unit can be converted into cm^3/cm^3 ($\varepsilon_v = \rho_{SSD}\varepsilon_w/(1+\rho_w\varepsilon_w)$, where ρ_w is the density of water). Results are listed in table II.2.

Table II.2. Specimen parameters

Specimen designation	Nominal water/cement ratio w/c	Curing method	SSD density g/cm^3	Porosity	
				ε_w (cm^3/g dry weight)	ε_v cm^3/cm^3
0.5 (S)	0.50	S	1.90[x)]	0.282±0.012[xx)]	0.418
0.4 (s)	0.40		2.03	0.219±0.005	0.365
0.5 (RT)	0.50	RT	1.93	0.241±0.006	0.375
0.4 (RT)	0.40		2.06	0.192±0.002	0.332

x) standard deviations of density measurements were ca. 0.01 g/cm^3

xx) Mean value ± 1 st. dev. The relatively large standard deviation for 0.5 (S) is mainly due to specimens originating from different batches.

As expected the porosities obtained by this procedure were found to be somewhat lower than those calculated from the weight lost when the virgin specimens were brought from the SSD to the P-dry state, i.e. during the first desorption. The first desorption porosities (in cm^3/g dry weight) were 0.5 (S): 0.295 ± 0.015, 0.4 (S): 0.224 ± 0.006, 0.5 (RT): 0.259 ± 0.008, and 0.4 (RT): 0.206 ± 0.001. The porosities for the RT cured specimens so obtained could be compared with the body of porosity data existing at this laboratory. The 0.4 (RT) porosity

agreed well with those data, whereas the 0.5 (RT) porosity seemed to be a little too low, probably caused by evaporation of some of the mixing water during the vacuum mixing, so that the effective w/c is somewhat lower than 0.50.

II.4. Pore size distribution. Internal surface area

The porosity of HCP is an important parameter for transmission of water through the material. However, its "importance" is strongly dependent on the way the porosity is distributed, as quantified through the pore size distribution function.

Pore size distribution functions of HCP are most commonly obtained from appropriate sorption isotherms, or by mercury intrusion porosimetry.

II.4.1. Sorption isotherms

II.4.1.1. General

At the surface of a solid the molecules of the solid are not surrounded by as many neighbour molecules as in the bulk of the solid. As a consequence, the free energy of the molecules in the surface is greater than that of the inside molecules. This excess free energy is responsible for the "activity" of the surface.

When a vapour is admitted to an evacuated solid, some of the molecules of the vapour attach themselves to the surface. This is the phenomenon of adsorption, which is a spontaneous process resulting in a decrease of the free energy of the system. The solid that adsorbs the vapour is called the adsorbent, the adsorbed vapour is called the adsorbate.

In most adsorption experiments, the temperature is kept constant and the amount adsorbed is determined as a function of the equilibrium vapour pressure:

$$w = f(p) \qquad \text{(II.1)}$$

where

w = weight of adsorbate per unit weight of adsorbent

p = vapour pressure
(e.g. in mmHg (torr))

The relationship (II.1) is called an adsorption isotherm.

At low pressures all the adsorbed vapour is in contact with the surface of the adsorbent. As the pressure is increased, a larger fraction of the surface becomes covered, and at still higher pressures a second adsorbed layer begins to build up on top of the first adsorbed layer. Thus monolayer adsorption goes over into multilayer adsorption. The second layer begins to build up appreciably even before the surface is covered with a complete monolayer (Brunauer and Copeland (1963)).

The most widely used expression of adsorbate content as a function of vapour pressure is given by the BET-equation, derived by Brunauer, Emmett and Teller (1938):

BET

$$w = \frac{V_m\, C(p/ps)}{(1 - p/ps)(1 + (C - 1)p/ps)} \qquad \text{(II.2)}$$

Here
- w = weight of adsorbate per unit weight of adsorbent
- V_m = weight of a complete monolayer of adsorbate, per unit weight of adsorbent
- p = vapour pressure
- p_s = vapour pressure at saturation
- C = a constant, related to the "activity" of the adsorbent surface

For most adsorbent-adsorbate systems, the BET equation (II.2) is valid in the range $0.05 < p/ps < 0.35$. The equation is commonly used for estimating surface area of adsorbents. Eq. (II.2) may be linearized for plotting purposes as follows:

$$\frac{p/ps}{w(1 - p/ps)} = \frac{1}{V_m C} + \frac{C - 1}{V_m C}\, p/p_s \qquad \text{(II.3)}$$

The slope and intercept of the straight line arizing from plotting $\frac{p/ps}{w(1 - p/ps)}$ versus p/ps give the monolayer capacity V_m and

the C-value. Given the area occupied by each adsorbate molecule, the surface area of the adsorbent can be calculated from V_m.

Monolayer and multilayer adsorption occurs on the surface of nonporous as well as of porous adsorbents. In porous adsorbents, at higher vapour pressures, the adsorbate may also be present as the result of capillary condensation.

The adsorbate, in the liquid state, can coexist in equilibrium with its vapour below the saturation vapour pressure, if the liquid/vapour interface is curved. The relationship between interface curvature and vapour pressure can be derived from the Young and Laplace equation (Gregg & Sing (1967))

$$\ln\frac{p}{p_s} = -\frac{\sigma v^e}{RT} \cdot \frac{2}{r_m}\,,$$
$$\frac{1}{r_m} = \frac{1}{2}\left(\frac{1}{r_1} + \frac{1}{r_2}\right) \qquad \text{(II.4)}$$

where

p = vapour pressure
p_s = vapour pressure at saturation
σ = surface tension of the liquid
v^e = molar volume of the liquid
R = the gas constant
T = absolute temperature
r_1, r_2 = principal radii of curvature (positive if the center of curvature is in the gas phase)

For a liquid contained in a circularly cylindrical capillary (fig. II.4), with the contact angle θ, we obtain

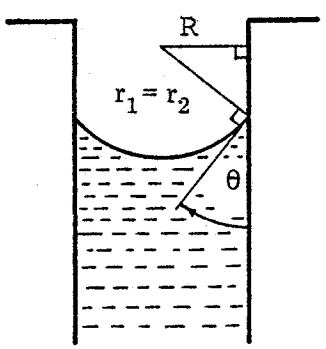

$$r_1 = r_2 = \frac{R}{\cos\theta}, \text{ and thus}$$

$$\ln\frac{p}{p_s} = -\frac{2\sigma v^e}{RRT}\cos\theta \qquad \text{(II.5)}$$

Fig. II.4. Circularly cylindrical capillary.

Equation (II.5), which is a special case of (II.4), is known as the Kelvin equation. We shall make use of these equations later, for pore structure analysis.

If a saturated adsorbent is brought to equilibrium with a vapour pressure less than the saturation pressure, adsorbate is lost to the surroundings through the process of desorption. Normally, at high vapour pressures, the amount of adsorbate held by the adsorbent at a given pressure is greater for the desorption isotherm than for the adsorption isotherm. This phenomenon is called hysteresis.

II.4.1.2. The t-method of pore structure analysis

Sorption isotherms may be used for analysing the pore structure, for example the distribution of pore sizes, of a porous adsorbent. During the last two decades, the so-called t-method of pore structure analysis has been applied quite extensively for that purpose. Based on the original work on this method, Radjy and Sellevold (1972) have developed a detailed phenomelogical theory for the application of the t-method of pore structure analysis to slit-shaped pores, and to circularly cylindrical pores (Sellevold and Radjy (1972).

In the case of slit-like pores, the t-method is centered on the V-t plot. The V-t plot is a graph of total volume adsorbed (V) at t, the statistical thickness of the adsorbed layer on the surface of an otherwise emply pore, versus t. The V-t plot is obtained from the sorption isotherm (amount adsorbed as a function of humidity, at constant temperature) and an appropriate t-isotherm (t as a function of humidity, at constant temperature), by elimination of the humidity. In the case of circularly cylindrical pores, the β-t plot, where β is the slope of V(t), is introduced in addition to the V-t plot.

The geometrical features of the V-t (and β-t) plot are interpreted in terms of pore statistics, and forms the basis to distinguish between two mechanisms for pore filling: Micropore (MP)-filling and (Kelvin) capillary condensation (KCC)-filling.

MP-filling takes place by the formation of successive layers of the adsorbate until the layers on opposite pore walls merge. KCC-filling occurs by capillary condensation (cf. section II.4.1.1.).

Sellevold and Radjy refer to a figure as reproduced in fig. II.5, which is a schematic representation of three types of commonly occurring V-t plots. The plots are linear up to $\hat{t}$, implying a "no-pore" region, where adsorption occurs on the walls of otherwise empty pores. At $\hat{t}$, an upwards deviation from the straight line means onset of capillary condensation, and a downward deviation means micropore filling, brought about by merging of adsorbed layers on opposite pore walls.

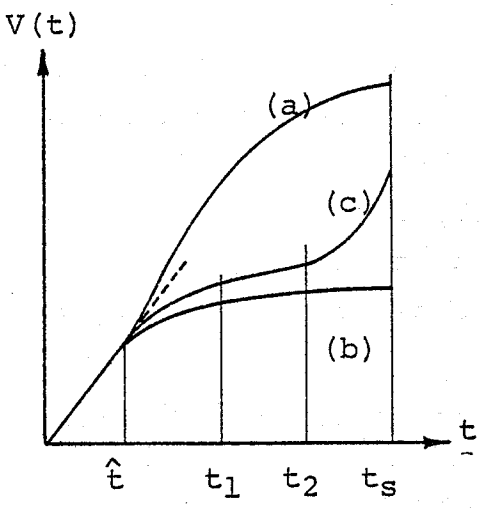

Fig. II.5. Representative V-t plots. From Sellevold and Radjy (1972).

Curve (a) has an upward departure from the initial straight line at $\hat{t}$, which means that Kelvin Capillary Condensation (KCC) analysis is appropriate in the range t to t_s. Either the slit or the cylindrical pore model can be used, the choice being decided by the closure conditions. The cylinder model, however, may be chosen only when the length average pore radius is much greater than $\hat{t}$.

Curve (b) has a downward departure at $\hat{t}$, and micropore analysis for slits is appropriate.

Curve (c) has a second linear range from t_1 to t_2, making this region a no-pore region. Micropore analysis for slits is appropriate in the range $\hat{t}$ to t_1, and KCC analysis for slits or cylinders from t_2 to t_s.

Once the regions of operation for the two filling mechanisms are determined, the appropriate analysis in each region can be performed. Radjy and Sellevold asserted three (internal) consistency criteria for the analysis:

1. The surface and volume closure conditions, i.e. the computed total surface area must equal the measured surface area, and the computed total pore volume must equal the total porosity of the adsorbent.

2. The fundamental restrictions of pore statistics, i.e. pore size distribution functions ≥ 0, etc.

3. The basic postulate that "the V-t plot and pore structure bear a unique and significant relationship to each other".

By reference to the third criterion it is proved that only sequential, and not simultaneous occurrence of micropore filling and capillary condensation is acceptable.

II.4.1.3. Experimental

Sorption isotherms were measured for three specimen types: 0.5 (S), 0.4 (S), and 0.4 (RT). Due to time limitations no sorption measurements were done for 0.5 (RT). At the time of measurement the 0.4 (S) and 0.4 (RT) pastes were about 8 months, and the 0.5 (S) about 4 months old.

The specimens were roughly crushed and predried at a mild vacuum over silica gel in desiccators at room temperature. The chunks were then further crushed and seived in a glove box containing ascarite to avoid carbonation. Powder in the size range between 149 and 250 μm was used for the sorption experiments. The powder was distributed in weighing bottles with ca. 1 g in each, and P-dried in vacuo ($p \approx 10^{-2}$ torr) in desiccators prior to use in the experiments. The drying periods varied from 7 to 26 days; ultimate rates of weight loss were about 0.1 mg/g dry material/day.

After the dry weight had been obtained, the weighing bottles

were placed in pairs in 9 desiccators. Each desiccator contained a saturated salt solution to control the humidity, as specified in table II.3. The desiccators were evacuated to a pressure slightly above the equilibrium water vapour pressures of the salt solutions, and kept in a thermostated box at 25 °C.

Table II.3. Saturated salt solutions for humidity control

Salt	Equilibrium humidity	Reference[x)]
$LiCl \cdot H_2O$	.11	a, b, c
$KCH_3COO \cdot 1.5\ H_2O$	.23	b, c
$MgCl_2 \cdot 6H_2O$	.33	a, b, c
$K_2CO_3 \cdot 2H_2O$	.43	a, c
$NaBr \cdot 2H_2O$	.57	b, c
NaCl	.75	a, b, c
KCl	.85	b, c
KNO_3	.92	a, b, c
K_2SO_4	.97	a, c

x) a: Wexler and Hasegawa (1954)
b: Stokes and Robinson (1949)
c: Rockland (1960)

The weighing bottles were taken out periodically and weighed, until the weight was reasonably constant, as will be discussed later.

In that way, a total of 9 points of the adsorption isotherm were determined simultaneously. Each point represents the mean value obtained from two companion samples.

After the adsorption branch of the isotherm was determined, the weighing bottles were kept in vacuo over pure water for about 1 day. Hereafter, a small quantity of water was dripped in each bottle to ensure complete saturation.

The saturated samples were then put back into the 9 desiccators, in such a way that each individual sample was exposed to the same humidity during desorption as it was during adsorption. Hereafter the desorption branch of the isotherm was determined in a way

similar to the adsorption measurements.

In all experiments results from two companion samples agreed extremely well. In both the adsorption and desorption experiments, however, it turned out to be difficult to reach constant weights. In fig. II.6 the weight gains are plotted as a function of exposure time. In general, the adsorption weights at the lower humidities unexpectedly decrease during the period plotted. This anomaly is not understood; similar unexplained behaviour was reported by Powers and Brownyard (1948). At the higher humidities the weight gain during adsorption become either constant, or increase slightly with time. The weight gains used to construct the adsorption isotherm were always (arbitrarily) chosen as the maxima of the curves in fig. II.6. Concerning the desorption weights, fig. II.6 demonstrates that the weight is steadily decreasing, though very slightly, with time for at least about 7 months. The end points of fig. II.6 were used to plot the nine points of the desorption isotherm.

II.4.1.4. Results

Sorption Isotherms

The sorption isotherms measured for the three specimen types 0.5 (S), 0.4 (S), and 0.5 (RT) are plotted in fig. II.7. Together with the sorption values, obtained below saturation from powdered specimens, the saturation points measured on discs as described in section II.3.2.3. are shown in these diagrams. For all specimen types, a smoth curve can be drawn through the adsorption points (the adsorption isotherm). The desorption points, however, exhibit considerable fluctuation, especially regarding the specimen types 0.5 (S) and 0.4 (RT) at the lower humidities. At $p/p_s = 0.23$ these specimens apparently contain more evaporable water than they do at $p/p_s = 0.33$. To the author's knowledge, no acceptable sorption mechanism could be responsible for this. In this connection it is worth recalling that the nine points of an isotherm were measured simultaneously, and thus in fact by nine independent experiments. Going critically through the experimental procedure, inclusive of checking the humidity over the saturated salt preparations, however, offered no explanation of the anomaly.

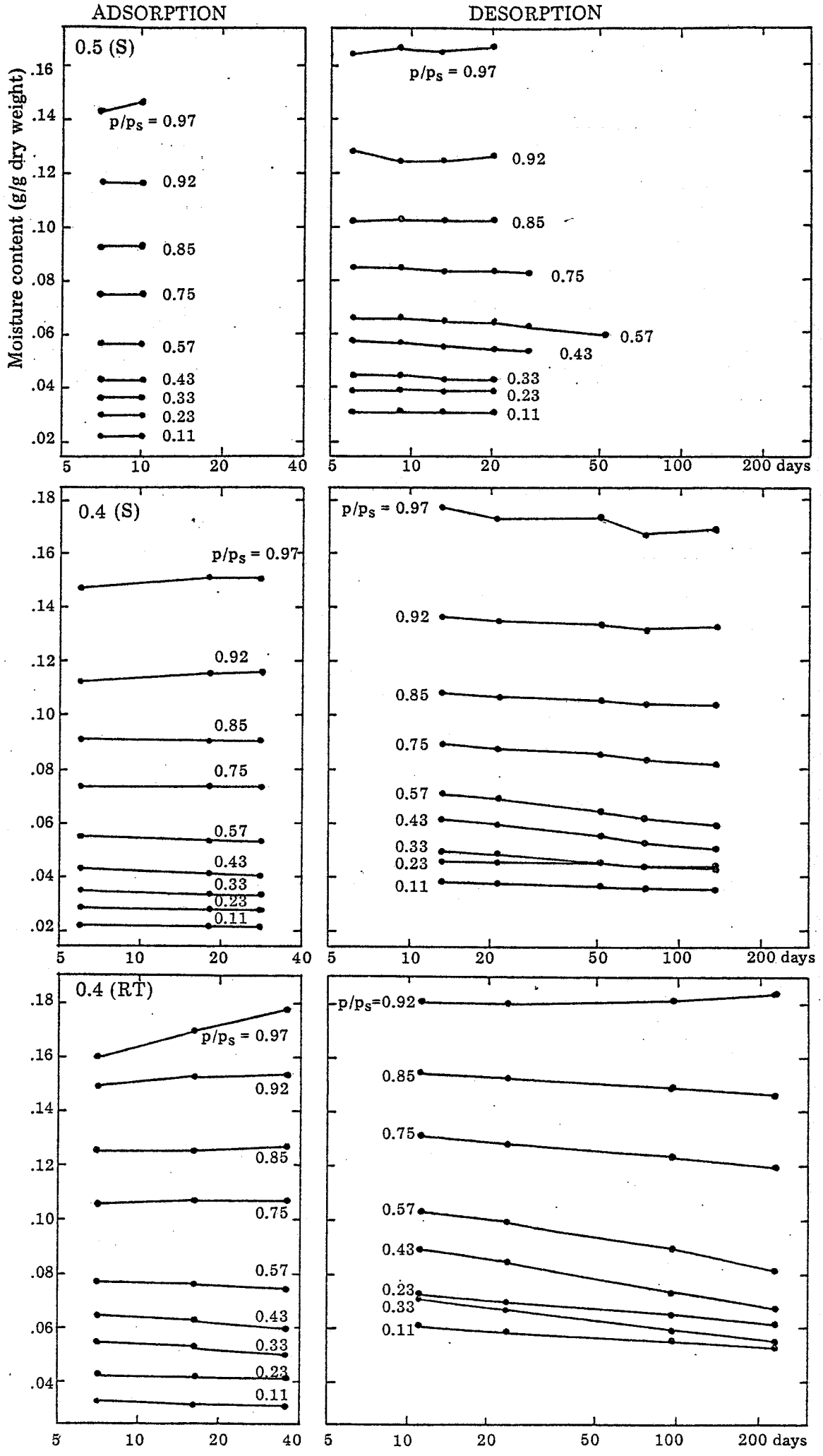

Fig. II.6. Sorption versus time

NB: Thin + Lightweight pp. 5 25

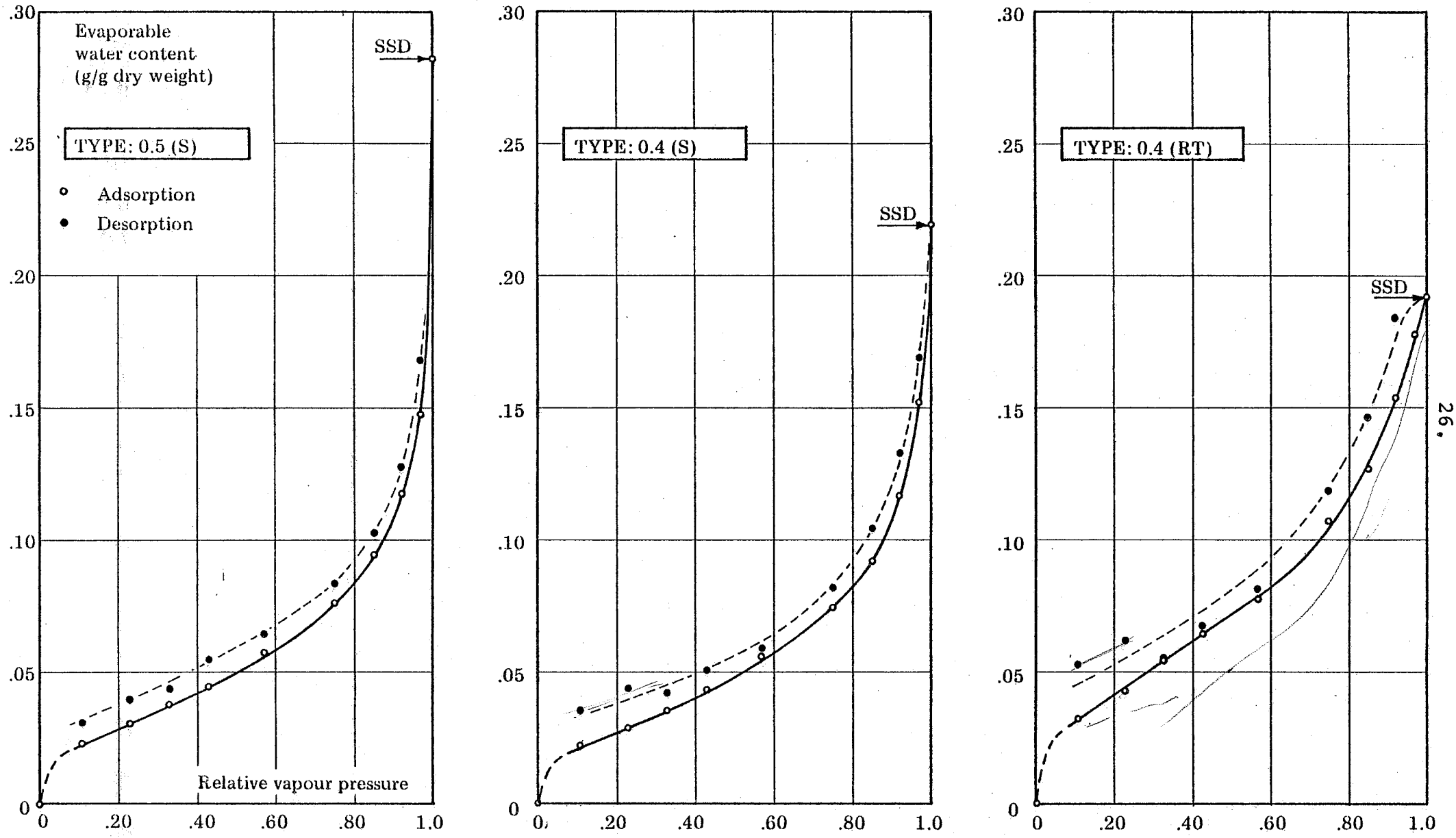

Fig. II. 7 Sorption isotherms

Internal surface area

BET-plots according to eq. (II.3), section II.4.4.1, are shown in fig. II.8. The straight lines shown are obtained by linear regression on points of the smooth adsorption isotherms. From the intercept and slope of these lines we can calculate V_m, the amount of adsorbate required to cover the internal surface with one layer of water molecules, and the BET C-value.

The internal surface area is calculated from

$$S_{BET} = \frac{V_m}{M} \cdot N \cdot A \qquad \text{(II.6)}$$

where S_{BET} = the internal surface area according to the BET-theory
V_m = the monolayer capacity
M = molecular weight of water (= 18g/mole)
A = the area covered by each water molecule
N = Avogadro's number (= 6.02×10^{23} molecules/mole)

With A = 11.4 $Å^2$, as suggested by Brunauer and Greenberg (1960), eq. (II.6) becomes

$$S_{BET}\ (m^2/g \text{ dry weight}) = 3813\ V_m\ (g/g \text{ dry weight}) \qquad \text{(II.7)}$$

The BET-parameters V_m and C are listed in table II.4 together with the internal surface area computed from (II.7).

Table II.4. BET parameters and internal surface area.

KKH

Specimen designation	V_m g/g dry weight	C	S_{BET} m^2/g dry weight
0.5 (S)	0.0269	22	103
0.4 (S)	0.0253 0,015	23	96
0.4 (RT)	0.0397	20	151

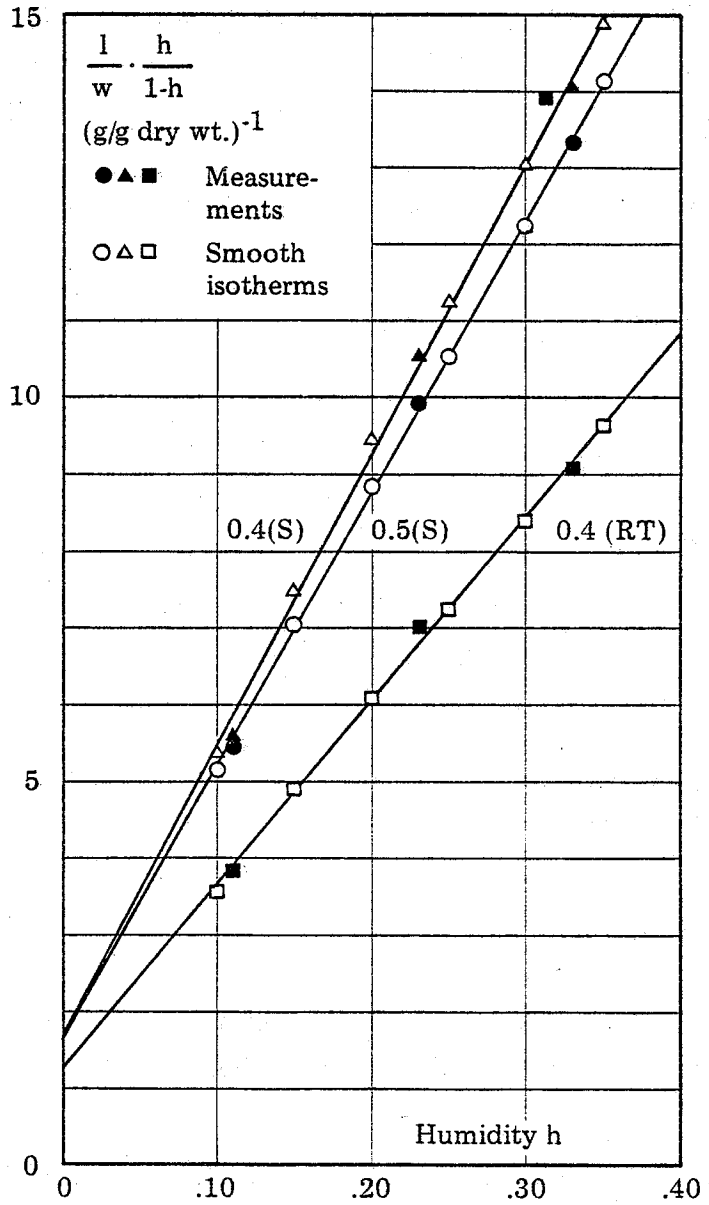

Fig. II.8 BET-plots, based on adsorption isotherms

Pore structure analysis

The t-curve used in constructing V-t plots is shown in fig. II.9. This curve was reported by Hagymassy, Brunauer, and Mikhail (1969). Below p/p_s = 0.50 it applies to an adsorbent with a C value of 23, and above p/p_s = 0.50 to adsorbents with C-values in the range 10-200. The t-curve is based on adsorption measurements at 25 °C and 30 °C. The value used for the thickness of a monolayer of water molecules was 3.0 Å.

The sorption isotherm to be used for pore structure analysis should ideally represent equilibrium conditions. As we have seen, all the specimens investigated exhibit considerable sorption hysteresis. The problem of deciding whether the adsorption or the desorption branch of the isotherm most closely represents true equilibrium has been the subject of a number of investigations and discussions, without having been fully resolved. Gregg and Sing (1967), and Everett (1967) take the question up in detail, and give complete references. In this work, the adsorption brances of the isotherms, which apparently are the ones best defined, were chosen for the pore structure analysis.

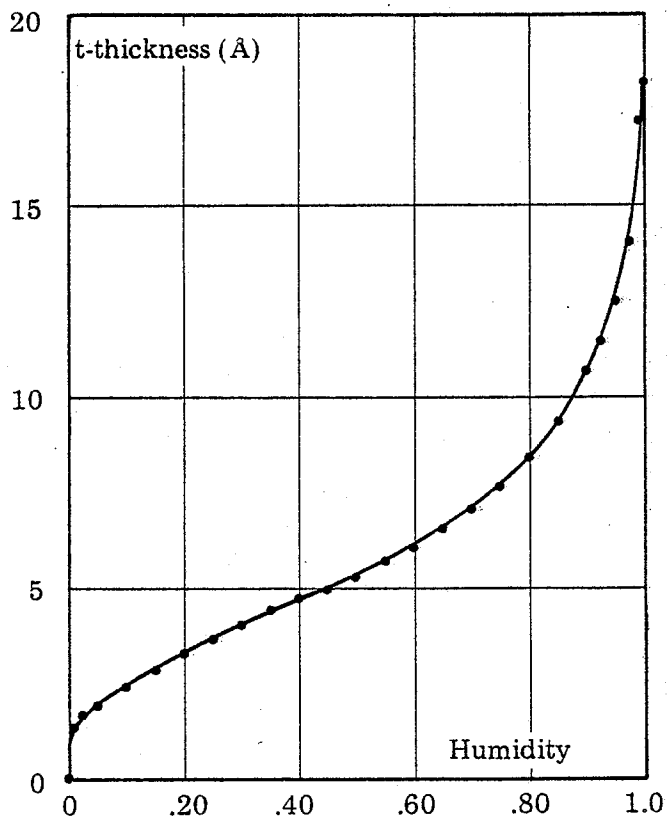

Fig. II.9. t-curve. Reported by Hagymassy et al. (1969)

The V-t plots, based on the adsorption isotherms, are shown in fig. II.10. The curves are drawn in accordance with the smooth isotherms, with the measured points shown.

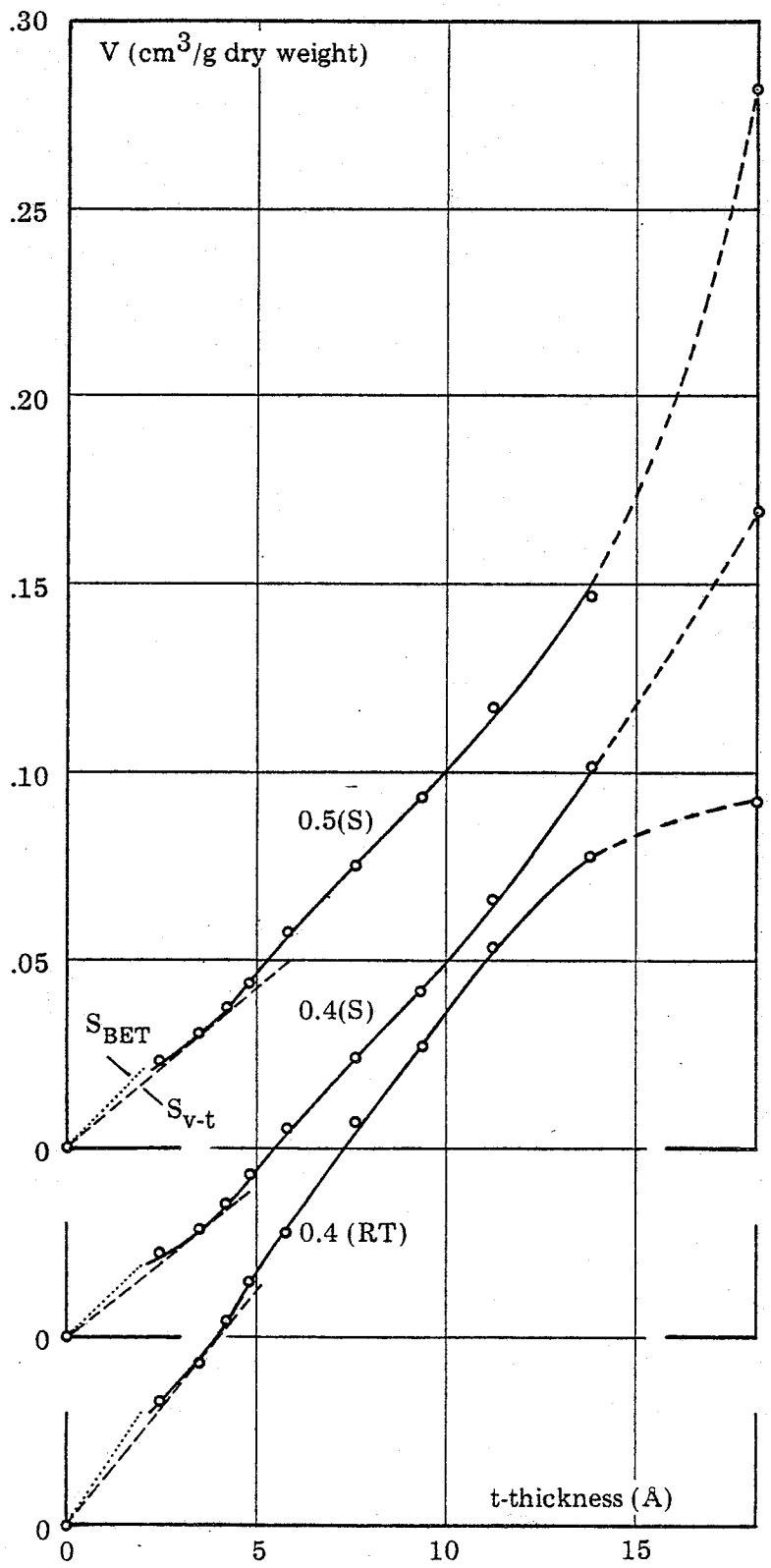

Fig. II.10. V-t plots, based on adsorption data

Following the analysis procedure of Sellevold and Radjy (1972) (cf. section II.4.1.2.), we start with examining the V-t plots in fig. II.10. All of these plots suffer from the lack of experimental points below t ≈ 2.5 Å, and consequently there is no precise information of whether the first portion of the plots is linear or not. However, considering the shape of the V-t plots at low t-values, and the accuracy of determination by reference to fig. II.6, II.7, and II.9, it seems justifiable to approximate the first portion of the plots with a tangent to the smooth curves, going through the origin, as shown with broken lines in fig. II.10.

The slope of the initial straight line equals the internal surface area of the specimen. In fig. II.9, lines corresponding to the BET-surface are shown, and the numerical values are listed in table II.7. It is seen that the surface computed from the V-t plots are comparable with the BET-values. Ideally, the difference between the two sets of values reflects the fitness of the t-isotherm.

The point of first departure from the initial straight line is located at t ≈ 4Å (p/ps ≈ 0.30) for all specimen types. Since we observe an upward departure, KCC-analysis is appropriate in the entire range from t ≈ 4Å (h = 0.30) to saturation.

The KCC analysis was performed using the "classical" approach. The various procedures commonly employed for evaluating pore size distritution functions (PSDF's) have been summerized by Sutherland (1967). The main assumptions made in the KCC analysis are

1. The surface tension and molar volume of the capillary condensate have the same values as those of bulk liquid at the experimental temperature

2. The pores have some specified geometri, e.g. cylinders or slits

3. The generalized Kelvin equation (II.4) describes the equilibrium properties of the capillary condensate

4. Any variation in the radius of the meniscus, arising from the influence of the adsorption forces of the pore walls is neglected.

The analysis method used in this work is a method that corrects for an adsorbed film, the thickness of which varies with the equilibrium vapour pressure. An outline of the method, assuming non-intersecting, circularly cylindrical open-ended pores, is given in the following.

Suitable intervals are chosen on the humidity scale of the adsorption isotherm, and the weight of water associated with each interval, is read off the isotherm. Starting from saturation, the pore volume in the first step is

$$\Delta V_1 = \Delta V_1^{o}\left(\frac{R_1}{R_{k1}}\right)^2 \qquad \text{(II.6)}$$

where

$$R_1 = R_{k1} + t_1 \qquad \text{(II.7)}$$

$$R_{k1} = -\frac{2\sigma v^e}{RT \ln h_1} \qquad \text{(II.8)}$$

ΔV_1 = pore volume in the first step

ΔV_1^{o} = "observed" volume desorbed in the first step, as obtained from the adsorption isotherm

R_1 = mean pore radius in the first step

t_1 = mean t-thickness in the first step, as obtained from the t-curve

R_{k1} = mean Kelvin radius obtained from the Kelvin equation (II.5), with zero contact angle, using

h_1 = the mean humidity of the first step ($h = p/p_s$)

Using the following values for the constants in eq. (II.8), or (II.5)

σ = 72.0 dynes/cm

v^e = 18.07 cm^3/mole

R = 8.314 x 10^7 ergs/mole/^{o}K

we get

$$R_k(\text{Å}) = -\frac{10.49}{\ln h} \qquad \text{(II.9)}$$

In the second step, the pore volume is calculated from

$$\Delta V_2 = \left(\Delta V_2^{o} - \Delta A_2\right)\left(\frac{R_2}{R_{k2}}\right)^2 \qquad \text{(II.10)}$$

where $$\Delta A_2 = \frac{\Delta V_1}{\pi R_1^2}\left(\pi(R_1 - t_2)^2 - \pi(R_1 - t_1)^2\right) \qquad \text{(II.11)}$$

ΔA_2 is the volume associated with the thinning of the surface layer in the pores emplied in step 1, during step 2, i.e. from thickness t_1 to t_2. The term $\Delta V_1/\pi R_1^2$ is equal to the length of pores with radius R_1.

Thus, in the n'th step we get

$$\Delta V_n = (\Delta V_n^{\circ} - \Delta A_n)\left(\frac{R_n}{R_{kn}}\right)^2 \qquad \text{(II.12)}$$

$$\Delta A_n = \frac{\Delta V_{n-1}}{R_n^2 1}\left((R_{n-1} - t_n)^2 - (R_{n-1} - t_{n-1})^2\right)$$

$$+ \frac{\Delta V_{n-2}}{R_n^2 2}\left((R_{n-2} - t_n)^2 - (R_{n-2} - t_{n-1})^2\right)$$

$$\vdots$$

$$+ \frac{\Delta V_1}{R_1^2}\left((R_1 - t_n)^2 - (R_1 - t_{n-1})^2\right) \qquad \text{(II.13)}$$

The pore surface ΔS_n and length ΔL_n in the n'th step are calculated from

$$\Delta S_n = \frac{2\Delta V_n}{R_n} \qquad \text{(II.14)}$$

$$\Delta L_n = \frac{\Delta V}{\pi R_n^2} \qquad \text{(II.15)}$$

The result of this analysis is a pore size distribution function, which can be presented as a histogram, i.e. a series of blocks, one for each interval, with the area of each block representing the volume, surface, or length of pores of the mean radius R of the interval.

The analysis can be performed quite analogously assuming pore geometries other than circular cylinders. In such case, the appropriate form of the generalized Kelvin equation (II.5) should be used, and eqs. (II.12) and (II.13) should be modified accordingly. The method is easily programmed for the computer, allowing small steps and better computing accuracy.

Table II.5. KCC-analysis, cylindrical pores. (part of "computer-worksheet".

CYLINDERS			0.5 (S)			0.4 (S)			0.4 (RT)		
Humidity p/p_s	t-thickness t (Å)	Pore radius R (Å)	Water content from isotherm w (cm^3/g)	Cumulative pore volume V (cm^3/g)	Cumulative pore surface S (m^2/g)	Water content from isotherm w (cm^3/g)	Cumulative pore volume V (cm^3/g)	Cumulative pore surface S (m^2/g)	Water content from isotherm w (cm^3/g)	Cumulative pore volume V (cm^3/g)	Cumulative pore surface S (m^2/g)
1.00	18.2	∞	0.2820	0	0	0.2190	0	0	0.1920	0	0
0.99	17.2	1061	0.1973	0.0862	0.9	0.1879	0.0316	0.3	0.1860	0.0061	0.2
0.98	14.8	534	0.1663	0.1184	1.8	0.1657	0.0549	1.0	0.1806	0.0094	0.5
0.97	13.5	358	0.1497	0.1359	2.6	0.1504	0.0711	1.8	0.1755	0.0171	0.7
0.95	12.5	217	0.1310	0.1561	4.1	0.1305	0.0926	3.3	0.1655	0.0281	1.5
0.93	11.6	156	0.1194	0.1689	5.5	0.1179	0.1068	4.9	0.1560	0.0391	2.7
0.90	10.6	110	0.1075	0.1824	7.6	0.1050	0.1215	7.1	0.1440	0.0530	4.8
0.87	9.8	85.2	0.0985	0.1931	9.8	0.0959	0.1323	9.4	0.1337	0.0656	7.4
0.85	9.3	73.9	0.0935	0.1987	11.2	0.0910	0.1378	10.8	0.1275	0.0729	9.3
0.82	8.7	61.6	0.0869	0.2066	13.5	0.0849	0.1450	12.9	0.1193	0.0831	12.3
0.80	8.3	55.4	0.0831	0.2111	15.1	0.0814	0.1492	14.3	0.1140	0.0897	14.6
0.75	7.6	44.1	0.0752	0.2207	19.0	0.0737	0.1586	18.1	0.1040	0.1023	19.7
0.70	7.0	36.4	0.0688	0.2286	22.9	0.0671	0.1668	22.3	0.0955	0.1132	25.1
0.65	6.5	30.8	0.0631	0.2357	27.2	0.0613	0.1742	26.7	0.0880	0.1230	31.0
0.60	6.0	26.5	0.0581	0.2418	31.5	0.0561	0.1807	31.2	0.0816	0.1311	36.7
0.55	5.6	23.2	0.0537	0.2475	36.0	0.0515	0.1867	36.1	0.0760	0.1386	42.7
0.50	5.3	20.4	0.0495	0.2527	40.8	0.0470	0.1924	41.3	0.0710	0.1448	48.4
0.45	4.9	18.1	0.0452	0.2583	46.7	0.0430	0.1974	46.6	0.0660	0.1513	55.2
0.40	4.7	16.1	0.0414	0.2637	53.0	0.0391	0.2030	53.1	0.0610	0.1586	63.8
0.35	4.4	14.4	0.0378	0.2682	58.9	0.0356	0.2073	58.8	0.0560	0.1654	72.7
0.30	4.0	12.7	0.0342	0.2715	63.8	0.0321	0.2105	63.4	0.0510	0.1708	80.6

Table II.6. KCC-analysis, slit-like pores. (Part of "computer-worksheet").

SLITS			0.5 (S)			0.4 (S)			0.4 (RT)		
Humidity	t-thickness	Pore radius (= half width)	Water content from isotherm	Cumulative pore volume	Cumulative pore surface	Water content from isotherm	Cumulative pore volume	Cumulative pore surface	Water content from isotherm	Cumulative pore volume	Cumulative pore surface
p/p_s	t (Å)	R (Å)	w (cm^3/g)	V (cm^3/g)	S (m^2/g)	w (cm^3/g)	V (cm^3/g)	S (m^2/g)	w (cm^3/g)	V (cm^3/g)	S (m^2/g)
1.00	18.2	∞	0.2820	0	0	0.2190	0	0	0.1920	0	0
0.99	17.2	539	0.1973	0.0862	0.9	0.1879	0.0316	0.3	0.1860	0.0061	0.2
0.98	14.8	274	0.1663	0.1186	1.8	0.1657	0.0549	1.0	0.1806	0.0117	0.5
0.97	13.5	186	0.1497	0.1359	2.6	0.1504	0.0710	1.7	0.1755	0.0171	0.7
0.95	12.5	115	0.1310	0.1560	4.0	0.1305	0.0926	3.2	0.1655	0.0283	1.4
0.93	11.6	83.9	0.1194	0.1688	5.3	0.1179	0.1066	4.7	0.1560	0.0390	2.5
0.90	10.6	60.4	0.1075	0.1822	7.2	0.1050	0.1212	6.7	0.1440	0.0528	4.5
0.87	9.8	47.5	0.0985	0.1928	9.1	0.0959	0.1320	8.7	0.1337	0.0653	6.8
0.85	9.3	41.6	0.0935	0.1983	10.4	0.0910	0.1374	9.9	0.1275	0.0725	8.5
0.82	8.7	35.1	0.0869	0.2060	12.4	0.0849	0.1444	11.8	0.1193	0.0825	11.1
0.80	8.3	31.8	0.0831	0.2105	13.7	0.0814	0.1486	13.0	0.1140	0.0890	13.0
0.75	7.6	25.8	0.0752	0.2198	17.0	0.0737	0.1577	16.2	0.1040	0.1012	17.3
0.70	7.0	21.7	0.0688	0.2275	20.2	0.0671	0.1657	19.6	0.0955	0.1118	21.8
0.65	6.5	18.7	0.0631	0.2344	23.7	0.0613	0.1728	23.1	0.0880	0.1213	26.5
0.60	6.0	16.3	0.0581	0.2403	27.1	0.0561	0.1790	26.7	0.0816	0.1291	31.0
0.55	5.6	14.4	0.0537	0.2457	30.6	0.0515	0.1848	30.5	0.0760	0.1362	35.6
0.50	5.3	12.8	0.0495	0.2506	34.2	0.0470	0.1902	34.5	0.0710	0.1421	40.0
0.45	4.9	11.5	0.0452	0.2559	38.6	0.0430	0.1950	38.4	0.0660	0.1483	45.1
0.40	4.7	10.4	0.0414	0.2609	43.2	0.0391	0.2002	43.2	0.0610	0.1551	51.3
0.35	4.4	9.4	0.0378	0.2651	47.5	0.0356	0.2043	47.3	0.0560	0.1615	57.7
0.30	4.0	8.3	0.0342	0.2684	51.1	0.0321	0.2073	50.7	0.0510	0.1666	63.5

The actual adsorption isotherms were analysed in the way described, assuming slit-like as well as circularly cylindrical pores. Tables II.5 and II.6 are part of the "computer-worksheets", showing the accumulation of pore volume and pore surface. Table II.7 summarizes the accumulated volumes and surface areas of the two pore models. The table also includes the computed length average pore radius in the case of cylindrical pores, and the total surface areas computed from the V-t plots.

Table II.7. KCC analysis results.

Specimen designation	Pore model	Accumul. volume cm^3/g dry wt	Porosity ε_w (table II.2) cm^3/g dry wt	Accumul. surface m^2/g	Surface from V-t plot m^2/g	S_{BET} m^2/g	Length average pore rad. Å
0.5 (S)	CYL.	0.272	0.282	64	84	103	26
	SLITS	0.268		51			-
0.4 (S)	CYL	0.210	0.219	63	80	96	26
	SLITS	0.207		51			-
0.4 (RT)	CYL.	0.171	0.192	80	126	151	24
	SLITS	0.167		64			-

We see that the length average pore radius is about 6 times greater than $\hat{t}$ = 4Å (cf. section II.4.1.2). A condition for the cylinder model to be consistent with the existence of an initial linear portion of the V-t plot is that R is much greater than $\hat{t}$.

Table II.7 also shows that the accumulated volumes agree with the total porosities within acceptable limits, i.e. the volume closure condition is satisfied. The surface closure condition for the KCC analysis requires that the accumulated surface is equal to the surface computed from the V-t plot. This condition is clearly not satisfied, since the accumulated surface areas are appreciably less than the V-t surfaces and much smaller than the BET-surfaces. Theoretically, the final choice of a pore model could be made with reference to the surface closure condition. However, both the cylinder and the slit models are far from able to account for the actual surface area, although the cylinder model accumulates a higher surface area than the slit model.

The volume cumulative distribution functions are shown in fig. II.11. Fig. II.12 presents the differential distribution curves as plots of $\Delta V/\Delta \ln R$ versus $\ln R$. This logarithmic form has been chosen because a large range of pore radii is covered more clearly than on a linear plot; using $\Delta V/\Delta \ln R$ as the ordinate makes the area under the curve represent pore volumes directly. The diagrams include pore sizes up to $R \approx 2100$ Å ($h \approx 0.995$). Due to the form of eq. (II.8), the humidity intervals have to be made increasingly small as the saturation point ($h = 1$) is approached, in order to achieve a reasonable resolution of the mean pore radii. In this range the adsorption isotherms are steep, and thus comparatively ill-defined which makes a fine subdivision meaningless. This problem, however, does not affect the portion of the curves at lower humidities.

II.4.1.5. Discussion

The paste used for sorption measurements were 8 and 4 months old. The progressing hydration of water cured specimens changes the shape of the isotherm, so that the evaporable water content increases at intermediate humidities, and decreases near saturation. Powers and Brownyard (1946) reported isotherms for room temperature cured cement pastes hydrated for periods from 7 days to six months. At least from 3 months age and onwards, the isotherms changed very little. This implies that our specimens can all be regarded as mature pastes.

The isotherms (fig. II.7) show that all of the three specimen types exhibit sorption hysteresis over the entire humidity range, which is in line with the great majority of published sorption isotherms for the system hcp + water. However, Hagymassy et al. (1972) reported sorption isotherms of hardened cement paste of $w/c = 0.40$, 0.45 and 0.70 with closed, and very small, hysteresis loops; the $w/c = 0.40$ paste even with practically no identifiable hysteresis at all. Hagymassy et al. argued that the contrasting results obtained by other investigators were due to the fact that they had not waited long enough to attain equilibrium. Using an experimental method similar to the one employed in the present work, they found the necessary time to equilibrium to be 2-3 weeks at adsorption, and 4-5 months

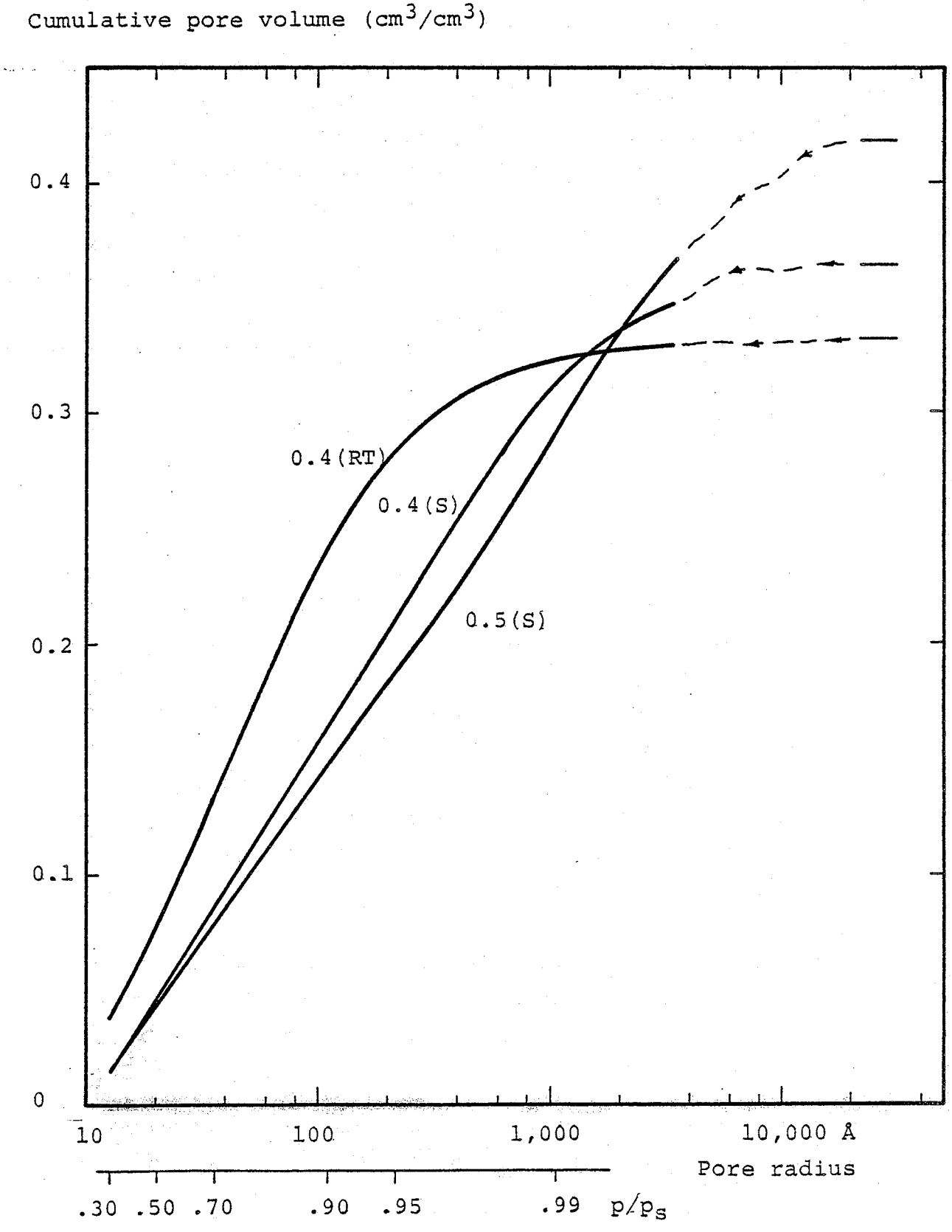

Fig. II.11. Volume cumulative distribution functions. Computed from adsorption isotherms.

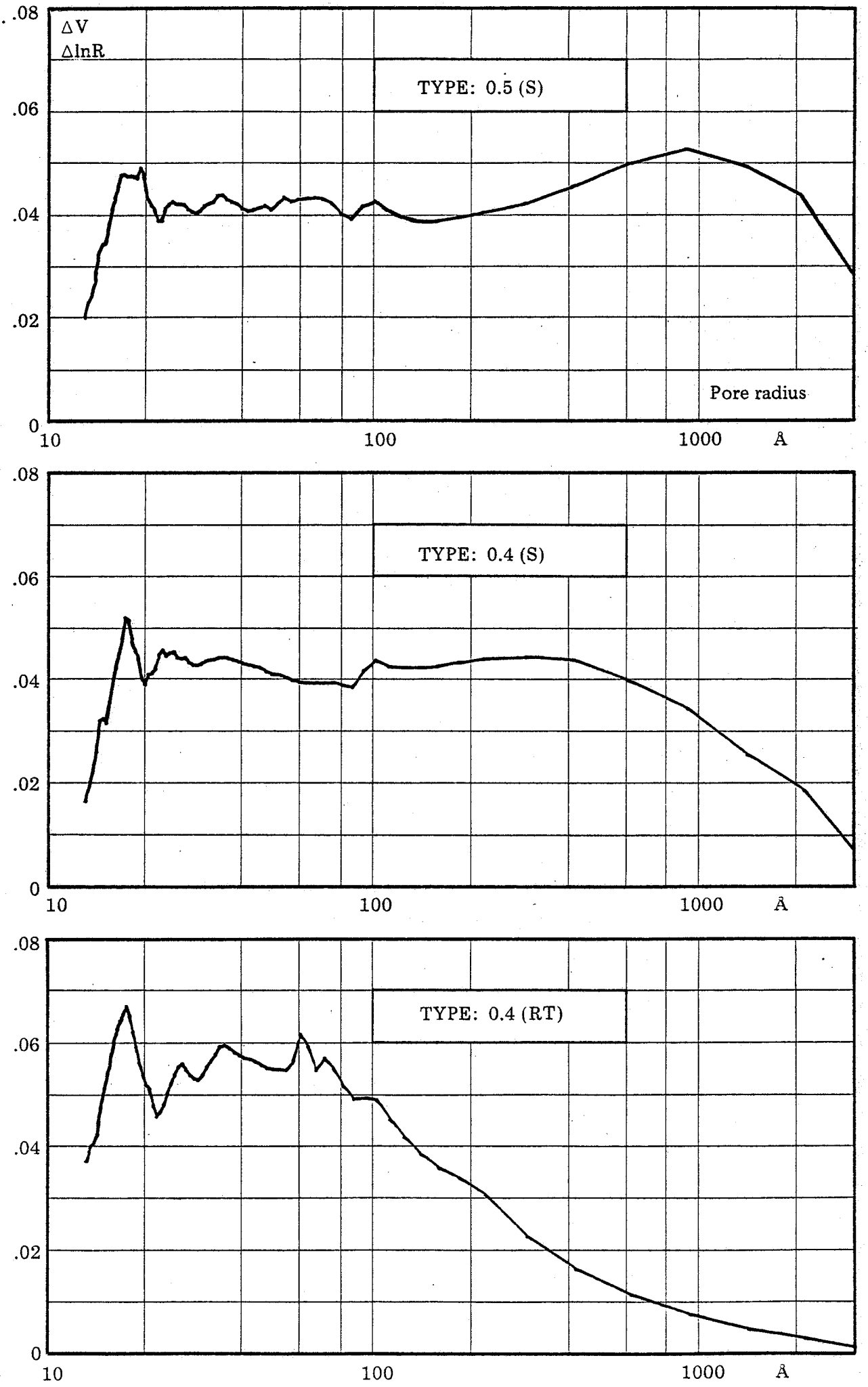

Fig. II. 12 Volume pore size distribution functions.
Computed from adsorption isotherms

at desorption. Our experiments extended to about 4 weeks and 7 months, respectively (fig. II.5), without yielding any tendency of closed loops.

The adsorption isotherms for the two steam cured specimens are practically identical in the entire humidity range up to a point very close to saturation. The isotherm of the 0.4 (RT) sample differ from these by showing a larger content of evaporable water at all humidities except those close to saturation. This qualitative difference in isotherm shapes between pastes hydrated at different temperatures has been recognized by several investigators. Sellevold (1969) presented quite extensive work regarding the influence of curing conditions on the microstructure of hcp. Among Sellevold's results are sorption data for a cement paste of w/c = 0.4, cured 14 days in lime water at 100 ^{o}C. The adsorption isotherm of this specimen shows significantly higher contents of evaporable water than the 0.4 (S) isotherm of the present work. Our isotherm can also be compared with data published by Hastrup (1976) for a w/c = 0.4 paste, steam cured at 97 ^{o}C for 10 days. These results show lower adsorption at all humidities. Thus the adsorption isotherm is apparently very sensitive to the exact details of the curing history.

The differences between the adsorption isotherms belonging to our three specimen types are reflected in the internal surface area and the pore size distribution derived from these. As it is generally found, the internal surface area is considerably smaller for the steam cured pastes compared with the one cured at room temperature (table II.4). This is in accord with the fact that steam curing produces a coarser pore structure, as is also demonstrated by the pore size distributions plotted in figs. II.11. and II.12.

The t-method of pore structure analysis is clearly very sensitive to the accuracy of the t-curve used, since the analysis is centered on the V-t plot. In the present case, the V-t plots indicated that all pores are filled by capillary condensation, and further use of the t-method was limited to establishing the lower limit of pore sizes encountered in the subsequent KCC-analysis. However, the correctness of the t-curve also influences the results of the KCC analysis, most pronounced in the small

radius end of the distribution. The two pore models investigated, slit-like and circularly cylindrical pores, both satisfied the volume closure condition within acceptable limits. None of these two models, however, were able to provide surface closure.

II.4.2. Mercury Intrusion Porosimetry (MIP)

II.4.2.1. General

As we have seen in the preceding sections, KCC analysis for determining pore size distribution suffer from severe limitations as regards the distribution of large pores. As a means for studying the large pore region of the distribution, already about 1920 it was suggested by Washburn and Co-workers to utilize the phenomenon of capillary depression (see for instance review by Scholten (1967)). The Young and Laplace equation (Gregg and Sing (1967))

$$\Delta p = \sigma(1/r_1 + 1/r_2) \qquad \text{(II.16)}$$

relates the pressure difference Δp across a curved interface to the interfacial tension σ and the interface geometry, expressed by the principal radii of curvature r_1 and r_2. When the interface is that between air and a liquid contained in a solid which it does not wet, i.e. the contact angle $\theta > 90^{\circ}$, we get by reference to fig. II.13 for a circularly cylindrical pore of radius R

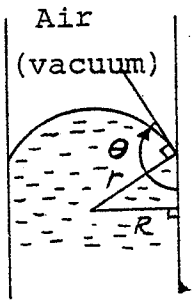

Fig. II.13. Capillary depression of a non-wetting liquid in a pore.

$$r_1 = r_2 = r = \frac{R}{\cos\theta}$$

$$\Delta P = P_{liq} - P_{air} = \frac{2\sigma\cos\theta}{R} \qquad \text{(II.17)}$$

For a slit-shaped pore of width 2R (fig. II.13), we get correspondingly

$$r_1 = r = \frac{R}{\cos\theta}$$

$$r_2 = \infty$$

$$\Delta P = P_{liq} - P_{air} = \frac{\sigma\cos\theta}{R} \qquad \text{(II.18)}$$

Consequently, pore size distributions in the form of (complementary) cumulative distribution functions can in principle be measured directly by forcing a non-wetting liquid into a porous specimen and measure the penetrating quantity as a function of the pressure applied. Measurements normally start in vacuo, making $P_{air} = 0$.

Mercury is the most widely used liquid for this type of measurement. It is nonwetting for most kinds of surfaces; in addition, it does not react with most non-metal solids, and it has a low vapour pressure.

A survey of the mercury intrusion porosimetry method of pore structure analysis as applied to cement systems was first given by Winslow and Diamond (1970). This work includes results on cement pastes of varying ages and water/cement ratios. Also, the contact angle was measured as a function of the drying procedure. For P-dried paste, Winslow and Diamond measured a contact angle of 130^{o}, and 117^{o} for oven-dried paste.

II.4.2.2. Apparatus

The mercury porosimeter used was a commercially available apparatus (Micromeritics Instrument Corporation, Norcross, Georgia), capable of exerting a pressure of 50,000 psi.

The sample to be investigated is contained in a glass sample cell as depicted in fig. II.14. It consists of two pieces: the part which contains the sample, and the cap with a precision bore tube constituting the pentrometer. A sample of maximum 4 cm^3 volume, 8 mm diameter, and 36 mm length is placed in the sample space of the holder part, which is then assembled to the cap through a greased ground joint. Hereafter the cell is installed in the pressuring chamber of the porosimeter.

The pressuring chamber, and thereby the sample, can then be evacuated to remove adsorbed gases and vapours from the sample. Hereafter mercury is admitted to the chamber to overflow into the sample cell and thereby fill the cell and surround the sample. The excess mercury is then drained away from the pressuring

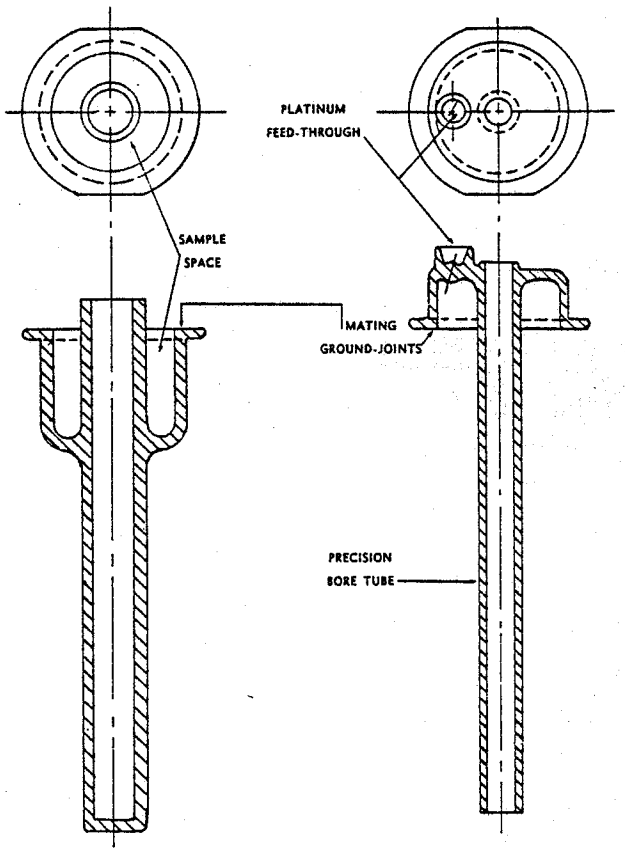

Fig. II.14. MIP sample cell

chamber and replaced by hydraulic fluid.

Pressure applied hydraulically now forces the mercury into voids and pores of the sample, causing the mercury level in the precision bore tube to decrease. This decrease in the mercury level is proportional to the penetrated volume, and is followed and recorded automatically by a probe mechanism. Increasing the pressure stepwise, and reading off the penetrated volume after each step comprises the results of a mercury porosimetry experiment.

The analysis procedure described above is the one given by the manufacturer of the instrument. Following this, however, we soon experienced certain short comings associated with the initial filling of the sample cell with mercury. We concluded that successful measurements could be performed only if the sample cell was filled with mercury under high vacuum and in clean surroundings (free from traces of hydraulic fluid), while being visually observed. Accordingly we constructed a glass apparatus for that purpose, fig. II.15.

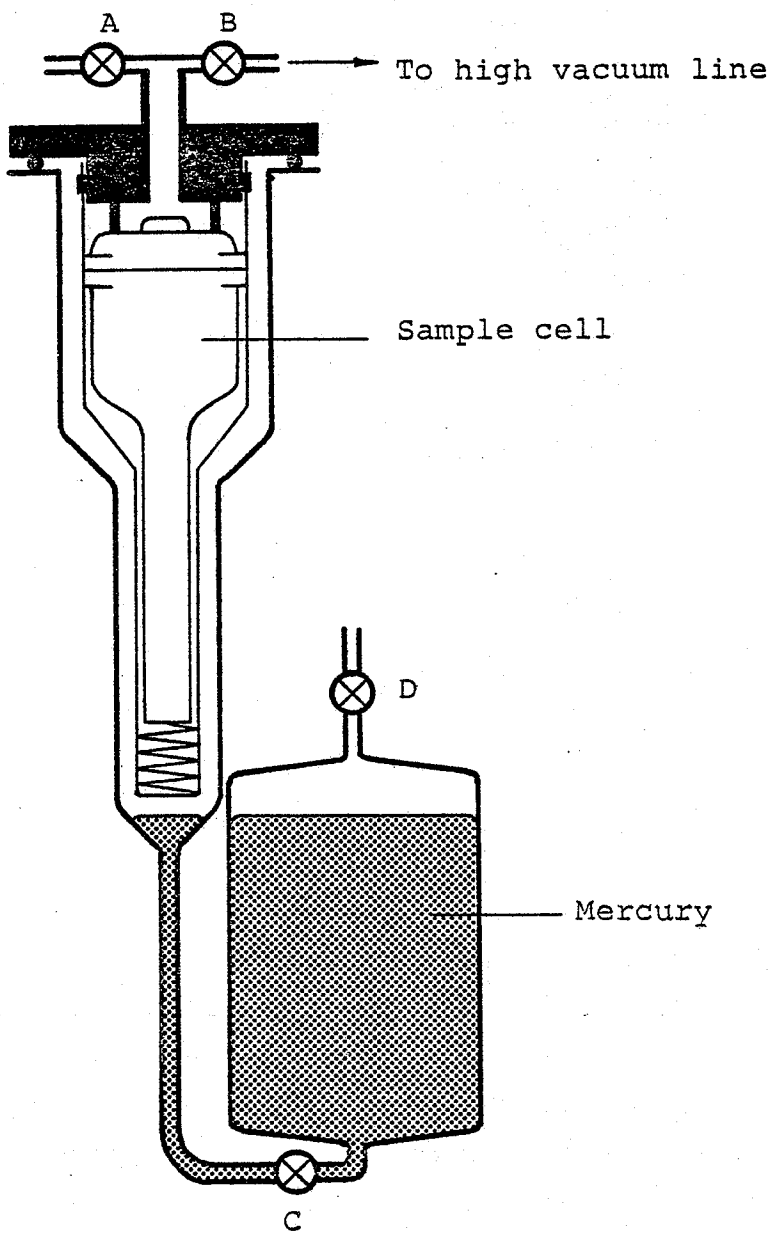

Fig. II.15. Apparatus for filling the MIP sample cell.

This device was attached to a high vacuum system. With stopcocks A and C closed, B open, the sample could be effectively evacuated prior to filling the cell with mercury. Also, by attaching the tube at D to the vacuum line, the mercury could be degassed before use. By closing cock B and opening C (D open to the atmosphere), mercury was allowed to rise around the sample cell and overflow into it, until the cell was filled. At this stage stopcock C was closed, and the mercury container was evacuated through D. Now closing D and opening C caused the excess mercury to drain back into the container while the vacuum around the cell was maintained. Hereafter we were able to visually follow what happened when the pressure around the cell was increased to 1 atm. when stopcock A was slowly opened. Inspection of that stage revealed the cause of some of the difficulties we had experienced when performing the filling process using the commercial apparatus. Sometimes the grease joint in the sample cell broke, and considerable amounts of air penetrated into the sample space. During the following run under high pressures in the commercial apparatus, air pockets in the sample space would introduce error in the test results. In addition, hydraulic fluid may penetrate through the broken grease joint and further disturb the results. We solved this problem by simply using a stiffer grease (Apiezon H) than that supplied with the instrument (Apiezon M).

After the sample cell had been filled with mercury using the glass filling device, the cell was transferred to the commercial apparatus for a run from 1 atm. to 50,000 psi.

II.4.2.3. Experimental

The specimens used in the MIP-experiments were about 7 months old. The hardened paste was crushed to powder in the size range 149-250 μm like the specimens used for sorption experiments (section II.4.1.3), and P-dried prior to use. The sample size was ca. 4 g.

The P-dried sample was poured into the sample cell, which was then assembled and placed in the glass filling device, and exposed to a high vacuum over night (which in fact may have dis-

turbed the P-dry state, as discussed later. After a successful filling of the cell with mercury it was transferred to the commercial apparatus.

The experiments were normally started at about 25 psi pressure, and extended to the limiting pressure of the apparatus, 50,000 psi. Two independent experiments were performed for each specimen type.

The raw result of an experiment - the pressure versus penetration relationship - must be subjected to certain corrections. The pressures encountered are large enough to make a compensation for the compressibility of the system necessary. Therefore so-called blank run results were obtained with the sample cell containing only mercury. Also, the interpretation of the results within the low pressure range can be somewhat ambiguous. The problem is that mercury penetration between the individual powder particles cannot always be distinguished from mercury intrusion into the large pores.

In order to investigate the interparticle penetration, a few additional experiments were performed using non-porous glass powder ground and sieved in the same manner as the HCP specimens. The sample size was ca. 7.5 g which corresponds to a particle volume similar to that of the HCP samples.

Finally, another potential source of error should be mentioned. During compression some heat evolves which causes the temperature within the pressure vessel to rise. Due to the subsequent thermal expansion of the mercury, readings of the intruded volume may be too small immediately after the pressure has been increased. In particular at the highest pressures we found it necessary to wait up to 30 minutes for a constant reading.

II.4.2.4. Results

The results from the blank run and glass powder experiments are plotted in fig. II.16 as apparently intruded volume versus the pressure applied. The two blank runs (sample cell containing only mercury) show almost identical results. Also, there seems to be a very nearly linear dependence of pressure on apparent

intrusion during compression of the system.

The glass powder was obtained by crushing a piece of non-porous glass, and sieving off the particle fraction used for the hcp samples. Results from the three experiments are very similar up to a pressure of about 10,000 psi. The difference between the

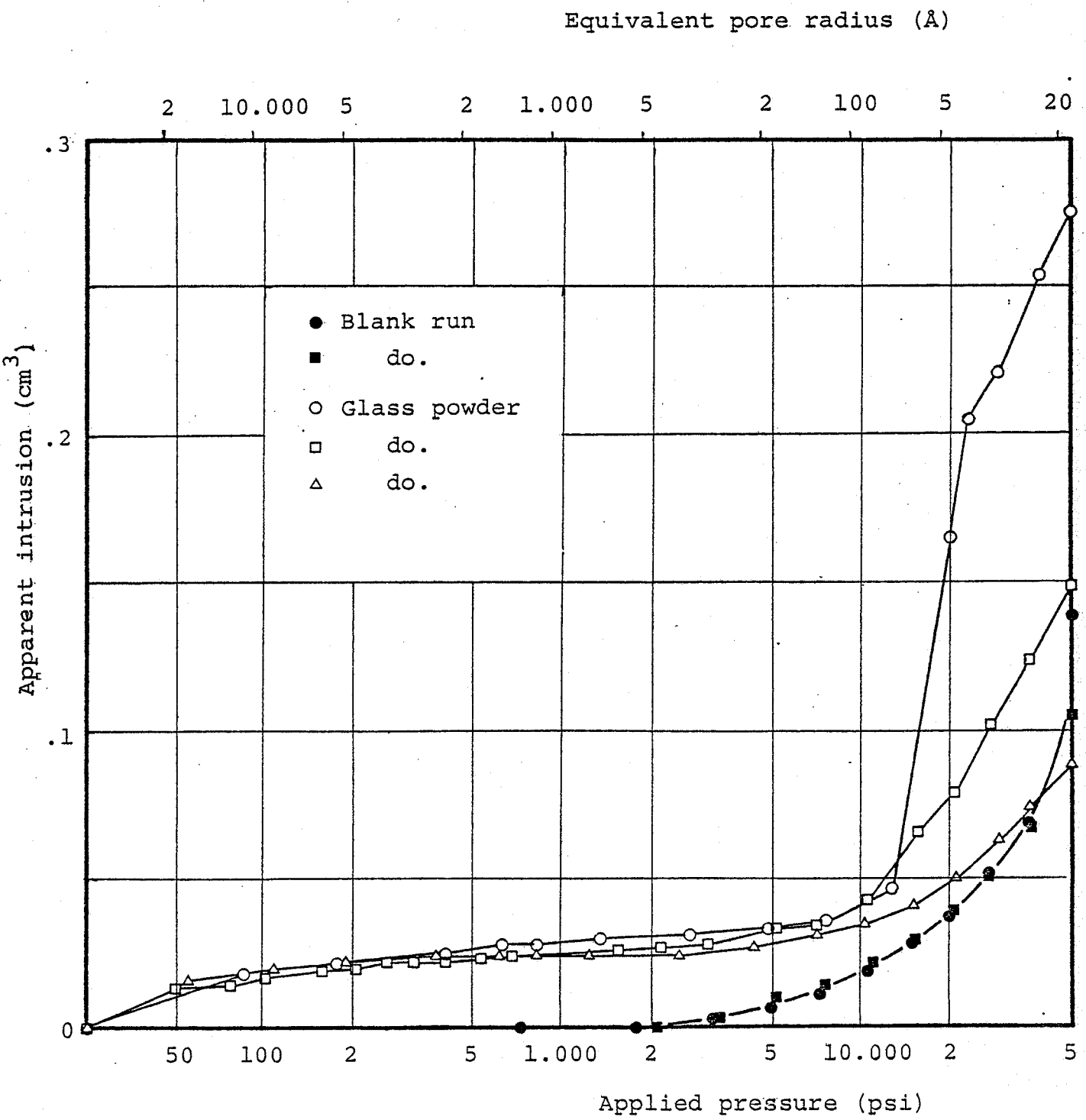

Fig. II.16. Results of blank runs and glass powder experiments.

curves from this pressure up to 50,000 psi may be due to the presence of cracks in the powder particles. The lower of the three curves shows an apparent intrusion in the range 2,000 to 50,000 psi which is smaller than that observed for the blank runs. Since the apparently intruded volume in that range is an approximately linear function of applied pressure, this observation is interpreted as the result of compressing a system where part of the mercury is replaced by (crack-free) glass particles.

The most important outcome of the glass powder experiments is the observation that the slope of the curves is very small at the lower pressures. Thus, for the glass powder at least, interparticle penetration is small. Although the distribution and shape of voids between the granules may be somewhat different for glass compared to hcp, these results give a rough estimate of the interparticle penetration part of the MIP curves for hcp.

Porosimetry results for the hcp samples are plotted in fig. II.17 as percentage of the total pore volume which resides in pores greater than a given radius. The "total pore volume" is defined by reference to the water porosity (table II.2). Assuming circularly cylindrical pores, the radius R of pores intruded at the pressure p is obtained from equation (II.17)

Following Winslow and Diamond (1970), for mercury intruding into P-dried HCP, we have assumed:

$$\theta = 130^{o},\ \sigma = 484 \text{ dynes/cm}$$

$$\text{Hence,}\quad R(\text{Å}) = 9.028 \times 10^{5}/p \text{ (psi)}$$

Two experiments were performed for each specimen type, as illustrated in fig. II.17 by open and full symbols. As it is usual for this sort of measurement, we observe good reproducibility.

The results shown in fig. II.17 are corrected for compressibility of the system by using blank run results. In order to illustrate the magnitude of correction, blank run results are sketched in the same figure, as well as results from the glass pow-

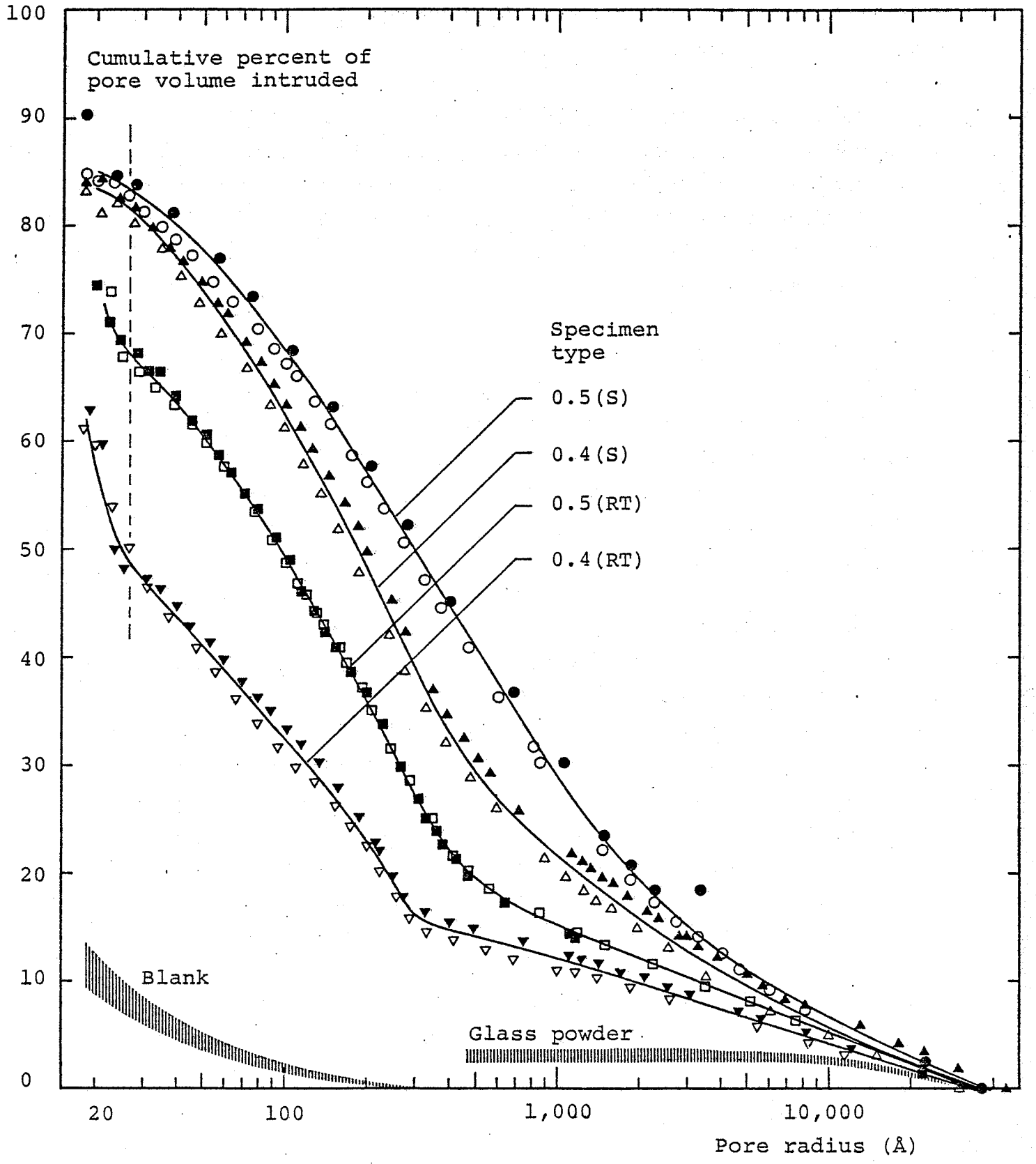

Fig. II.17. Volume (complementary) cumulative distribution functions of HCP obtained by mercury intrusion porosimetry.

der experiments. The latter forms a basis for separating intrusion between individual grains from the intrusion into hcp. The data suggest that interparticle penetration is negligible at pressures corresponding to pore radii less than about 10,000 Å.

According to eq. (II.17), the computed radius corresponding to a given intrusion pressure depends linearly on the cosine of the assumed contact angle. Diamond (1970) measured contact angles for P-dried paste (130°) and oven-dried paste (117°), and estimated a contact angle of 126° for D-dried hcp. The effect of assuming a contact angle less than 130° is to shift the curves in fig. II.17 to the left. In the case of oven-drying the horizontal movement would correspond to a factor of 1.42 in the case of oven-drying, and 1.09 in the case of D-drying. As we noted earlier, the pressure after the over-night evacuation of our previously P-dried specimens may in fact have been less than 8×10^{-3} torr. However, the resulting drying is presumably closer to D-drying than to oven-drying, which makes the error negligible.

The curves for the RT-cured specimens exhibit a sudden upturn at the highest pressures (smallest radii). We suspect this to be an artifact, perhaps caused by local crushing in the samples. In chapter IV we shall make use of the pore volume of hcp presented to mercury, in connection with the flow of water vapour through hcp. For that purpose we have included data only up to a pressure corresponding to R = 25 Å to secure that the upturn part of the cumulative distribution curves at the highest pressures is excluded. The MIP results are presented as volume (cm^3/cm^3) complementary cumulative distribution curves in fig. II.18 (together with results from the sorption experiments).

The volume pore size distribution functions are presented in fig. II.19 as plots of $\Delta V/\Delta \ln R$ versus $\ln R$. For comparison fig. II.19 also includes data from the sorption experiments.

II.4.2.5 Discussion

The (complementary) cumulative distribution curves in fig. II.15 show the same general characteristics as found by most other investigators using mercury intrusion porosimetry on hardened cement paste.

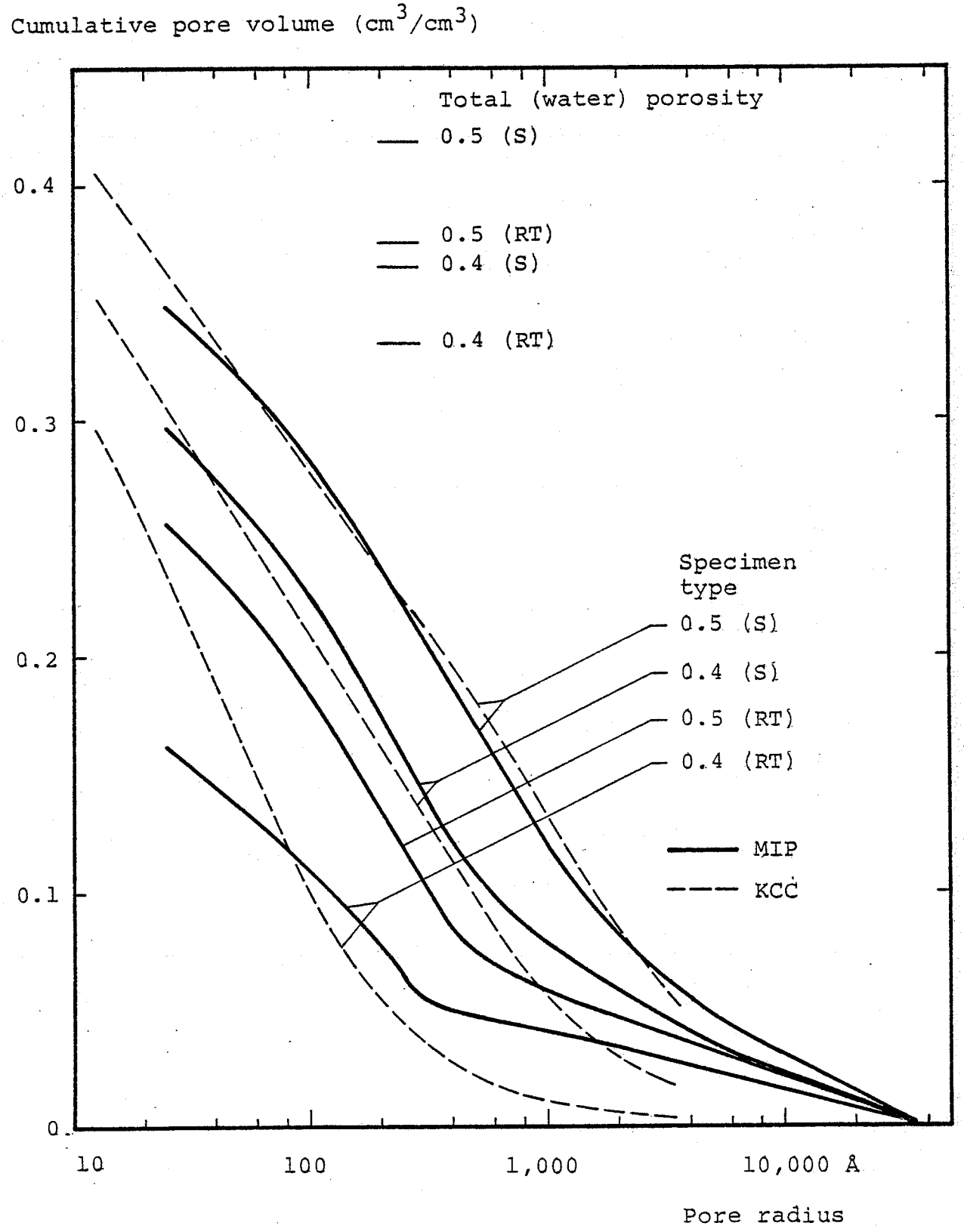

Fig. II.18. Volume (complementary) cumulative distribution functions derived from mercury intrusion porosimetry (full lines) and adsorption data (broken lines).

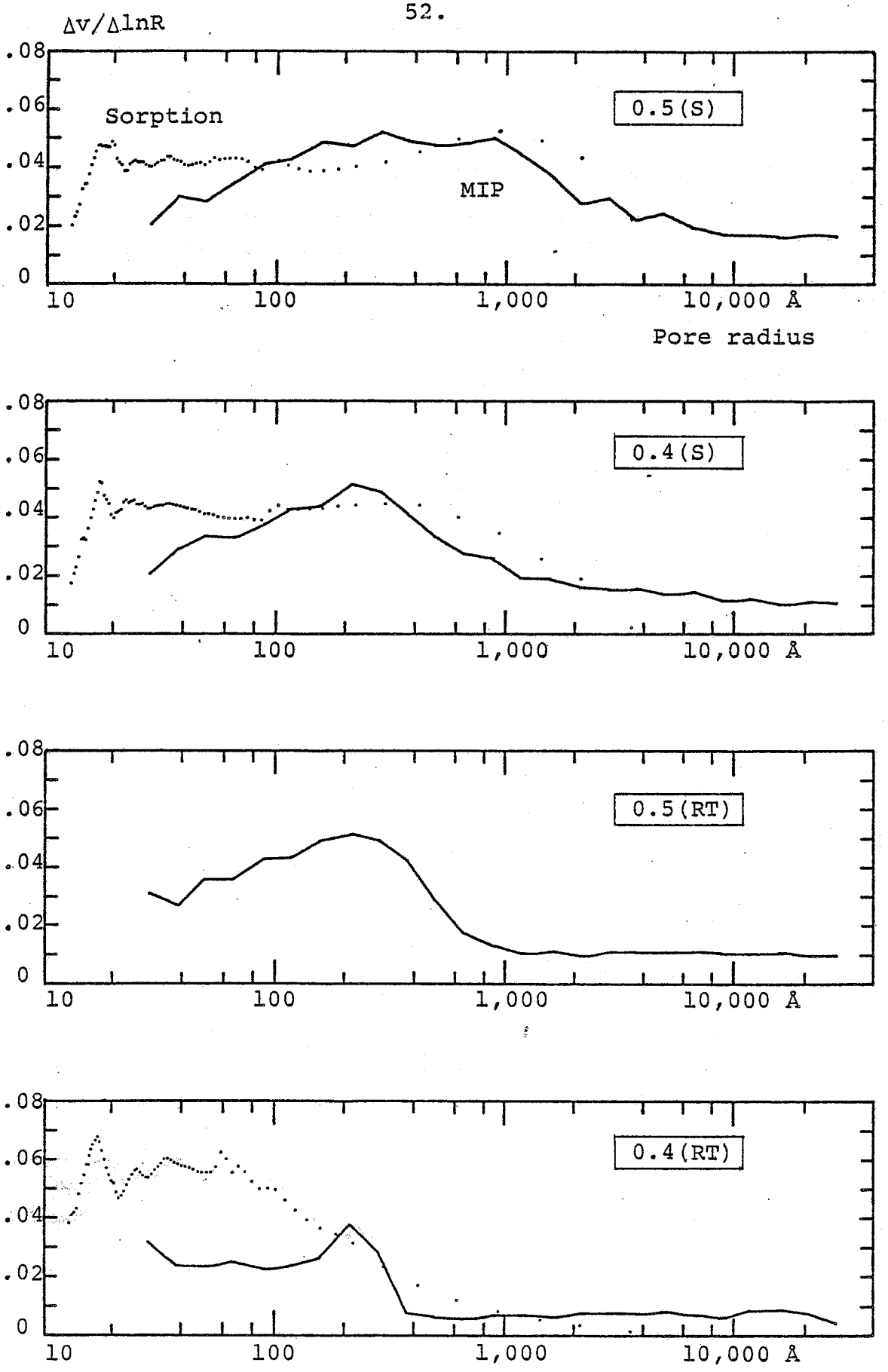

Fig. II.19. Volume pore size distribution functions. Computed from mercury intrusion porosimetry (MIP) data (lines) and adsorption isotherms (dots).

The curve for the densest sample - 0.4 (RT) - displays a so-called "Threshold radius" of about 300 Å, immediately below which a comparatively great portion of the intrusion commences. The treshold radius was interpreted by Winslow and Diamond (1970) as representing the minimum radius of pores which are geometrically continuous throughout all regions of the hydrated cement paste. Pores of greater radii are present, but are only available to penetration from the exterior as long as the pressure has not exceeded the "threshold pressure". Above the threshold pressure, however, interior pores with radii greater than the threshold radius, but with narrow entryways, can be intruded, producing an upturn of the distribution curve. The presence of such "ink-bottle" shaped pores - wider pores with narrower entryways - has the general effect of overestimating the volume belonging to small pores, since an ink-bottle pore will be tallied at the pressure where its entryway is intruded.

Sellevold (1974), and Bager and Sellevold (1975) provided supporting evidence for this interpretation of the experimental data. In their work, Bager and Sellevold measured mercury intrusion of hcp samples in different particle size ranges and found a systematic increase in the apparent content of large pores with decreasing particle size. As the cumulative curves flattened out in the large pore radius range, the threshold radius became less well defined, which should be expected according to Winslow and Diamond's interpretation.

A consequence of this view is that a finer powder measures a pore size distribution closer to the "true" one. As the powder becomes finer, however, the problem of separating pore space from interparticle space increases. In the present work, powder in the size range 149-250 μm was used, and experiments with non-porous glass powder of similar size demonstrated that interparticle penetration below ca. 10,000 Å was negligible or nil.

As pointed out by Bager and Sellevold (1975), results of MIP studies reported by different authors are different in two respects. One is the value of the threshold radius, which is apparently very sensitive to the details of the specimen preparation. The second difference concerns the existence of pores in the radius range below $\sim$ 50 Å. Auskern and Horn (1973) found very few

pores in this range - their cumulative curves flattened out at the highest pressures. The cumulative curves obtained in the present work are in line with those obtained by Bager and Sellevold in these two respects.

As mentioned earlier, the cumulative curve for the 0.4 (RT) sample shows clearly the presence of a threshold radius about 300 Å. For the 0.5 (RT) sample a threshold radius is also distinguishable, about 450 Å, whereas the steam cured specimens show distribution curves of more gradual slope, suggesting that these specimen types contain a greater portion of large continuous pores.

Both the cumulative distribution curves (figs. II.17 and II.18), and the differential distribution functions (fig. II.19) demonstrate that steam curing produces a coarser pore structure than does curing at room temperature, this tendency being most pronounced for the w/c = 0.4 paste. This observation is in accord with similar results reported by Sellevold (1974) concerning hcp of w/c = 0.35 and 0.45. These changes of the pore structure, taking place as a consequence of the higher hydration temperature, also cause a considerable variation in the total amount of intruded mercury (down to 25 Å pore radius), expressed as percent of the total pore volume measured by water. The densest one of the RT cured pastes (w/c = 0.4) is intruded about 50%, and the w/c = 0.5 paste about 69%, while the steam cured samples 0.4 (S) and 0.5 (S) show higher, and nearly identical, degrees of intrusion - 82% and 84% respectively.

The volume of mercury intrusion at R = 25 Å could be denoted the "mercury porosity". Inspection of fig. II.18, which contains both water and MIP porosities, reveals that in addition to being smaller than the water porosities, the MIP porosities occur in a different order of sequence among the 4 specimen types.

II.4.3. Comparison between pore size distributions obtained from sorption isotherms and from mercury intrusion porosimetry

Pore size distributions obtained from sorption isotherms are ill-defined in the large radius region of the distribution. This region is fairly well described by MIP measurement, whereas this

method does not include so small pores as the isotherm (KCC) method. Potentially, the two methods should therefore be complementary to one another.

Diamond (1971) critically compared the two methods and demonstrated that while there seems to be reasonable agreement between pore size distributions obtained from MIP and KCC in the region of overlap for a number of porous materials, this is apparently not the case for (room temperature cured) hcp. Diamond found that the mercury intrusion method indicates that the entire distribution is much coarser than KCC results suggest.

In the present work, comparison of the two methods can be made directly from measurement on the same samples, which was not the case in Diamond's analysis. Our results are shown as volume cumulative distribution in fig. II.18, and as (differential) pore size distributions in fig. II.19. For the two steam cured pastes, we actually find a reasonable agreement in the "common region" of MIP and KCC (ca. 25 - 800 Å), whereas the results for the RT-cured specimen confirms Diamond's observation that the MIP-distribution is coarser than the KCC-distribution. In this context we should recall that the MIP-distributions in fig. II.18 are upper bound curves, due to the ink bottle effect. MIP consistently overemphasizes the relative importance of small pores, if anything.

One of the difficulties in comparing the two sets of curves is associated with the "missing" pore volume of the MIP analysis, i.e. that only part of the pore volume seen by water is intruded by mercury. The most straight forward assumptions are that the missing volume resides 1) in pores smaller than the minimum pore size intrudable at the maximum mercury pressure, or 2) in regions with very small entryways, but with pore size distributions similar to those of the intruded sample volume. Following the first assumption, the MIP curves in fig. II.18 should be extended into the region of pore radii less than 25 Å to reach total pore volumes equal to the water porosities. The upturn of the cumulative curves in fig. II.17 for the RT-cured pastes below R = 25 Å would justify at least part of such an extension, if that upturn is not ascribed to local crushing in the sample.

On the other hand, the first assumption implies that no ink-bottle effects are present, which does not comply with the existence of threshold pressures. Also, the upturn of the curves in the fine end of the distribution would fit the second assumption when interpreted as the result of local crushing. Following the latter assumption, the MIP curves should be in some way strained vertically to reach the water porosities.

While noting that there is a fair agreement between the pore size distributions for the steam cured pastes as obtained from MIP and from adsorption experiments in the common range of these two methods, we should remember that both methods are based on a simple assumed pore geometry (circularly cylindrical pores) which is far from being a realistic model of the pore structure (cf. chapter I). However, such results can be important indicators of certain aspects of the pore structure. In chapter IV we shall make use of the pore size distribution data for analysing water vapour permeability results in relation to pore structure.

III. WATER VAPOUR PERMEABILITY

The subjects discussed in this chapter are concerned with various aspects of water transport in hardened cement paste and related materials. Apart from describing measurements and results within the scope of the actual project, the chapter includes reviews of the relevant literature.

III.1. Terminology

The flow of water through a microporous substance is commonly referred to as "diffusion" or as "permeability-flow" of water in the material. Usually the term diffusion is used to characterize flow in a concentration gradient, while permeability is used in connection with flow in a pressure gradient.

In a microporous substance such as hardened cement paste, water transmission is the result of several combined flow mechanisms, even at constant total pressure. Water vapour flows in a partial pressure gradient (equivalent to a concentration gradient), adsorbed water flows in a surface concentration gradient, and capillary condensed water flows in a pressure gradient (basically, of course, all flow is in a free energy gradient). Thus, transport of moisture (water vapour) from one face of the material to another, strictly cannot be characterized solely by diffusion or by permeability.

In many situations it is convenient to express the overall transport of moisture in terms of humidity differences, i.e. differences in relative water vapour pressure. In that case the overall transport coefficient is adequately referred to as the water vapour permeability.

In this chapter, we shall use the various terms much in accordance with general practice, although this in some cases may not be strictly consistent with the definitions outlined above.

III.2. Phenomenological description of mass transport

The basic laws governing mass transport are Darcy's law and Fick's first law.

Darcy's law is an empirical relationship between the volume of flowing fluid passing unit area per unit time, i.e. the volume flux, and the hydraulic gradient. It may be written

$$q = -B \frac{\partial p}{\partial x} \qquad \text{(III.1)}$$

where
- q = volume flux ($L^3L^{-2}T^{-1}$), or linear flow rate (LT^{-1}) in the x-direction.
- p = pressure in the fluid ($ML^{-1}T^{-2}$)
- B = permeability coefficient ($M^{-1}L^3T$)

If the flowing fluid is compressible, as in gas phase flow, the volume flux is determined not only by B and $\frac{\partial P}{\partial x}$, but is a function of the pressure P as well. This is an inconvenience which can be overcome as follows. Using the equation of state for an ideal gas,

$$p \cdot V = n \cdot R \cdot T, \qquad \text{(III.2)}$$

where
- p = pressure
- V = volume
- n = number of moles
- R = the gas constant
- T = absolute temperature

the mass density ρ of the gas can be expressed as

$$\rho = \frac{nM}{V} = \frac{M}{RT} \cdot p, \qquad \text{(III.3)}$$

where M is the molar weight of the gas. Thus, for an ideal gas at constant temperature the density of the gas is proportional to the pressure. Now, multiplying eq. (III.1) by p,

$$q \cdot p = -K \cdot \frac{\partial p}{\partial x}, \qquad \text{(III.4)}$$

makes the left-hand side proportional to the mass flux, i.e. the rate of mass flowing through unit area, which is independent of pressure. Eq. (III.4) is a new permeability equation in which the flux, in PV-units (MT^{-3}), is determined by $\partial p/\partial x$ and the PV-permeability coefficient $K(L^2T^{-1})$. K is related to B in eq. (III.1) by

$$K = p \cdot B \qquad \text{(III.5)}$$

Eq. (III.1) can also be expressed in terms of mass flux. Multiplying eq. (III.1) by the density of the fluid, ρ, yields

$$J = -\nu \frac{\partial p}{\partial x} \qquad \text{(III.6)}$$

where

J = mass flux in the x-direction ($ML^{-2}T^{-1}$)
ν = mass permeability coefficient (T)
p = (partial) pressure ($ML^{-1}T^{-2}$)

We shall make use of eq. (III.6) later, in connection with the cup method. If the flowing matter can be regarded as an ideal gas, the permeability coefficients in eqs. (III.1), (III.4), and (III.6) are related to one another by

$$B = \frac{1}{p} \cdot K = \frac{1}{p} \cdot \frac{RT}{M}\nu \qquad \text{(III.7)}$$

Fick's first law states that the rate of mass flowing through unit area of a section is proportional to the concentration gradient measured normal to the section,

$$J = -D \frac{\partial c}{\partial x} \qquad \text{(III.8)}$$

where

J = mass flux in the x-direction ($ML^{-2}T^{-1}$)
c = concentration (ML^{-3})
D = diffusion coefficient (L^2T^{-1})

If p in eq. (III.6) denotes the partial pressure of a gas, e.g. water vapour, flowing through a porous material, we can obtain

a relation between D and ν. From eq. (III.6):

$$J = -\nu \frac{\partial p}{\partial x} = -\nu \frac{\partial p}{\partial c} \frac{\partial c}{\partial x}$$

Comparison with (III.8) yields

$$D = \nu \frac{\partial p}{\partial c} \qquad \text{(III.9)}$$

The quantity $\frac{\partial p}{\partial c}$ can be evaluated from the appropriate sorption isotherm by differentiation.

Migration of gas molecules adsorbed on a sorbent surface can be described by an equation analogous to (III.8), viz.

$$J^{\sigma} = -D^{\sigma} \frac{\partial \Gamma}{\partial x} \qquad \text{(III.10)}$$

where

J^{σ} = surface flux ($ML^{-1}T^{-1}$)
D^{σ} = surface diffusion coefficient (ML^{-2})
Γ = surface concentration (ML^{-2})

All of the aforementioned equations are directly applicable to steady state mass transport, i.e. in situations where the concentration (pressure) is a function of the space coordinate only, independently of time. When concentration in a given position changes with time, i.e. under transient conditions, transport is governed by Fick's second law.

Fick's second law is a differential equation of diffusion which may be deduced using Fick's first law (see for instance Crank (1967)). For one-dimensional diffusion (in the x-direction) the equation takes the form

$$\frac{\partial c}{\partial t} = \frac{\partial}{\partial x} \left(D \frac{\partial c}{\partial x} \right), \qquad \text{(III.11)}$$

where t is time (T). If the diffusion coefficient D is independent of concentration, Fick's second law becomes

$$\frac{\partial c}{\partial t} = D \frac{\partial^2 c}{\partial x^2} \qquad \text{(III.12)}$$

Fick's laws are analogous to Fourier's equations governing heat conduction. An equation analogous to (III.3) for purely radial diffusion in a (long) cylinder is

$$\frac{\partial c}{\partial t} = \frac{1}{r} \frac{\partial}{\partial r} \left(Dr \frac{\partial c}{\partial r} \right) \qquad \text{(III.13)}$$

where r is radius, and for radial diffusion in a sphere

$$\frac{\partial c}{\partial t} = \frac{1}{r2} \frac{\partial}{\partial r} \left(Dr^2 \frac{\partial c}{\partial r} \right) \qquad \text{(III.14)}$$

Equations (III.12) - (III.14), with constant diffusion coefficient, may be solved analytically in a number of cases, depending on the type of initial and boundary conditions. A problem of practical interest is represented by the drying of a body with an initially uniform moisture concentration, and with a constant surface concentration, corresponding to the ambient humidity, throughout the drying period. Crank (1967) presents solutions of (III.12) - (III.14) in that case, permitting 1) calculation of the concentration distribution in the body at a given time, 2) calculation of the concentration in a given position as a function of time, and 3) calculation of the amount of diffusing substance which has left the body at a given time. Fig. III.1 illustrates the moisture content (W) versus time (t) presented in a plot of the non-dimensional parameters $\bar{u} = (W - W_\infty)/(W_o - W_\infty)$ and $Fo = Dt/l^2$, where W_o and W_∞ is the initial and final moisture contents, respectively, and D is the constant diffusion coefficient.

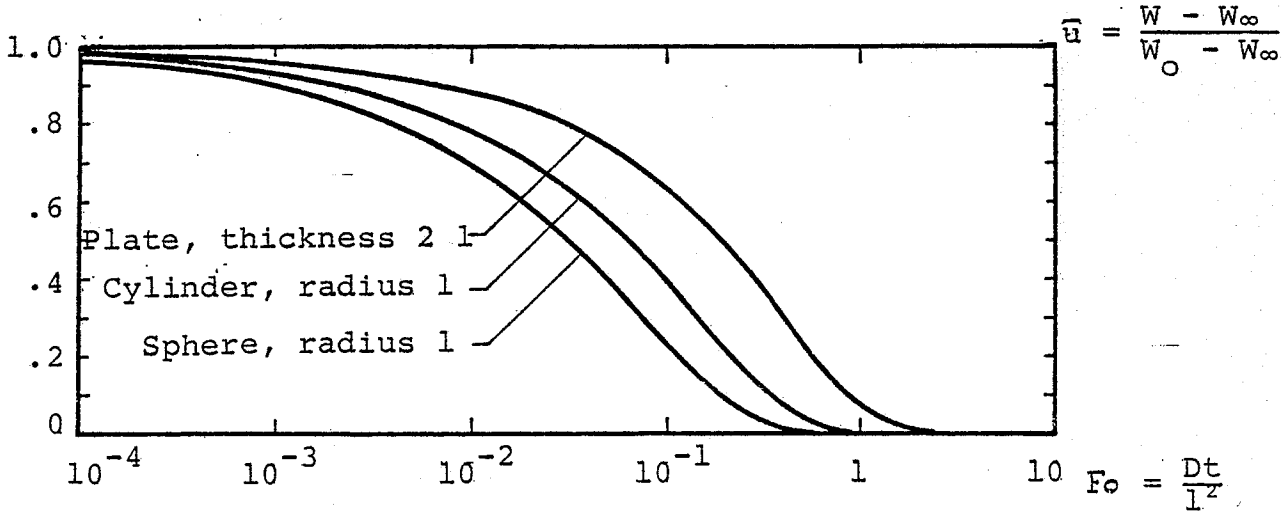

Fig. III.1. Moisture content W versus time t, represented by the non-dimensional parameters $\bar{u} = (W - W_\infty)/(W_o - W_\infty)$ and $Fo = Dt/l^2$ for a body initially with a uniformly distributed moisture content W_o drying to a final moisture content W_∞. During drying the surface concentrations are constant and correspond to W_∞; diffusion coefficent D is constant.

As we shall see later, the transport coefficient associated with moisture migration in hardened cement paste is in general a strong function of the moisture content. In that case analytical solution of the diffusion equation is rarely possible, and in general one has to resort to numerical procedures. However, in narrow intervals of concentration the diffusion coefficient may be regarded as a constant and the linear differential equations apply. Also, methods exist for evaluating concentration dependent diffusion coefficients based on solutions of the constant coefficient diffusion equation (III.12).

III.3. Basic transport mechanisms

In the preceding section we have treated mass transport from a purely phenomenological point of view. In this section we shall briefly consider the mechanisms of mass transport in pores of dimensions typically found in hardened cement paste.

First, we consider a gas flowing through a single circularly cylindrical capillary (Carman (1956), Barrer (1967)).

At higher mean pressures, or in a capillary with a radius much greater than the mean free path of the gas, mutual collision between individual gas molecules is prevailing, and the gas behaves as a continuous fluid. So long as the pressure difference between the ends of the capillary is not so large that turbulance is promoted, viscous flow, also called streamline or Poiseuille flow, occurs. The PV-permeability coefficient for Poiseuille flow is given by

$$K_p = \frac{r^2 P}{8\eta} \qquad \text{(III.15)}$$

Where

K_p = Poiseuille PV-permeability
r = radius of the capillary
η = viscosity coefficient of the gas

The viscosity coefficient η is a function of temperature and various molecular parameters.

If the pressure of the gas is reduced until its mean free path is an appreciable fraction of the capillary radius, the rate of flow exceeds that calculated from viscosity by Poiseuille's law. This is attributed to "slippage" at the capillary walls. In Poiseuille flow there is a parabolic velocity profile across the tube section, with zero velocity at the wall. In slip flow, it is assumed that there is a non-zero velocity of the gas layer immediately adjacent to the capillary wall. There is no rigorous theoretical treatment of slip flow; the usual approach is to assume that a modified Poiseuille flow is occurring.

If the pressure is further decreased, or if the capillary is sufficiently narrow, so that the mean free path is much greater than the capillary diameter, viscosity plays no part in flow, since molecules collide only with the capillary wall, and not with one another. In this case flow is referred to as molecular streaming or Knudsen flow and is characterized by a PV-permeability coefficient given by

$$K_k = \frac{2}{3} \cdot r \cdot \bar{v} \cdot \frac{2 - f}{f} = \frac{2}{3} \cdot r \cdot \frac{2 - f}{f} \sqrt{\frac{8RT}{\pi M}} \qquad \text{(III.16)}$$

where

K_k = Knudsen PV-permeability
r = capillary radius
$\bar{v}$ = mean thermal velocity of the gas molecules
f = the proportion of molecules which undergo diffuse reflection at the pore walls
R = the gas constant
T = absolute temperature
M = molecular weight of the gas

It is generally assumed that $f \approx 1$ which reduces eq. III.16 to

$$K_k = \frac{2}{3} \cdot r \sqrt{\frac{8RT}{\pi M}} \qquad \text{(III.17)}$$

The mean free path of a gas is roughly proportional to the ratic absolute temperature/pressure. For water molecules in air it is of the order 1000 Å at 25°C and 1 atm. The Knudsen permeability is seen to be independent of pressure.

So far we have considered the flow of a single gas under the influence of a pressure gradient. For a mixture of gases, when the composition is different at the two ends, mutual diffusion or interdiffusion may contribute to the net flux of the single components

through the capillary. At constant total pressure, if the capillary radius is much greater than the mean free path, this so-called ordinary molecular diffusion or mutual diffusion is the only contributor to transport. This sort of transport is characterized by a mutual diffusion coefficient which is a function of total pressure, temperature and molecular characteristics of the gases, and is independent of the size of the capillary. If, however, the capillary radius is much less than the mean free path, transport is by Knudsen diffusion. The Knudsen diffusion coefficient is given by eq. III.16. In the Knudsen region, each component in a mixture diffuses independently of the others, since in this case molecules collide only with the capillary walls. Also, the flux is independent of the existence of a total pressure gradient so long as the partial pressure gradient remains unchanged. As in the case of pressure flow, there is a transition region between the two limiting cases represented by ordinary and Knudsen diffusion.

Regarding liquid flow in a capillary, we may restrict ourselves to viscous or Poiseuille flow. The permeability coefficient is given by

$$B = \frac{r^2}{8\eta} \qquad \text{(III.18)}$$

where

B = permeability coefficient
r = radius of the capillary
η = viscosity of the liquid

In the process of surface adsorption, gas molecules are captured by the attractive force of the solid surface of the adsorbent. The adsorbent surface will have certain low energy sites to which the adsorbed molecules will tend to be attracted. These molecules will vibrate about their mean equilibrium position in the potential well, and once in a while will surmount the activation barrier to occupy a new site. If a concentration gradient exists along the surface there will be a net transport down the gradient as more molecules will be hopping out of regions of high concentration than in from adjacent regions of lower concentration. A phenomenological description of surface flow is given by eq. (III.10).

A circularly cylindrical capillary can be regarded as an idealized pore in a porous solid. In a real porous material such as hcp the conducting channels comprise an irregular network of pores, some linked and others forming "blind" pockets. In order to interpret measured (phenomenological) transport coefficients in terms of basic flow mechanisms occurring within the porous solid, one has to assume a more or less idealized model of the pore space (see for instance Barrer (1967)). In a later chapter we shall apply a simple model represented by a system of circularly cylindrical capillaries lying in the direction of flow.

III.4. Permeability of water saturated hardened cement paste and concrete. Literature review.

Obviously, studies of liquid water flow through a specimen under the influence of an applied pressure gradient yields information about the permeability of the specimen only in its specific saturated state. As we shall see, however, valuable information regarding the microstructure of the specimen have been deduced from such studies.

Powers el al. (1954) performed a systematic investigation on the permeability of hardened cement paste to water. The permeability was calculated from the steady-state water flux through a specimen under influence of a constant pressure gradient according to eq. (III.1). The main conclusion from this work was that the most important material parameters influencing the permeability of virgin hcp specimens were degree of hydration (age) and water-cement ratio. Both parameters are related to the porosity of the paste: the water-cement ratio determines the initial porosity, which subsequently decreases due to the volume increase that takes place when the cement is hydrated. This work includes a further interesting observation. After having been dried only down to 79% humidity the pastes (w/c = 0.50) exhibited permeabilities about seventy times those of the virgin specimens. Powers et al. believe that the capillary space is in the form of isolated cavities,each cavity being surrounded by gel (cf. section I.2). Shrinkage produced by drying may rupture some of the webs of gel and thus increase the permeability.

In a later work Powers, Copeland, and Mann (1959) more specifically interpreted permeability results by reference to the capillary structure of cement paste. Since the capillary pores in the paste are on the average much larger than the gel pores, continuity or discontinuity in the capillary pore system is decisive for the permeability. Powers et al. concluded that for any given cement there is a maximum water-cement ratio above which complete hydration does not produce enough gel to block all the capillaries, i.e. the capillary pore system remains continuous even at complete hydration. For the particular type II cement this w/c was about 0.7. At water-cement ratios below that value, capillaries become discontinuous before all of the cement has become hydrated.

A consequence of these findings is that when water is forced through mature hcp specimens like those of the present work with w/c = 0.4 and 0.5 it must pass regions of the fine textured gel phase. Also, since all our specimens were dried prior to use, we should expect higher permeabilities than those found for virgin specimens.

The permeability of concrete which contains 65-75 vol. % of aggregate particles usually differs from that of the neat cement paste. If the aggregate has a very low permeability its presence reduces the effective area over which flow can take place. Furthermore, since the flow path has to circumvent the aggregate particles, the effective flow path becomes considerably longer and the permeability is reduced. On the other hand, the boundary zone between paste and aggregate particles is often very porous, mainly due to settlement (bleeding) of the paste below aggregate particles. Such zones represent flow paths of very low resistance and hence increases permeability. Powers et al (1954) determined the permeability of various coarse aggregates free from visible flaws and found values which were comparable to those of mature hardened cement paste.

Ruettgers et al (1934/35) & (1935/36) performed an extensive investigation on the permeability of concrete. They concluded that the main factors controlling permeability of mature concretes

were water-cement ratio and maximum size of aggregate. Increasing the water-cement ratio may have a double effect: in addition to producing a more permeable paste the tendency of bleeding in the fresh paste is enhanced, so that there is a greater risk of very porous boundary zones between paste and aggregate particles. Ruettgers et al. also measured permeabilities of cement mortar and neat cement pastes. However, we hesitate to draw too rigorous conclusions from the latter results, and tend to remain at the more general and qualitative statements about the concrete results which were obtained under comparable experimental conditions.

III.5. Estimation of diffusion coefficients for hardened cement paste, mortar and concrete from drying tests and related experiments. Literature review.

A fairly large amount of experimental results regarding drying of cement paste, cement mortar and concrete has been reported in the literature. Such results have been used, one way or the other, to determine diffusion coefficients, on a purely phenomenological basis, for water (moisture) removal from the porous material, based on Fick's second law (III.12). Some of the published work along these lines is reviewed below.

Pihlajavaara (1963) describes the general character of drying experiments. When an initially water saturated and "surface wet" specimen is placed in an atmosphere of low humidity, the specimen weight versus time curve displays three distinct domains (cf. fig. III.2). During a first short period water is lost at

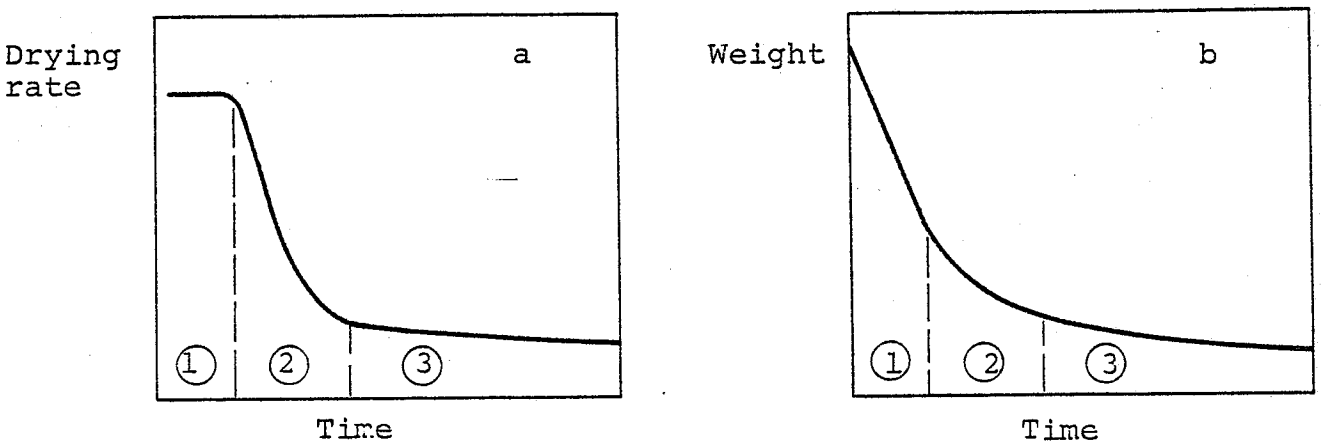

Fig. III.2. Schematic representation of the drying periods. 1) constant rate period, 2) First falling-rate period, 3) Second falling-rate period.

a constant rate due to evaporation of excess surface water. As the surface water film disappears, the drying rate at first decreases fairly quickly. This "first falling rate period" can be regarded as the transition from the constant rate period with surface evaporation to a "second falling rate period" of relatively low and steadily decreasing drying rate, where internal transport processes are rate determining.During the constant rate period (1) and the first falling rate period (2) the weight versus time results are sensitive to the velocity of the ambient air, and in general the drying process is not isothermal.

If the specimen has been sealed during curing, or if it is initially conditioned at a moisture content below saturation, practically the entire drying course belongs to the second drying period, for which Fick's second law (III.11) can be applied with the boundary condition represented by a constant surface moisture concentration, in equilibrium with the ambient air humidity.

Pihlajavaara (1963) performed a large number of drying experiments with cement mortar. Material data were: water/cement ratio (by weight) w/c = 0.56, cement paste/aggregate ratio 1/1.2 by volume, maximum particle size of aggregate 1.4 mm. Plates, 0.5, 1 and 2 cm thick, cast in plastic rings 13.5 cm in diameter and cured corresponding to approximately one month in water at 20°C, were used in the experiments. The plates were placed in two climate rooms at 21°C, with humidities of 0.70 and 0.40, respectively. Pihlajavaara recorded specimen weight versus time, and compared these data with the solution of the diffusion equation represented by fig. III.1. For a given value of $\bar{u}$, the diffusion coefficient D can be computed by dividing the value of Fo, obtained from fig. III.1, by t/l^2 as determined experimentally. Using this procedure, Pihlajavaara obtained diffusion coefficients as a function of $\bar{u}$. The results are shown in fig. III.3 in a recalculated form as D versus the relative moisture content. It appears that the diffusion coefficients so measured depend on both the humidity range of the experiment and the specimen thickness. Judged from some additional results, however, the assumed boundary condition may have

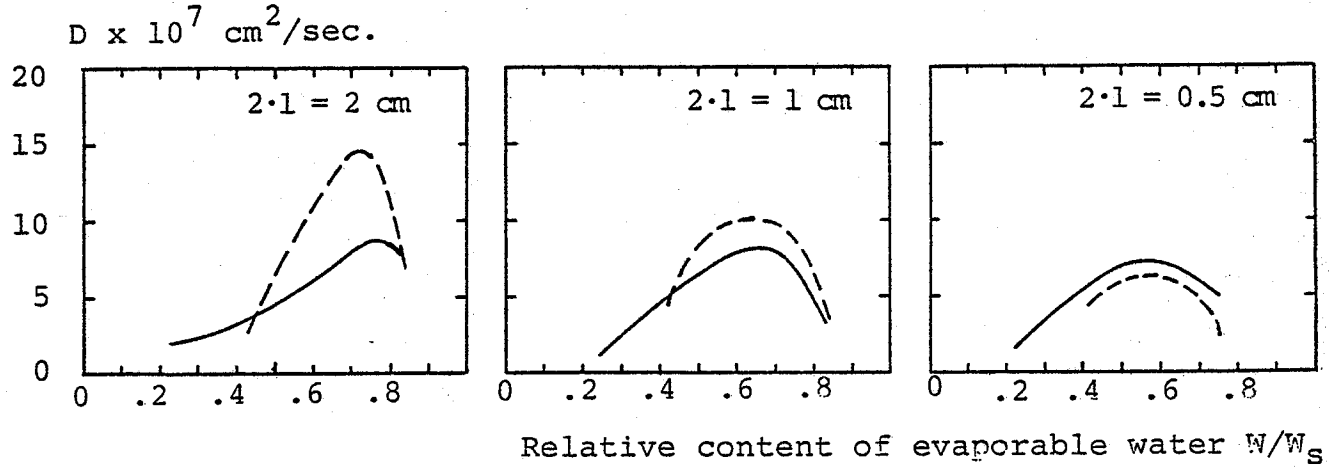

Fig. III.3. Diffusion coefficient D as a function of relative moisture content W/W_S (W_S = saturation moisture content). Based on data from Pihlajavaara (1963) for cement mortar plates of various thicknesses (2·1) drying from saturation to equilibrium with a humidity of 0.7 (broken lines) or 0.4 (full lines).

been violated at the higher moisture contents, although some attempts were done to correct for this.

In a later work, Pihlajavaara (1965) evaluated diffusion coefficients for cement mortar using a different procedure. The mortar mix was similar to that used in the 1963 publication. The specimens were plates of 1.2 cm thickness and 13.5 cm diameter. A series of successive drying experiments were performed, starting from saturation. The humidity of the ambient air in the seperate steps were 0.85, 0.70, 0.55, and 0.40. Assuming that the desorption steps are sufficiently narrow to secure a reasonably constant diffusion coefficient within each step Pihlajavaara estimated the diffusion coefficient from the best fit of the experimental data to the theoretical curve in fig. III.1. The results are shown in fig. III.4, again as a plot of diffusion coefficient versus relative moisture content. The two curves appearing in fig. III.4 are both based on drying of 1.2 cm thick plates; the upper curve was obtained when the plate dried from one face only, the back face being sealed, whereas the lower curve refers to symmetrical drying from the two faces. Pihlaja-

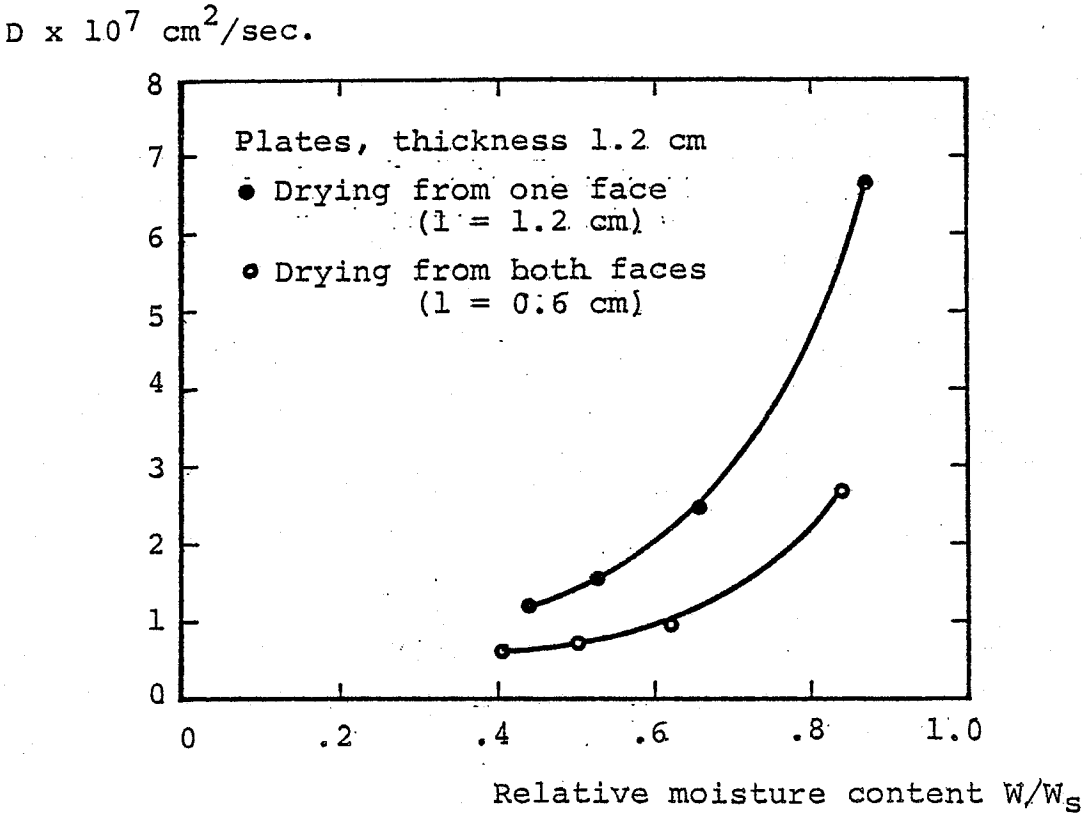

Fig. III.4. Diffusion coefficient D as a function of relative moisture content for cement mortar plates drying from one face (full points) or both faces (open points). Reproduced from Pihlajavaara (1965).

vaara suggests that the diffusion coefficient is a function of the thickness of the plates or, in other words, a function of the drying rate. However, the results from the earlier drying tests performed by Pihlajavaara (fig. III.3), at least the ones going down to h = 0.40, do not justify such a conclusion. Also, evidence from other sources (Lowe et al (1971), Jain and Kesler (1964)) precludes the likelihood of any size dependence of the diffusion coefficient.

We note that the diffusion coefficients in fig. III.4 are considerably smaller than those in fig. III.3, and the curves do not show a similar drop at higher water contents. We can find no other explanations of the difference between the two sets of curves than the fact that the specimens may actually be very different. The 1963 specimens were cured corresponding to approximately one month in water at 20°C, whereas the 1965 specimens were subject to a complicated curing history: after one month of water curing at 20°C, the specimens were used for a six months

drying test (20°C, h = 0.40), hereafter oven dried at 105°C for one month, and finally stored in water at 20°C for 2½ years. In both cases, however, we note a significant dependence of the diffusion coefficient on the moisture content. The two sets of results are shown on the common plot in fig. III.8.

Bray (1969) performed an extensive series of diffusion experiments. He used hardened cement paste specimens of w/c = 0.35 and 0.45 cured in boiling water for at least 21 days, followed by sealed curing at room temperature. Bray employed two experimental techniques to determine diffusion coefficients. One method, called the "stepping method", consists in measuring weight versus time relationships during adsorption or desorption in small intervals of concentration, and fit the data to the appropriate solution of the diffusion equation (III.12). This procedure is similar to that used by Pihlajavaara (1965). The procedure in the second method is to obtain the weight versus time relationship in an adsorption step from humidity zero to a given upper humidity, and subsequently perform a similar measurement in the corresponding desorption step from the upper humidity to zero. From these measurements an adsorption (D_a) and a desorption (D_d) diffusion coefficient are determined as those D values which cause the experimental and theoretical (constant coefficient) curves to coincide at the mid-point weight in the step. The diffusion coefficient corresponding to the upper humidity is then computed as the average value of D_a and D_d, i.e. $D = \frac{1}{2}(D_a + D_d)$. Bray refers to Crank and Henry (1949) who reported this method. Crank and Henry assumed a number of analytical relationships between diffusion coefficient and concentration and computed differences between D_a and D_d ranging to ±25%, whereas D differed from the exact value by less than 3%. Some of Bray's results obtained from the "stepping method" are shown in fig. III.5. The experiments started at low humidities and proceeded through a series of successive adsorption steps, followed by a series of successive desorption steps. Results from the "averaging method" are shown in fig. III.6. In this case, only one curve is obtained for each specimen type, implying that differences between D_a and D_d values are due to the concentration-dependent diffusion

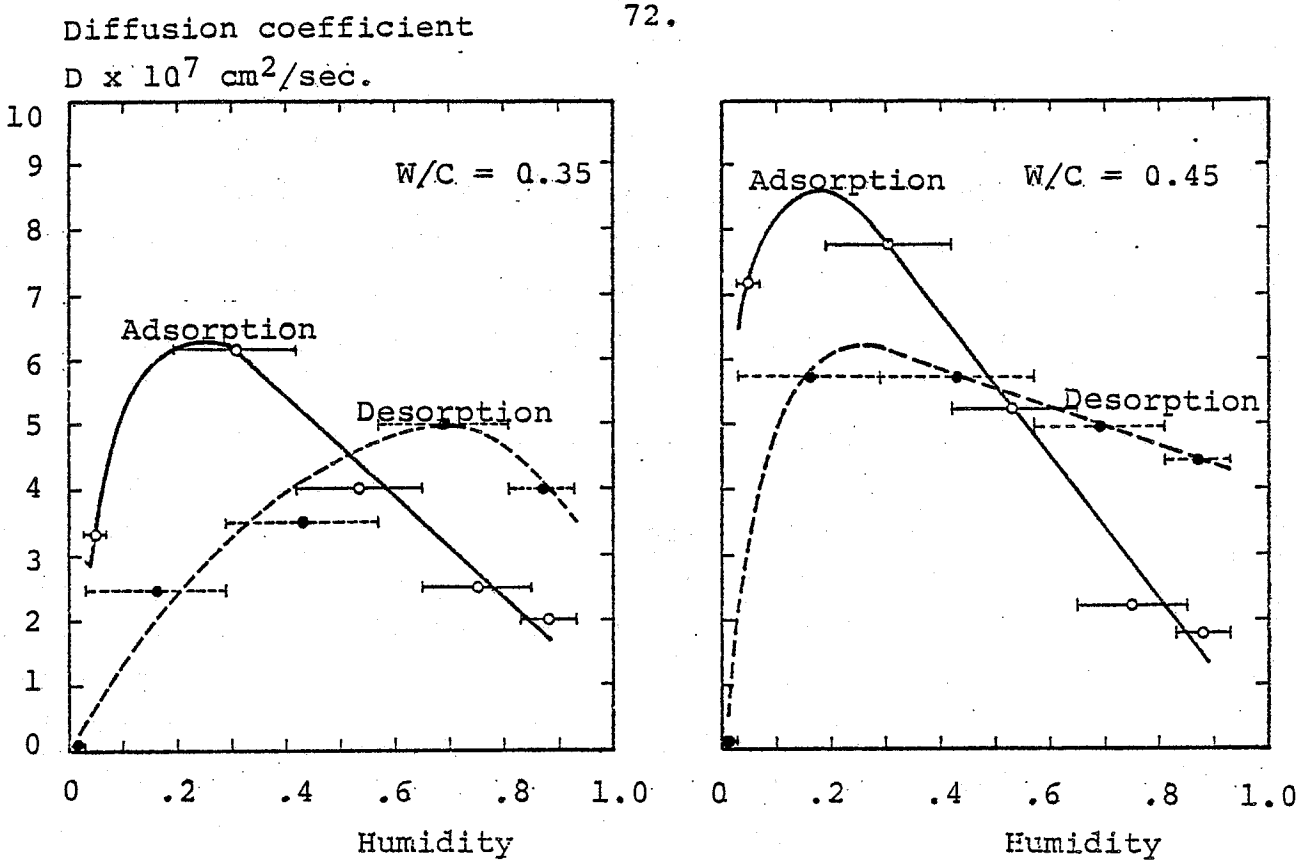

Fig. III.5. Diffusion coefficient versus humidity for hardened cement paste at 45°C. The plots are based on data from Bray (1969), "stepping method".

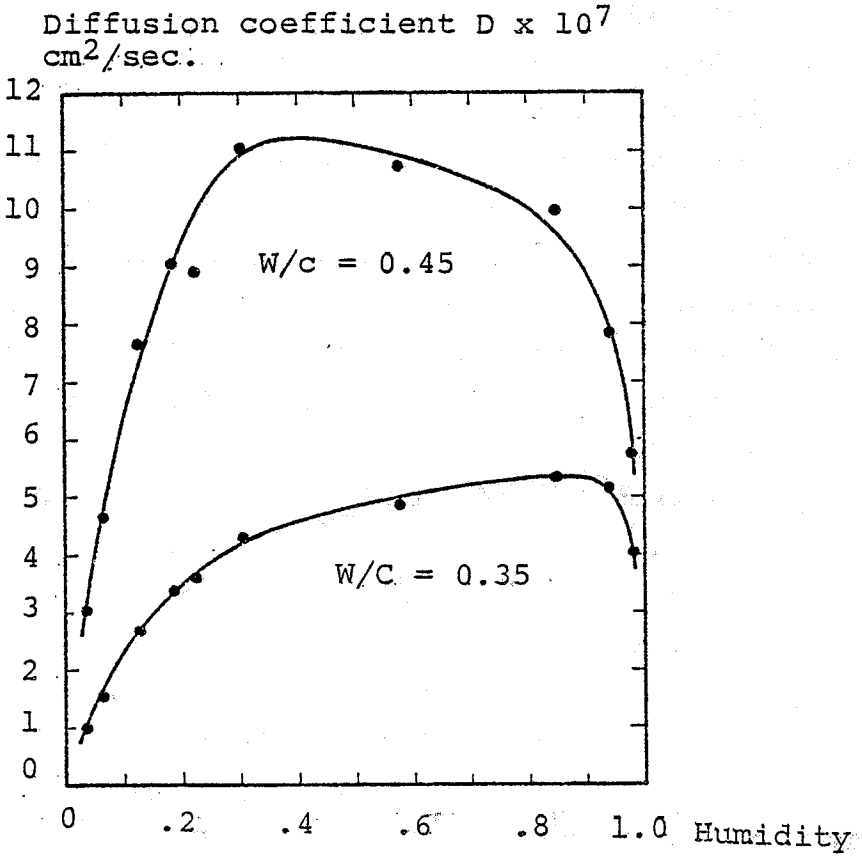

Fig. III.6. Diffusion coefficient versus humidity for hardened cement paste at 57.4°C. Data from Bray (1969), adsorption-desorption method.

coefficient. Bray performed his experiments at 45°C and 57.4°C. Although a direct comparison between similar experiments at the two temperatures cannot be made, it is clear that the diffusion coefficient increases with temperature, in line with findings of Hughes et al (1966) and Hancox (1967 and 1968). However, we can do no better than saying that lower coefficients would have been obtained at 25°C.

Hancox (1968) estimated diffusion coefficients for cement paste (w/c = 0.28 and 0.50, cured in water for at least 6 months) from drying experiments. The drying range was from saturation to almost zero humidity. For the first about 60% loss of evaporable water the diffusion coefficient was found to depend on moisture content, although no figures were reported. For the last 40% of the evaporable water content drying could be described by constant diffusion coefficients (see fig. III.8).

Lowe, Hughes, and Walker (1971) performed drying experiments with concrete spheres (w/c = 0.50, ca. 500 kg cement per m^3, max. aggregate size 9.5 mm, moist cured for at least 28 days). These tests were done at 30°C, from saturation to an ambient humidity of 0.70. The estimated diffusion coefficient was found to decrease drastically with moisture content (fig. III.8).

Based on fitting of experimental drying data from a number of sources, Bazant and Najjar (1971) suggested a mathematical expression of the diffusion coefficient of concrete as a function of (pore) humidity, of the form

$$D(h) = D_1 \left(\alpha_o + \frac{1 - \alpha_o}{1 + \left(\frac{1 - h}{1 - h_c}\right)^n}\right) \qquad \text{(III.19)}$$

where h is pore humidity and D_1 is the value of the diffusion coefficient at saturation (h = 1.0). The meaning of parameters α_o, h_c, and n appear from fig. III.7. Bazant and Najjar noticed that the values of parameter h_c, characterizing the location of the drop in the curve, were about the same for different concre-

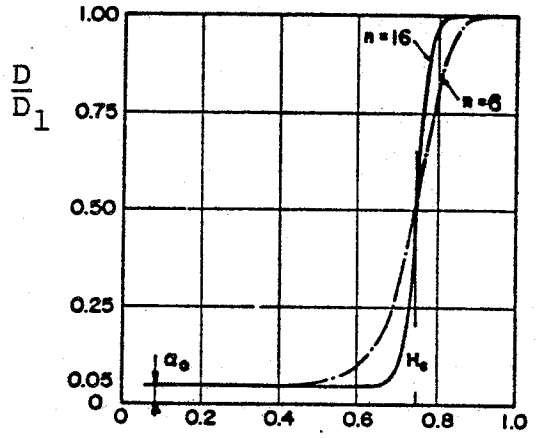

Fig. III.7. Diffusion coefficient relative to its value at h = 1.0 versus pore humidity h, according to eq.(III.19) . Reproduced from Bazant and Najjar (1971).

tes or cement pastes, about $h_c = 0.75$. The values of parameter α_o, representing the ratio min. D/max. D, were also quite close and equal to about 0.05. The values of the exponent n, characterizing the spread of the drop in D (h) were between n = 6 and n = 16. The absolute values of the diffusion coefficient, characterized by the parameter D_1, were found to scatter more than the other parameters, especially in dependence on the water/cement ratio.

In their analysis Bazant and Najjar presume that the desorption isotherm can be approximated by a straight line, which makes the reported diffusion coefficients proportional to the permeability coefficients (cf. eq. III.6). This approximation may be reasonable for some concretes, but not for cement paste (cf. fig. II.7). Water vapour permeability versus humidity curves for cement mortar reported by Nilsson (1976) (fig. III.10) actually match the type of curve in fig. III.7 for water-cement ratios 0.60 and 0.80. The water vapour permeability versus humidity curves that we have obtained (fig. III.17) have also some resemblance to the curve in fig. III.7.

amount of data used in Bazant's and Najjar's analysis originated from drying experiments on relatively immature concretes (7 days old or younger), and most of them with water-cement ratios above 0.60, which gives some of the explanation of the very high D_1 values reported (22 - 44 x 10^{-7} $cm^2/sec.$).

By reference to fig. III.8 we note that the concrete results of Lowe et al. seem to be in line with those of Bazant and Najjar, while diffusion coefficients for mortar and cement paste show a different pattern. As was discussed in connection with saturated flow permeability, the presence of aggregate particles can increase or decrease the diffusion coefficient. On one hand, dense particles reduce the effective flow area, and the flow path becomes longer. On the other hand, due to bleeding the boundary zone between paste and aggregate may be more porous than the bulk paste phase and thus represent flow paths of very low resistance. Nilsson (1976) reported data for various concretes (w/c = 0.60, 28 days water curing) which showed an increase of diffusion coefficient with increasing max, aggregate size, as well as with increasing content of "coarse" (4-8 mm) aggregate, which suggests that the latter effect has dominated. Nilsson's results serve to illustrate differences between cement mortar and concrete, but strictly only at the specified water-cement ratio and maturity. It has not been possible to find any further informations in the literature that could elucidate the effect of aggregate on the diffusion coefficient. Since we must expect that both concrete composition (type, content, and grading of aggregate) and details of the specimen preparation may strongly affect the moisture transport properties, and probably further so as a function of the water-cement ratio, it seems that we are forced to treat results from hardened cement paste, mortar and concrete separately.

Most of the diffusion results discussed above are presented on the common plots of fig. III.8. The data appear as diffusion coefficients versus relative moisture content in fig. III.8.a. For those cases where sorption data were available, fig. III.8.b plots diffusion coefficients versus humidity (relative vapour pressure). For curve no. 13 which originates from a drying experiment at a humidity of 0.70 it was assumed that the desorp-

Curve no.	Material	w/c	Curing	Ads./ des.	Exp. temp. (°C)	Ref.
1,2	Cement mortar	0.56	28 days in water	des.	21	Pihlajavaara (1963) (fig. III.3)
3,4			"Old specimens", see p. 70			Pihlajavaara (1965) (fig. III.4)
5	Cement paste	0.45	21 days in boiling water	ads.	45	Bray (1969)
6				des.		
7		0.50	6 months in water	des.	21	Hancox (1968)
8		0.28				
9		0.50	steam-cured (97°C)	ads.	25	Computed from data of the present work
10				des.		
11		0.40	RT-cured (25°C)			
12						
13	Concrete	0.50	28 days in fog room	des.	30	Lowe et al. (1971)

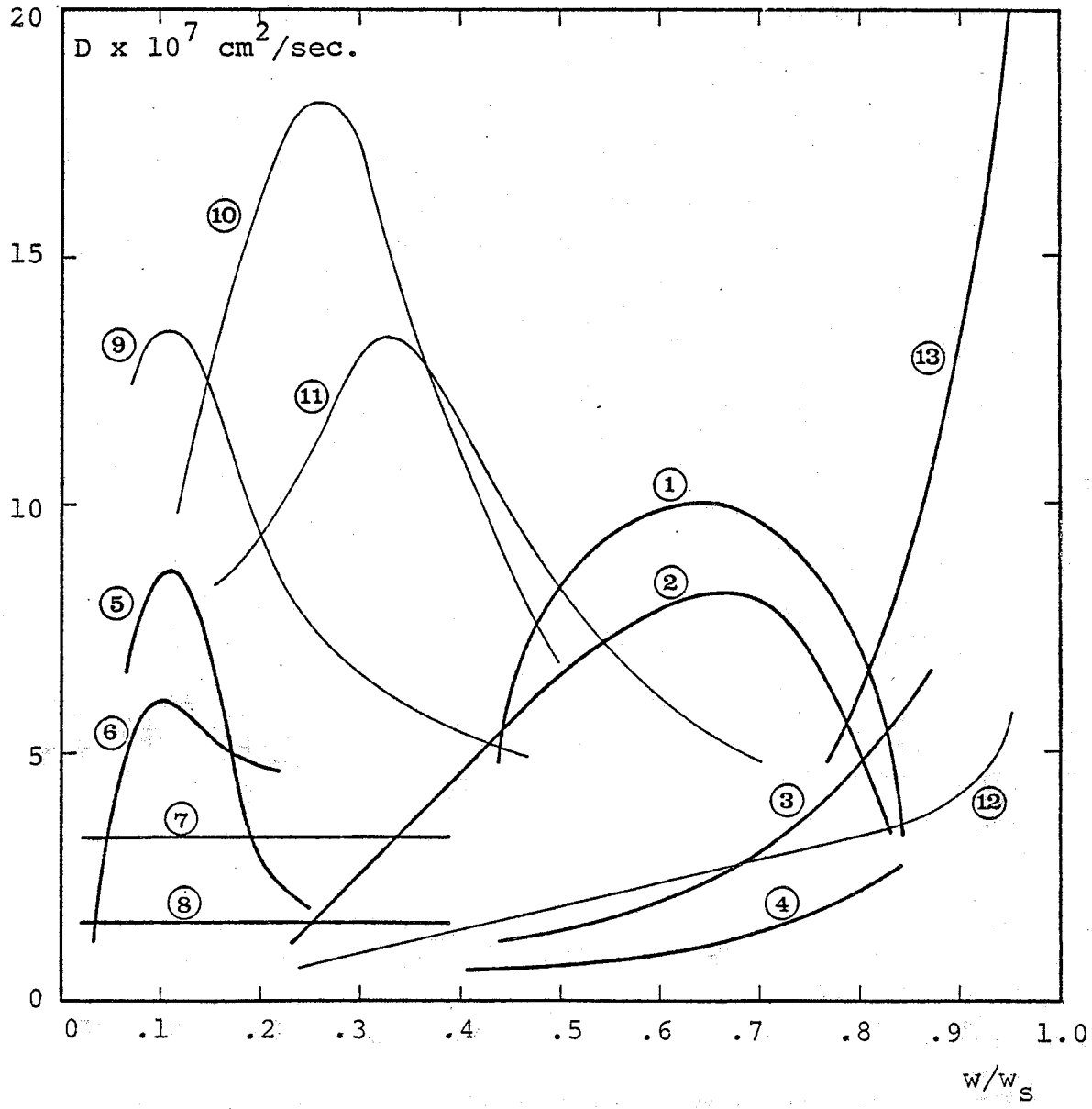

Fig.III.8.a.Diffusion coefficient versus relative moisture content obtained from various sources.(See also fig. III.8.b)

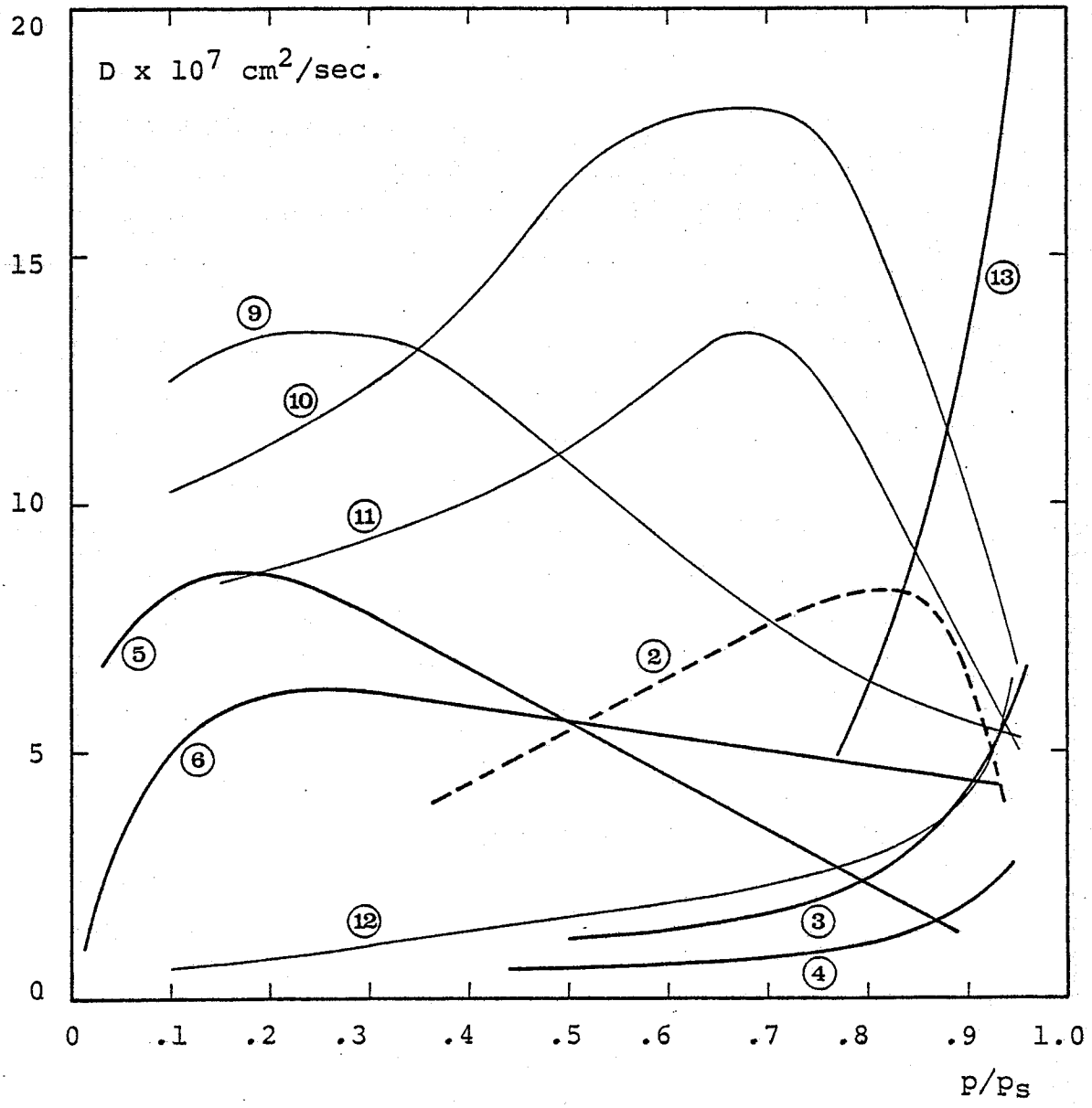

Fig. III.8.b. Diffusion coefficient versus relative vapour pressure (humidity). (See also fig. III.8.a).

tion isotherm of the concrete is linear from h = 0.70 to saturation. Although no sorption data relevant to curve no. 2 were given, we found it justifiable to include it in fig. III.8.b for comparison, using the sorption data given for curves no. 3 and 4.

We note as a common feature for all specimen types that the diffusion coefficient depends significantly on the moisture content or on the humidity. Several curves exhibit a maximum at some intermediate moisture content (humidity). Recalling that the diffusion coefficient represents the mass flux caused by a unit concentration (water content) gradient, a comparatively low diffusion coefficient near saturation may cause a considerable flux in terms of humidity gradient if the sorption isotherm is steep near saturation. When the transport coefficient is expressed as water vapour permeability, i.e. the mass flux caused by a unit vapour pressure (or humidity) gradient, which formulation is perhaps intuitively more acceptable, we typically find an ever-increasing transport coefficient versus humidity curve, as we shall see later. Our own results illustrate that transformation of such a curve may yield a diffusion coefficient versus humidity (moisture content) curve with a maximum (cf. figs. III.8 and III.17-19). Later on we shall try to interpret the moisture transport coefficient in terms of basic transport mechanisms by reference to water vapour permeability versus humidity curves.

The curves shown on the common plots (fig. III.8) include both concrete, mortar, and cement paste specimens. As was discussed previously, it seems that we must treat results from each material separately. The material group best represented is hardened cement paste; but the various curves involve differences regarding both water/cement ratio, curing condition, and experimental temperature, and the available data are too scarce to indicate possible influences of these factors on the diffusion coefficient. However, at least we note that the reported diffusion coefficients fall within approximately one order of magnitude.

III.6. The cup method

III.6.1 Principle

The cup method, sometimes also called the dish method, is a steady state method, recommended by the ASTM (1974 a and 1974 b), and used extensively for characterizing the water vapour permeability of building materials. The material to be tested, in the form of a thin disc, is sealed to the mouth of an impermeable cup (dish), which contains either a desiccant or water (fig. III.9).

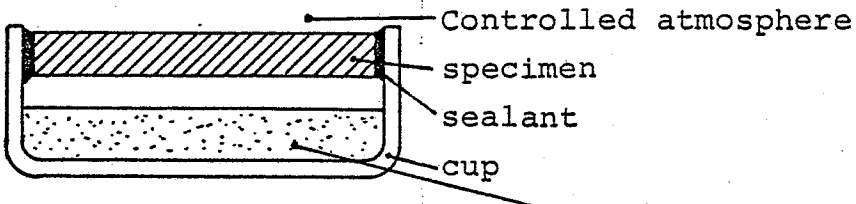

Fig. III.9. Assembly for the cup method.

The assembly is placed in an atmosphere of constant temperature and humidity, and the weight gain or loss of the assembly is used to calculate the rate of moisture movement through the specimen. Ideally then, at steady state conditions characterized by a constant transfer rate, the flux of water vapour under the influence of a known humidity drop can be measured.

III.6.2 Theory

The basic form of the flow equation is (III.6):

$$J = -\nu \frac{\partial p}{\partial x} \qquad \text{(III.20)}$$

In the cup method, constant vapour pressures p_1 and p_2 are isothermally maintained at the two faces of the specimen disc, and the constant flux J is measured when the steady state condition is reached. Eq. (III.6) may be written

$$J dx = -\nu \, dp \qquad \text{(III.21)}$$

Integrating from x = 0 to x = L (L = specimen thickness) and from p_1 to p_2 yields

$$J \cdot L = -\int_{p_1}^{p_2} \nu \, dp = -\frac{\int_{p_1}^{p_2} \nu \, dp}{p_2 - p_1} (p_2 - p_1) \qquad \text{(III.22)}$$

Rearranging yields

$$J = \bar{\nu} \frac{\Delta p}{L} \qquad \text{(III.23)}$$

$$\bar{\nu} = \frac{1}{p_2 - p_1} \int_{p_1}^{p_2} \nu \, dp \qquad \text{(III.24)}$$

where

$\bar{\nu}$ = the mean water vapour permeability

$\Delta p = p_1 - p_2$, p_1 and p_2 being the water vapour pressures at $x = 0$ and $x = L$, respectively

L = specimen thickness

Since ν is, in general, a function of the moisture content (or humidity), the cup method actually measures the mean permeability $\bar{\nu}$.

The vapour pressure dependent permeability $\nu(p)$ can be evaluated from measurements of $\bar{\nu}$, as outlined for instance by Bazant and Najjar (1972). Generalize eq. (III.24) to the form

$$(p_j - p_i) \cdot \bar{\nu}_{ij} = \int_{p_i}^{p_j} \nu dp \qquad \text{(III.25)}$$

Now choose a constant value for p_i, say $p_i = \alpha$, and obtain Y_j as a function of p_j:

$$Y_j = (p_j - \alpha) \, \bar{\nu}_{\alpha j} = \int_{\alpha}^{p_j} \nu dp \qquad \text{(III.26)}$$

or differentiating

$$\nu(p_j) = \frac{dY_j}{dp_j} \qquad \text{(III.27)}$$

Thus, to obtain $\nu(p)$, the following procedure may be followed: 1) measure a systematic series of $\bar{\nu}_{\alpha j}$ ($\bar{\nu}_{\alpha 1}$, $\bar{\nu}_{\alpha 2}$ ....) keeping the water vapour pressure of one side of the specimen constant

(= α), 2) construct a graph of $Y_j = (p_j - \alpha) \cdot \bar{\nu}_{\alpha j}$ versus p_j, and 3) differentiate this curve with respect to p_j to obtain $\nu(p_j)$ versus p_j.

III.6.3 General comments on cup experiments

In principle any two water vapour pressures at the faces of the specimen may be chosen. The desiccant inside the cup may be a saturated salt solution to maintain any given humidity. Even a so-called "inverted water method" is included in the ASTM Standard (1972 a) in which the cup, containing water (fig. III.9), is inverted so that the water is in contact with the specimen surface at all times during the test.

Experimentally, the cup method is relatively simple. However, various sources of error associated with apparatus design and experimental procedure may seriously affect the results. The main sources of error personally recognized, and included in reviews of the method by Newns (1950), Chang and Hutcheon (1956), and Joy and Wilson (1966) are summerized below.

Design of equipment:

1. Insufficient sealing of the specimen to the mouth of the cup may clearly introduce large errors, in particular for low permeability specimens. Also, if the sealing arrangement is so as to mask part of the plane surfaces at the edge of the specimen, errors may arise due to the effective flow area being larger than the geometrically determined area.

2. The desiccant must be able to absorb moisture reasonably quickly, and must possess a sufficient capacity of moisture uptake to maintain a constant humidity during the experiment.

3. The presence of stagnant air layers at the specimen faces may affect the results. Such effects are very difficult to correct for, and the problem should be avoided whenever possible, for instance by establishing rapid air circulation at the faces.

4. The test temperature must be kept constant throughout the experiment. While the humidity is relatively unaffected by small

temperature variations when controlled by saturated salt solutions, the absolute water vapour pressure which is the quantity entering in eq. (III.23) is not.

Experimental procedure:

5. Obtaining the rate of moisture transfer through the specimen usually requires that the cup is taken out of the experimental set-up during weighing. The consequent disturbance of the measurement should be kept to a minimum by choosing a rational weighing procedure.

6. Carbonation of the specimen during test may affect the result. Severe carbonation changes the microstructure of hardened cement paste and causes weight gain (Pihlajavaara (1965), Verbeck (1958)).

7. Changes of barometric pressure produce over-all pressure differences across the specimen. For materials of coarse porosity this may cause pressure flow to occur through the specimen.

8. In the derivation of eq. (III.23) it is assumed that ν is independent of the vapour pressure gradient, so that the mean permeability $\bar{\nu}$, which is the quantity measured in a cup experiment, is independent of the specimen thickness. Only if this is true can a permeability coefficient obtained through the cup method be regarded as a material property.

III.6.4 Published results of water vapour permeability of hardened cement paste, mortar and concrete by the cup method.

An extensive investigation of moisture transport in cement mortar and concrete has recently been published by Nilsson (1976). For cement mortar (max. size of aggregate 1 mm) of varying water/cement ratios Nilsson evaluated the (true) water vapour permeability coefficient as a function of humidity using the procedure described in section III.6.2. Judged from the informations given, the results were obtained in desorption using a cup with low inside humidity. Nilsson's results, shown in fig. III.10., demonstrate a very marked dependence of permeability on humidity, especially for w/c = 0.60 and 0.80.

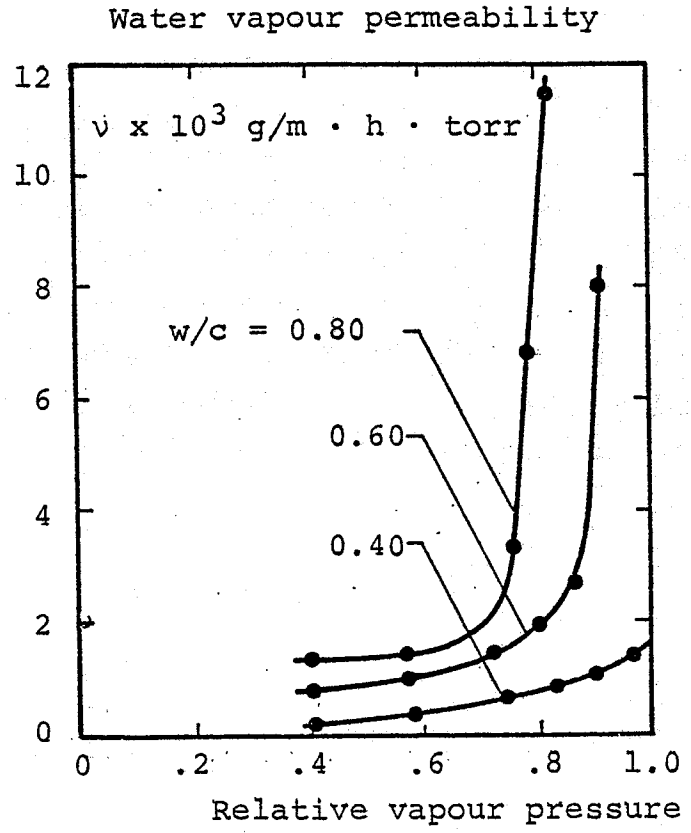

Fig. III.10. Water vapour permeability versus humidity for cement mortar. Reproduced from Nilsson (1976).

Wierig (1965) measured water vapour permeability of mortar and concrete of various water/cement ratios, curing times and cement types. Also, the influence of the test temperature was investigated. Wierig used a cup containing concentrated sulfuric acid (≈ zero humidity) and maintained humidities of 0.50 and 0.95 outside the cup. The permeabilities reported are mean permeabilities $\bar{\nu}$ as obtained from eq. (III.23). Wierig noted ratios of measurements at an upstream humidity of h = 0.95 to those at h = 0.50 ranging from 2 to 4 or more for mature specimens. The dominating factors influencing the permeability were found to be curing time and water/cement ratio.

Tveit (1966) reported measurements of moisture permeability for a large number of porous building materials. In these tests various absorbents were used in the cups, depending on the intended humidity. The tests were carried out at different humidity levels, with a difference between upstream and downstream humidity which was on an average 0.18 at each level. The measurements were started at the h = 0.75 level and successive test

series were carried out at about h = 0.55, 0.35, 0.12 (i.e. during desorption) and finally at about h = 0.95 (i.e. during adsorption). Results for a concrete (w/c = 0.60) and a cement mortar (unknown w/c) are shown in fig. III.11. We note that the concrete permeabilities are lower than those found by Nilsson for cement mortar of the same water-cement ratio. The largest differences are observed in the region near saturation, maybe due to the fact that the h = 0.95 result was obtained during adsorption (cf. section III.7.4). Results for a concrete (w/c = 0.60) and a cement mortar (unknown w/c) are shown in fig. III.11. shown in fig. III.11.

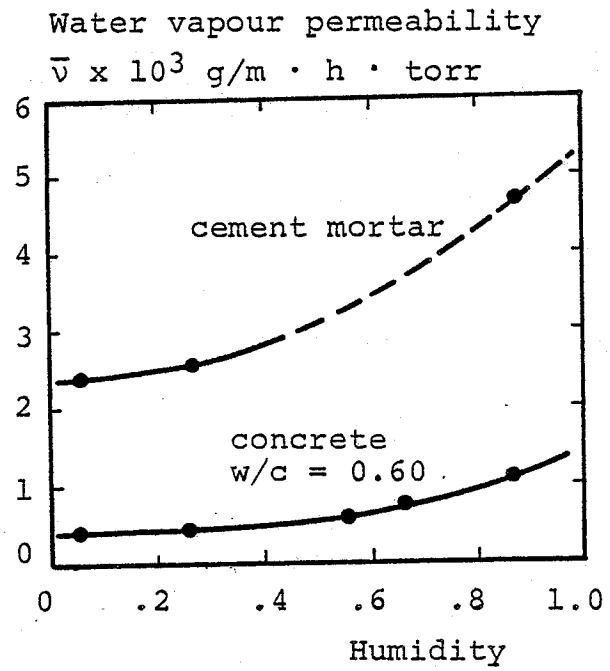

Fig. III.11. Water vapour permeability versus humidity for a concrete and a cement mortar. Reproduced from Tveit (1966).

We shall return to the work described above in connection with the discussion of our own results.

III.7. Present investigation

III.7.1. Scope and programme.

The purpose of the investigation described in this section was to study moisture movement through well defined specimens of hardened cement paste as affected by the moisture condition of the material, and to try to relate moisture migration to pore structure.

The cup method was used in the way described in section III.6.2 to obtain water vapour permeability coefficients as a function of pore humidity. The fixed value of humidity was chosen as zero and realized by using a desiccant in the cup.

The measurements included four specimen types: two water/cement ratios (0.40 and 0.50) and two curing procedures (S-curing and RT-curing). In addition, for each specimen type one series of experiments was performed using specimens initially in a dry condition, while in another series the specimens were initially in a resaturated condition. The total of eight series of experiments is summarized in table III.1.

Table III.1. Experimental programme.

Series no.	Designation	w/c	Curing	Initial specimen condition
1	0.4 (RT) ADS	0.40	RT	Dry
2	0.4 (RT) DES			Resaturated
3	0.4 (S) ADS		S	Dry
4	0.4 (S) DES			Resaturated
5	0.5 (RT) ADS	0.50	RT	Dry
6	0.5 (RT) DES			Resaturated
7	0.5 (S) ADS		S	Dry
8	0.5 (S) DES			Resaturated

III.7.2. Experimental apparatus and techniques

The specimens used were discs which were cut from hcp cylinders 22 mm in diameter, and subsequently polished down to a thickness of about 1 mm. The RT-cured specimens were cured for about 7 months, and the S-cured pastes had been stored in lime water for at least 2 months. All discs were P-dried prior to use (see section II.3.2). The ADS series was started with the specimens in that initial condition. In the DES series the discs were resaturated prior to use, by first subjecting them to saturated water vapour and then saturate them by vacuum soaking. (cf. section II.3.2).

The cup design is shown in fig. (III.12). A number of sealing arrangements, desiccants and placings of dessicant in the cup was tried at length before reaching at this arrangement with the

"inverted" cup, which gave reproducible results. The specimen disc was sealed to the mouth of the glass cup by means of two rubber O-rings, lightly greased and kept in place by a brass support ring and a brass screw cap. Apart from offering easy operation, this arrangement has the advantage of permitting small dilatations of the specimen.

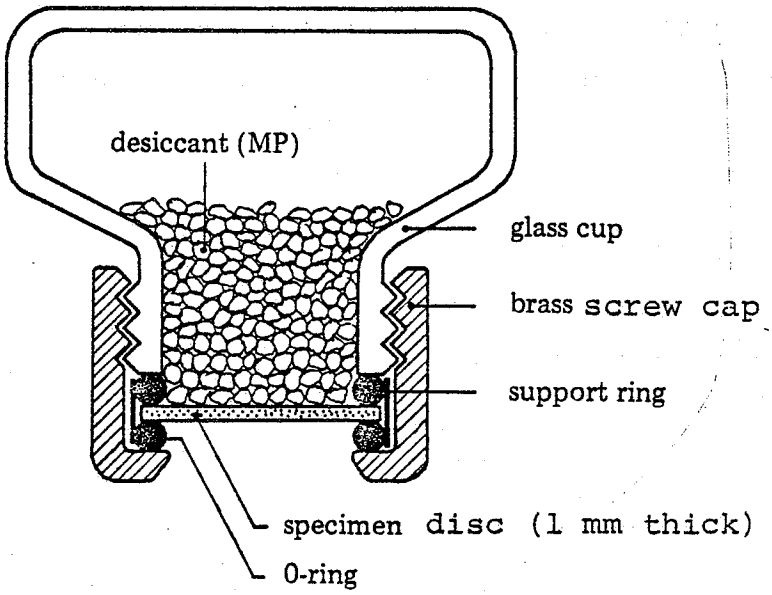

Fig. III.12 The cup assembly.

The cup was used in the inverted position shown to secure the condition of zero humidity at the downstream specimen face. The desiccant, magnesium perchlorate hydrate (MP) has a suitable moisture capacity and rate of moisture uptake. A separate experiment showed that the maximum rate of uptake by the MP was at least 5 times as high as the fastest weight gain observed in the permeability experiments. Prior to use, the MP was conditioned to contain slightly above 2 moles of water which was checked by thermogravimetric analysis. After completion of an experiment it was checked that the MP did not contain more than 4 moles of water (cf. section II.3.2.2).

The experimental set-up is shown schematically in fig. III.13. A total of 4 cups (two sets of two companion specimens) were placed in a desiccator equipped with a small fan to provide vigorous circulation of air around the cups and thus eliminate any stagnant air layer at the disc surface. A humidity conditioned air stream was circulated through the whole system by means of a membrane pump. The air stream was conditioned by

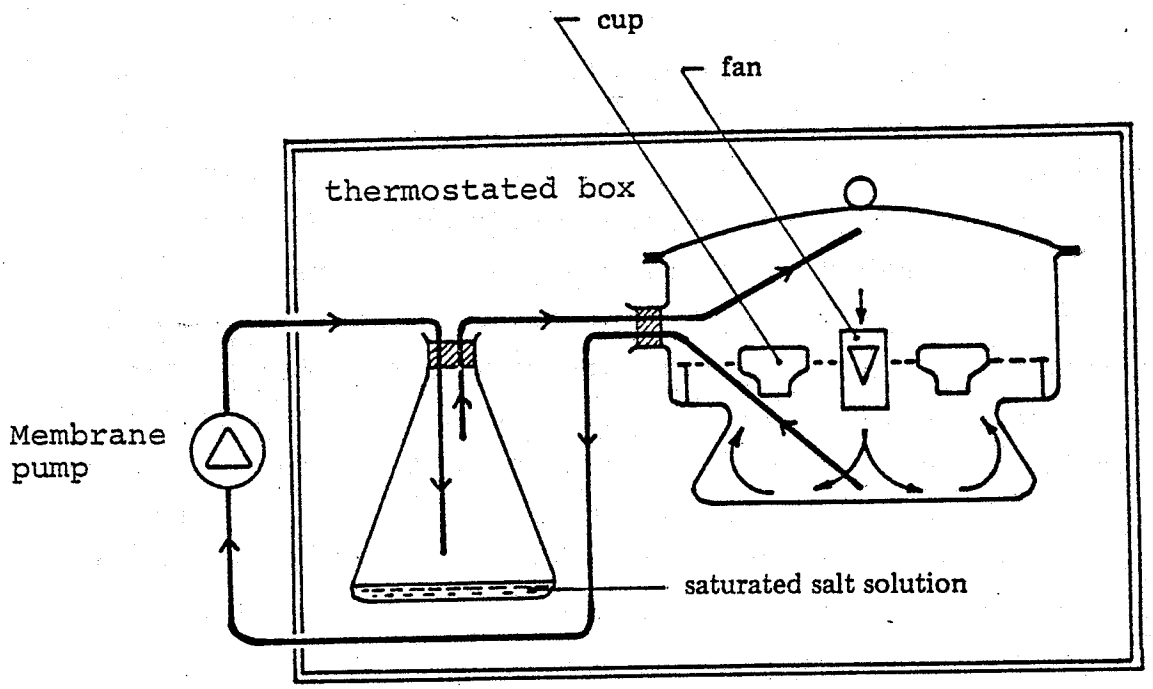

Fig. III.13. The experimental set-up

passing it over an appropriate saturated salt solution (virtually "wet crystals"), cf. table II.3. The humidity in the desiccator was monitored by means of an electronic humidity gauge to check that it was constant during the experiments. In the measuring range of the gauge, which included all the humidity levels used except the lowest one (h = 0.11), the humidity throughout an experiment was found to be within ± 1% of the mean value. The complete system was situated in a thermostated box maintained at 25°C.

With suitable intervals of time the cups were removed from the desiccator, put into weighing bottles, weighed, and returned to the apparatus. Such a weighing procedure was completed within about 5 minutes. Variations in the humidity level in the desiccator after a weighing was followed by means of the electronic gauge and was found to be insignificant. At each weighing, the cups were turned and shaken gently to homogenize the MP.

Measurement of weight gain was continued until a well defined straight line plot of cup weight versus time, characterizing the steady state situation, was obtained. The duration of a single experiment varied from two to five days. In the ADS series (nos. 1, 3, 5, and 7 in table III.1) the same discs were used at increasing upstream humidities. In the DES series each specimen was used in only one experiment, i.e. at only one value of the up-

stream humidity. This procedure was chosen because the DES specimens were initially in the SSD condition, in order to avoid a possible cumulative error due to fine desiccant particles sticking to the specimen surface. Visual inspection of the specimens after each experiment, however, did not give any indication of such a problem. In all desorption experiments the cups were placed in the apparatus in an upward position between the first two weighings in order to secure that the surface towards the desiccant was not wet. Also, in some cases when the rate of moisture transport was high, the cups were placed in that way over night in order to avoid "over-usage" and possible dissolution of the magnesium perchlorate in the vicinity of the disc face; in those cases, however, the data obtained within each working day were sufficient to establish a straight line relationship between weight gain and time.

The experiments were performed in due consideration of the general comments on cup experiments listed in section III.6.3. Some of the items have already been commented on in the previous section. A rough estimate of the masked edge effect (item 1) can be obtained using a formula reported by Joy and Wilson (1966) according to which the masked edge causes an excess water vapour transmission less than 5%, which is small enough to be ignored. Changes of barometric pressure (item 7) may be ignored because viscous flow of gas probably does not occur in pores of the dimensions encountered, as we shall discuss later. A dependence of the permeability on the vapour pressure gradient (specimen thickness) (item 7) would not be detected in the present investigation, since all specimens were about 1 mm thick. Wierig (1965) varied the thickness of mortar specimens from 1 to 4 cm in a single series of experiments and reported an increase in permeability with thickness. However, in Wierig's cup there was a 3 cm air gap between the desiccant (concentrated sulfuric acid) and the specimen, which can in fact account for most of the reported increase (cf. item 8). Finally, carbonation may affect the results (item 6). The CO_2 content of some of the specimens was determined by thermogravimetric analysis after they were used in the experiments. Concentrations of CO_2, expressed as weight percentage of ignited weight, was found to be generally from about 2% or less and up to about 7% for the steam cured specimens used in the ADS series. Unless carbonation is concentrated in a

very thin layer at the disc surface, these CO_2 contents may be regarded as small. Pihlajavaara (1965) compared porosity and pore size distribution of non-carbonated and carbonated samples of hcp and found that carbonation decreased the total porosity and shifted the pore size distribution somewhat towards higher concentrations of fine pores. However, in Pihlajavaara's experiments the CO_2 content increased from 5% for what was referred to as non-carbonated paste to about 35% for the carbonated samples. Also, Winslow and Diamond (1970) checked the possible effects of carbonation on pore size distributions measured by mercury intrusion porosimetry. Samples were deliberately exposed to the atmosphere in an intermediate condition of dryness for about three weeks to insure maximum opportunity for carbonation to take place and were then dried and tested in the normal manner. Winslow and Diamond found no differences in the resulting pore size distributions when they compared with replicate samples that had only minimum possible exposure to the atmosphere.

III.7.3. Results

Each experiment yields eventually straight line relationships between weight gain and time, corresponding to the steady state. The water vapour flux J is obtained by dividing the slope of this line by the exposed disc area which was taken to be 2.5 cm^2. The mean permeability in the humidity interval in question is then obtained from eq. (III.23). The water vapour pressure difference over the disc is calculated from the humidities at the two faces, and the saturation water vapour pressure at the test temperature (= 23.76 torr at 25°C).

Examples of weight gain versus time results are shown on the two diagrams of fig. III.14. Each diagram represents one "experimental unit", which includes two companion specimens of w/c = 0.5, and two of w/c = 0.4, all either RT- or S-cured. Fig. III.14 shows runs with RT-cured pastes at an upstream humidity of h = 0.43, during adsorption (upper diagram) and desorption (lower diagram). The adsorption results show that the steady state was reached after 15-20 hours. In this case the specimens had been used in a previous experiment at h = 0.11, so that the period from 0 to 15-20 hours represents the transition from the steady state flow at the upstream humidity h = 0.11 to that of h = 0.43.

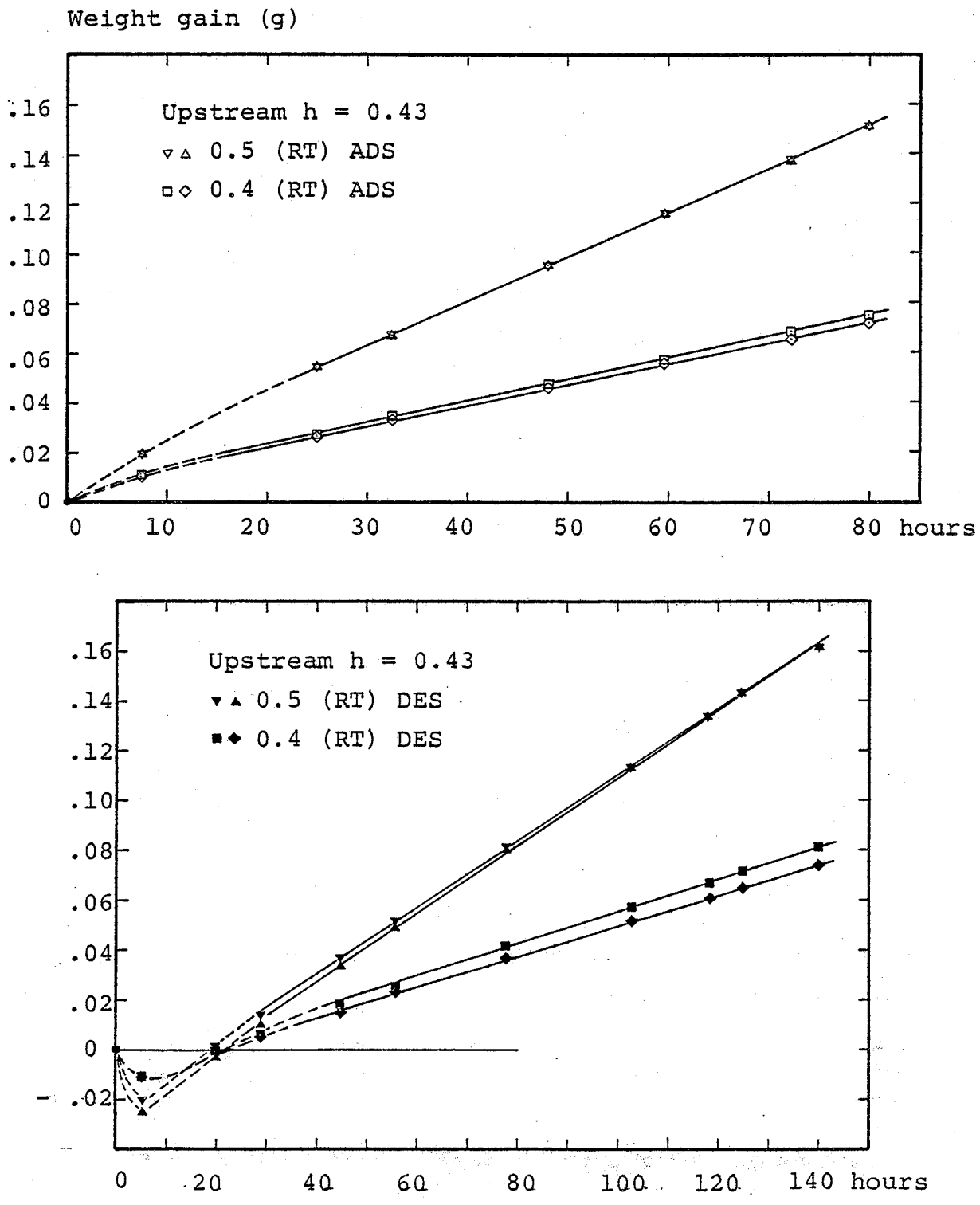

Fig. III.14. Examples of weight gain versus time results. RT-cured specimens, upstream humidity h = 0.43. Upper diagram: adsorption; lower diagram: desorption.

In general the magnesium perchlorate hydrate had to be renewed between two experiments. In the present work we were interested solely in the steady state transport. However, our apparatus design and experimental procedure could probably be further developed to permit systematic studies of the transient period as well.

The lower diagram of fig. III.14 shows the corresponding desorption results. As was the case for all desorption experiments the specimens were resaturated prior to use in the experiment. Although the first portion of the curves are not determined very accurately (the cups were in an upright position between the first two weighings, as noted previously) we can see that the water loss from the discs to the air stream exceeds the mass transport through the disc in the first period of exposure. The steady state was reached in this case after 30-40 hours.

The mean permeabilities obtained are shown in fig. III.15. As can be seen, in general the $\bar{\nu}$ values obtained from two companion specimens agreed very well. The reproducibility between experiments may be judged from the results of 6 identically performed experiments (0.5 (S) DES, upstream humidity 0.92) which showed a coefficient of variation for $\bar{\nu}$ equal to 6.8%.

Following the procedure described in section III.6.2 in order to evaluate the permeability as function of humidity, plots of $p_j \cdot \bar{\nu}_{oj}$ ($= L \cdot J_{oj}$) should be obtained. An example is shown in fig. III.16. Finally, these curves are differentiated to yield permeability as a function of (pore) vapour pressure. The results are shown in fig. III.17 as water vapour permeability versus humidity.

As stated in section III.2, the diffusion coefficient can be calculated from the water vapour permeability coefficient. The relation between permeability and diffusion coefficient is given by eq. (III.9). Transforming the permeability involves a differentiation of the appropriate sorption isotherm. In order

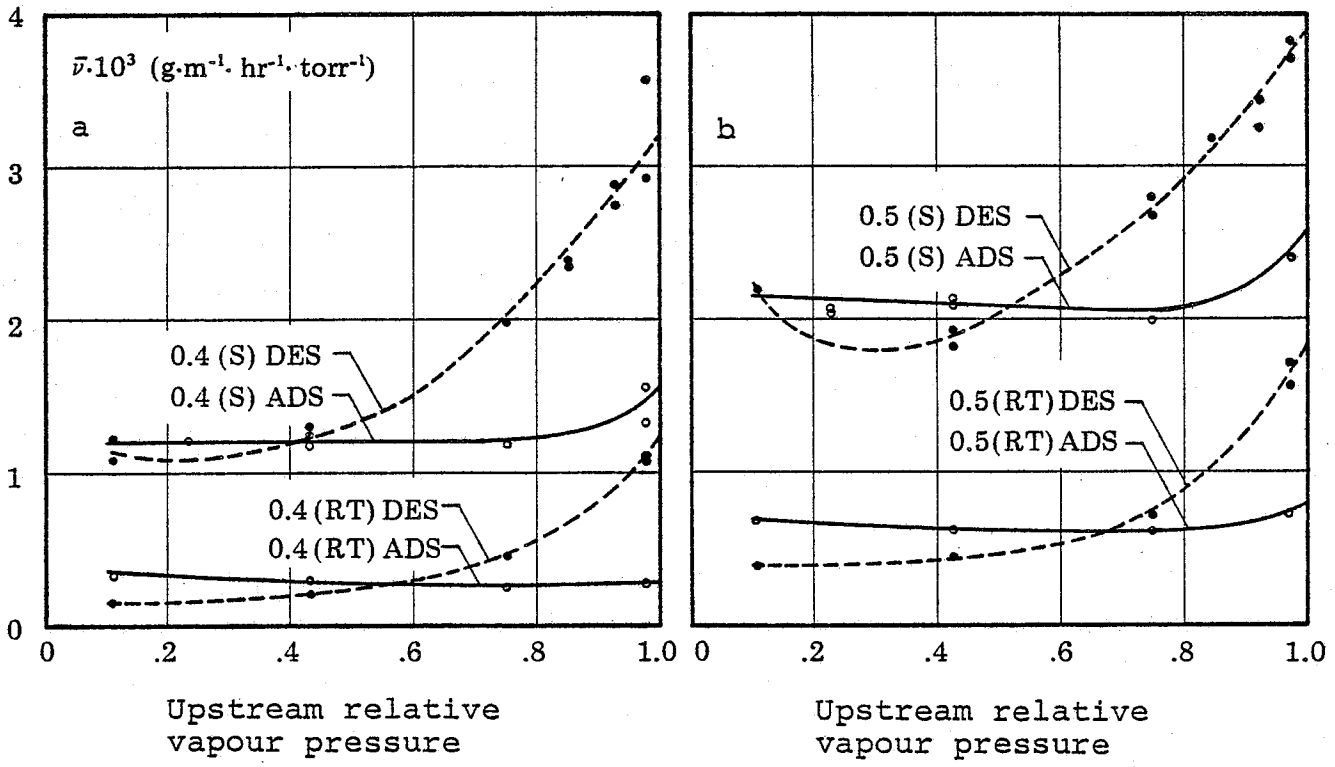

Fig. III.15. Mean permeabilities versus upstream humidity. a) w/c = 0.40, b) w/c = 0.50.

to make the present results comparable with some of the results reported in the literature, diffusion coefficients for the specimen types 0.5 (S), 0.4 (S), and 0.4 (RT) have been calculated. For the ADS permeabilities in fig. III.15 the adsorption isotherms in fig. II.6 were used, and for the DES permeabilities the corresponding desorption isotherms were used in the computation. The results are shown as plots of the calculated diffusion coefficients versus humidity in fig. III.18, and versus relative content of evaporable water in fig. III.19.

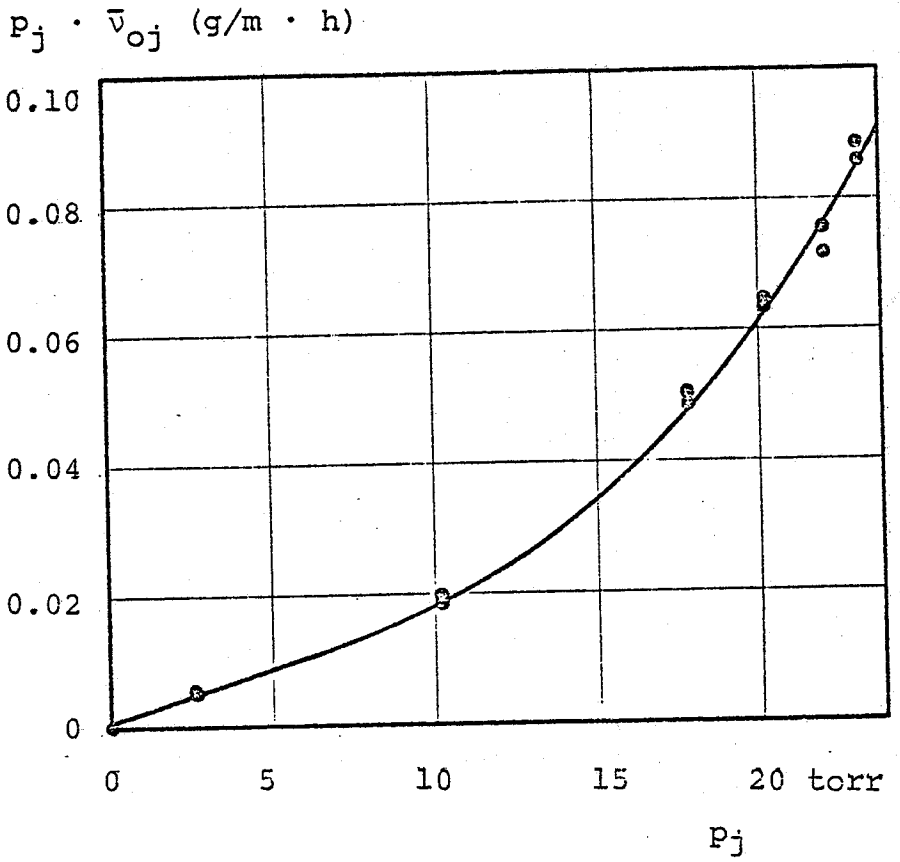

Fig. III.16. Example of a $p_j \cdot \bar{v}_{oj}$ versus p_j relationship. (0.5 (S) DES).

Permeability

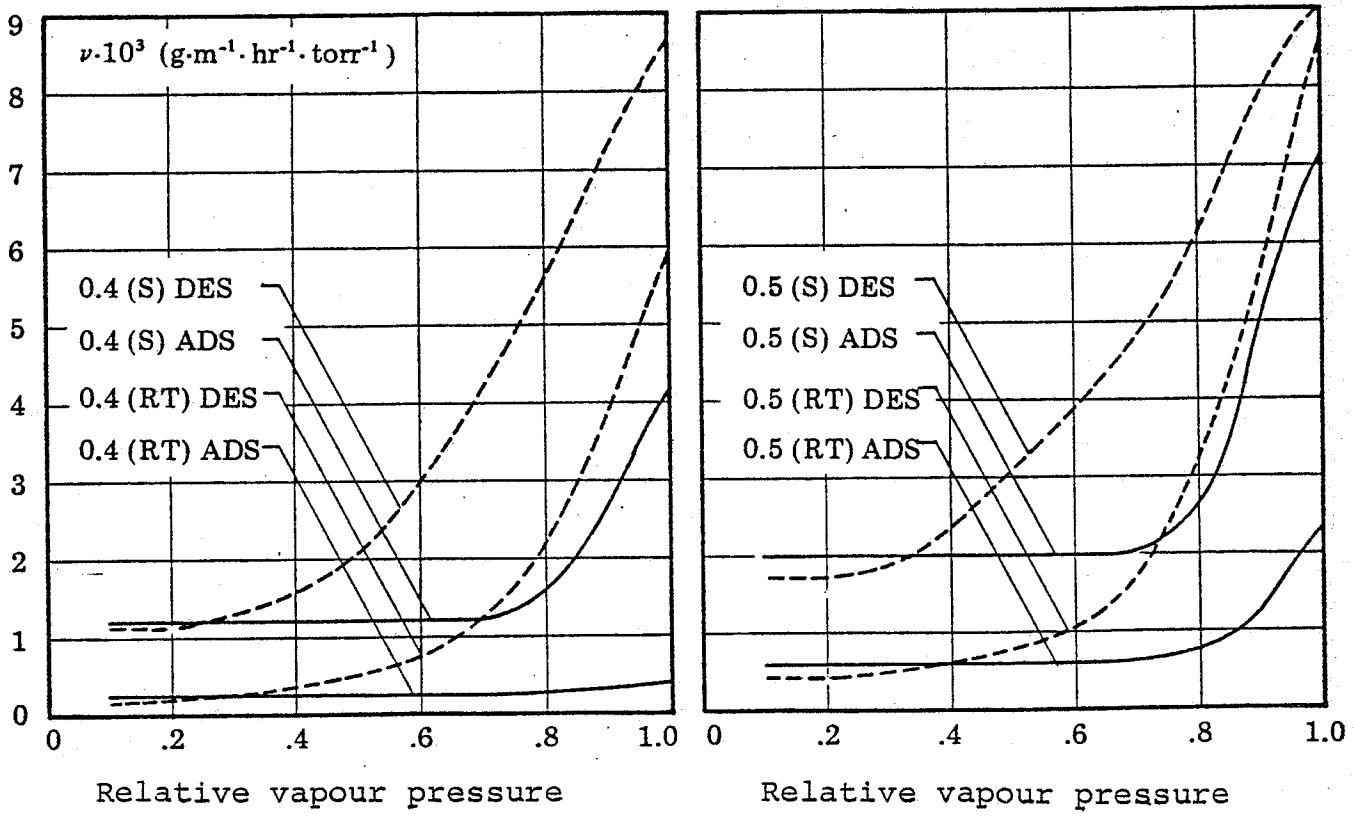

Fig. III.17. Water vapour permeability as a function of humidity.

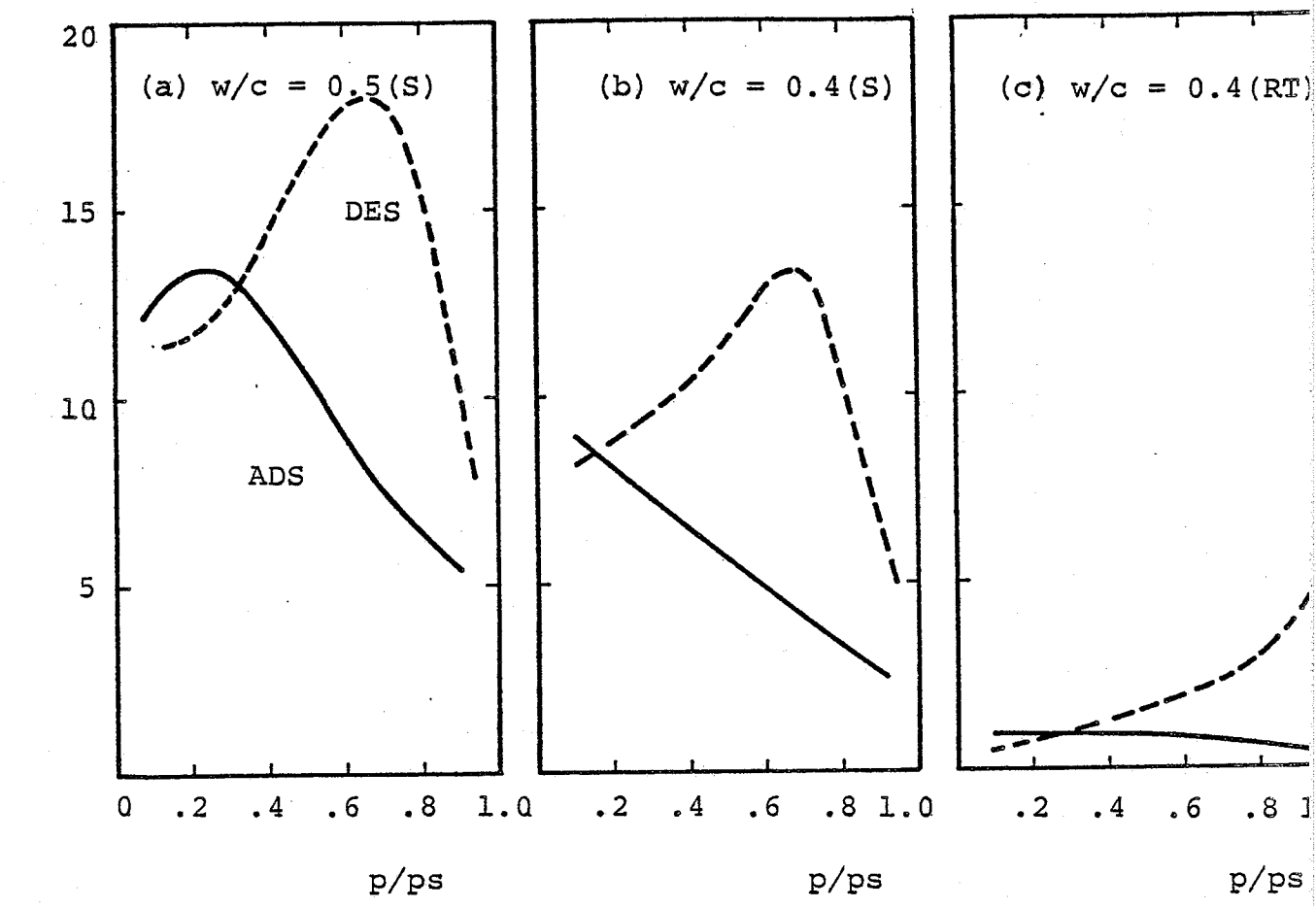

Fig. III.18. Calculated diffusion coefficients versus humidity. (p/ps

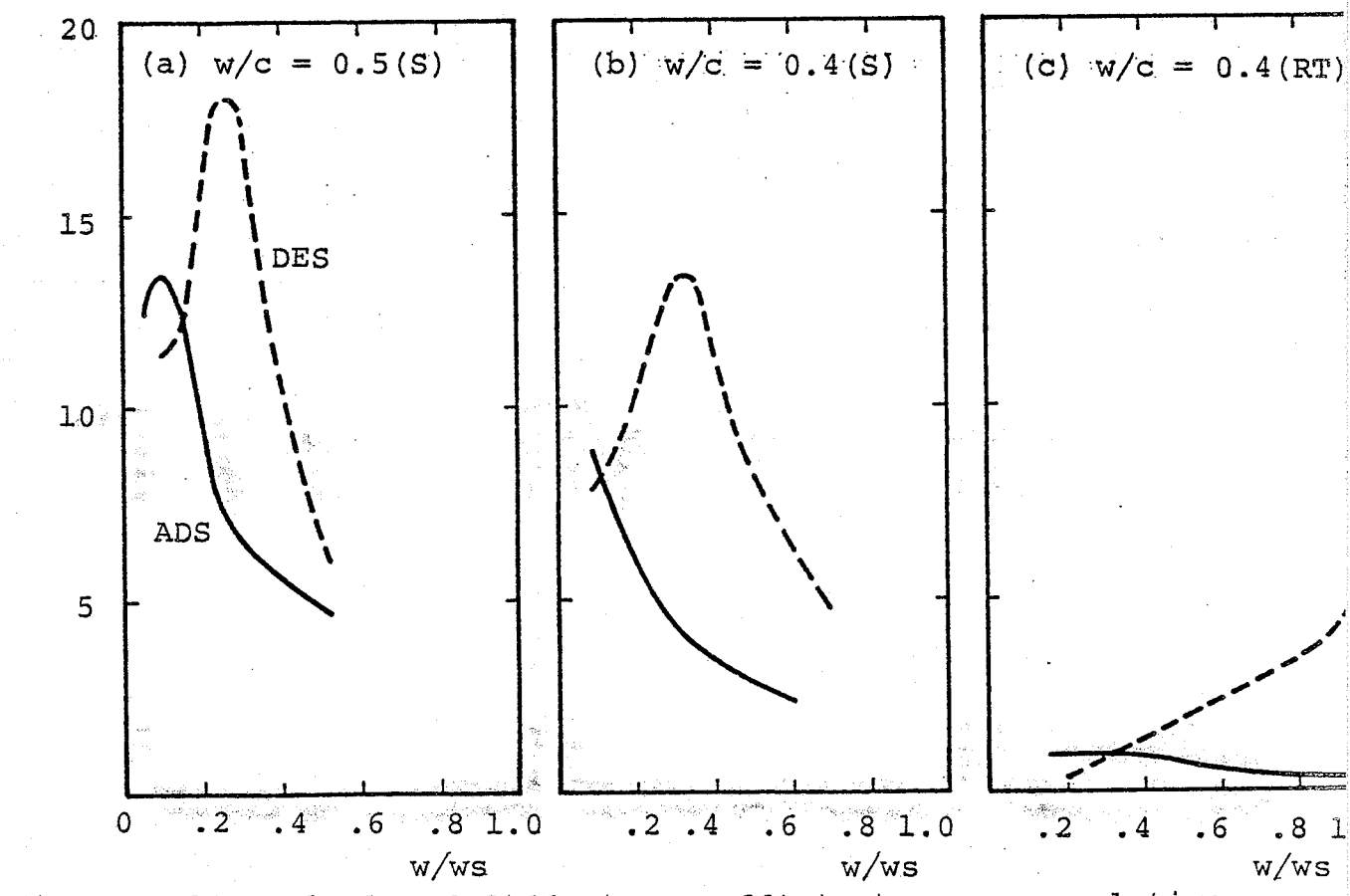

Fig. III.19. Calculated diffusion coefficients versus relative content of evaporable water. (w/ws)

III.7.4 Discussion of results

The most striking features of the main results in fig. III.17 are the strong dependence of water vapour permeability on humidity, and the great difference between permeabilities measured in adsorption and in desorption which may be referred to as permeability hysteresis. We shall discuss the various characteristics separately below.

a) The strongest variation of permeability with humidity is registered in desorption. The effect is substantial, ranging from about an eight-fold decrease in permeability for the S-cured pastes to about a thirty-fold decrease for the RT-cured paste when going from near saturation to a humidity of 0.20. Corresponding variations in adsorption are smaller.

b) There seems to be a very marked difference between adsorption and desorption permeabilities. Adsorption permeabilities are lower than corresponding desorption values over practically the entire humidity range. The adsorption permeabilities are remarkably independent of humidities less than about 0.70 which results in a substantial "permeability hysteresis".

c) Raising the water/cement ratio from 0.40 to 0.50 increases the permeability at lower humidities approximately by a factor of 2. In the same humidity range S-curing is seen to produce permeabilities about four times those of RT-cured specimens. In the subsequent chapter we shall try to interpret these observations in terms of pore structure.

By reference to the various presentations of our results we can make some comparisons with both permeability and diffusion results from other sources as described earlier.

Nilsson's results regarding the water vapour permeability of cement mortar (fig. III.10) with w/c = 0.40 can be compared with the 0.4 (RT) DES curve in fig. III.17. The two curves have much the same shape, but our permeabilities for hardened cement paste are about 2-3 times higher than those for the mortar. However, as we discussed previously we do not know whether the

difference hcp/mortar can contribute to explain the difference in permeabilities. A further difference between the two materials which could be mentioned in this connection is that our specimens were dried prior to use. According to Powers et al. (1955) this may considerably increase the permeability (cf. section III.4).

The mean permeabilities $\bar{\nu}$ reported by Wierig (1965) (cf. section III.6.4) included a set of results which may be compared with data from this project: for a cement mortar of w/c = 0.40 permeabilities at upstream humidities 0.95 and 0.50 were $\bar{\nu} = 0.42 \times 10$ and 0.07×10^{-3} g/m · h · torr, respectively. By reference to the 0.4 (RT) DES curve in fig. III.15 we find that Wierig's permeabilities are about half of those found in the present work.

In fig. III.19 the water vapour permeabilities have been converted to diffusion coefficients and plotted against the relative content of evaporable water. Some of these curves appear on the common plot in fig. III.8 to facilitate comparison with results obtained from other sources. The shape of the curves for the steam cured specimens, with a distinct maximum at some intermediate humidity, is similar to the shape of Bray's and Pihlajavaara's curves, which was discussed further in section III.5. Bray's results (curves 5 and 6 in fig. III.8) refer to cement pastes cured in a way similar to the S-curing used in this project. Furthermore, Bray performed these experiments at 45°C, which yields diffusion coefficients that are higher than those obtained at 25°C. On that background it is clear that the diffusion coefficients for the steam cured specimens in the present work are considerably higher than those reported by Bray.

In the next chapter we shall consider the water vapour permeability results in relation to the pore structure of the hcp specimens.

IV. PERMEABILITY IN RELATION TO PORE STRUCTURE

Mass transport in microporous solids is a complicated process which does not generally yield itself to rigorous analysis. The theoretical difficulties arise firstly from the interaction of different transport mechanisms acting in various series-parallel combinations, and secondly from difficulties associated with a realistic, and yet tractable, description of the pore structure as regards sizes, geometry and spatial distribution.

Most methods of pore structure analysis, for example MIP, at best yield pore size distribution functions based on assumed pore geometries. The spatial distribution of the pores, as an important requirement for realistic modelling, is not obtained by any of these methods.

One is, therefore, reduced to simple models with limited goals. This sort of theoretical analysis can, at best, be a semi-quantitative aid in identifying the flow mechanisms, and perhaps even in elucidating certain aspects of the pore structures.

With these reservations, we will attempt below to analyse the results in terms of an appropriate model.

IV.1. Flow in a single pore

Following Radjy (1974), consider in detail the transport of moisture through a circularly cylindrical pore in a steady state isothermal situation.

Assume that the transport occurs by a combination of any of the following mechanisms: a) Knudsen flow; b) surface diffusion; c) capillary suction. We will neglect the contributions due to Poiseuille flow in the vapour phase, implying that the pore diameter is sufficiently small compared to the mean free path of water molecules. The analysis is performed for steady state transport through the pore with an imposed relative vapour pressure of zero at the downstream end, while the upstream relative vapour pressure is varied from zero to unity. These boundary conditions make the results compatible with the type of experiments con-

sidered herein.

Consider a pore of radius, R, and length, L, as shown in fig.IV.1.

Prior to considering moisture transport through such a pore in terms of mechanisms, treat the pore as a black box, moisture conducting device. The mean (PV-) permeability, $\bar{K}_{13}$, is defined by (cf. eq. III.4):

$$\bar{P}_{13}^{g} \cdot q_{13} = \bar{K}_{13} \frac{\Delta P_{13}^{g}}{L} \qquad \text{(IV.1)}$$

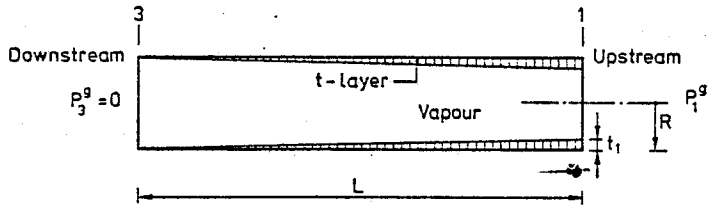

Fig. IV.1. Cylindrical pore with adsorbed t-layer prior to capillary condensation. The t-profile need not be linear.

where $\bar{P}_{13}^{g}$ is the mean vapour (gas) pressure across the "13"-section, q_{13} the linear flow velocity (cm sec^{-1}) or the volume flux ($cm^3 \cdot cm^{-2}$ sec^{-1}), referred to the mean pressure $\bar{P}_{13}^{g}$, $\bar{P}_{13}^{g} \cdot q_{13}$ the overall flux in pressure-volume (PV) units, and $\Delta P_{13}^{g} = P_1^{g} - P_3^{g}$.

Now referring to fig. IV.1 start with both the downstream and the upstream sides at a vapour pressure of zero. As the upstream pressure is gradually increased, during an initial period prior to capillary condensation, the situation in fig. IV.1 will develop; the pore will conduct moisture by surface diffusion through the t-layer and by Knudsen flow through the vapour phase. It is shown elsewhere (Radjy (1974)) that the permeability coefficient $\bar{K}_{13}^{o}$ - the superscript "o" denoting the lack of capillary condensation - is given by:

$$\bar{K}_{13}^{o} = \Omega_{13} K_{o}^{g} \qquad \text{(IV.2)}$$

where K_o^g is the uncorrected Knudsen flow permeability - as if there were no pore blocking and no surface diffusion, and Ω_{13}, the so-called "surface factor", is a correction term accounting

for deviations from simple molecular flow. Surface adsorption in a pore reduces the Knudsen contribution to flow due to pore blocking, while increasing the surface diffusion contribution. Both of these effects are expressed in terms of Ω. The surface factor is in general a function of the pore size, R, and the surface diffusion coefficient D^{σ},cf. eq.(III.10). Computations have been performed (Radjy (1974)) for R and D^{σ} in ranges from 20 to 1000Å and 10^{-8} to 10^{-3} cm^2 sec^{-1}, respectively, and show that Ω ranges correspondingly from approximately 0.7 to 5000. The surface factor is more sensitive to D^{σ} for the smaller pore sizes, since both the pore blocking and the surface diffusion effects are more important for such pores. For a very small pore, and a completely immobile t-layer ($D^{\sigma} = 0$), pore blocking will be most efficient with Ω approaching to zero. On the other hand as the t-layer becomes more mobile ($D^{\sigma} > 10^{-6}$ $cm^2 \cdot sec^{-1}$), surface diffusion can more than compensate for pore blocking resulting in large values of Ω. ($\Omega = 5050$, for $R = 20$Å and $D^{\sigma} = 10^{-3}$ cm^2 sec^{-1}). In situations where pore blocking is to a large extent compensated for by surface diffusion or in large pores where surface effects are not important, Ω will be of the order of unity. The computations referred to previously show that for D^{σ} and R in the respective ranges from 10^{-8} to 10^{-6} cm^2 sec^{-1} and 20 to 1000Å, Ω is of the order of unity.

In the absence of any precise experimental information regarding D^{σ}, and noting from fig. II.15 that much of the pore space corresponds to a size less than 1000Å, we will as a first approximation assume that $\Omega \simeq 1$. Accordingly, eq. (IV.2) reduces to

$$\bar{K}^{o}_{13} = \bar{K}^{g}_{o} \qquad \text{(IV.3)}$$

where the Knudsen permeability is given by eq. (III.17)

$$K^{g}_{o} = \frac{2}{3} \bar{v} R = \frac{2}{3} R \sqrt{\frac{8\mathcal{R}T}{\pi M}} \qquad \text{(IV.4)}$$

where $\bar{v}$ is the mean thermal velocity of the gas molecules, $\mathcal{R}$ is the gas constant, T the absolute temperature and M the molecular weight.

Next consider the influence of capillary condensation on the transport process. Let h_R be the critical relative vapour pres-

sure above which capillary condensation is expected to occur in the pore in question. Once the upstream relative vapour pressure, h_1, has exceeded h_R, a meniscus will advance into the pore from the upstream side, as depicted in fig. IV.2. Moisture conduction is now by a compound series/parallel process: capillary suction in the "12" section in series with parallel transport occuring in the vapour phase and the t-layer in the "23" section. The mean permeability $\bar{K}_{13}$ is now written as (Radjy (1974)):

$$\bar{K}_{13} = \alpha \, \bar{K}^{o}_{13} \qquad \text{(IV.5)}$$

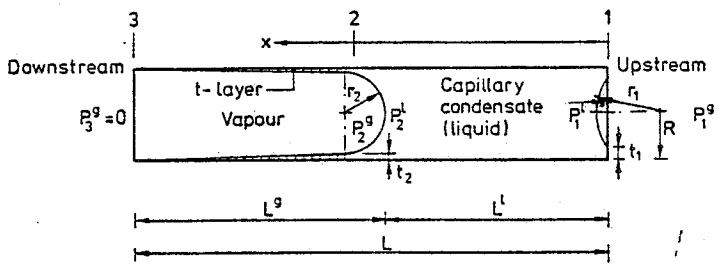

Fig. IV.2. Pore of fig.IV.1 after capillary condensation. The t-profile need not be linear.

where α is the flow amplification factor due to capillary suction. With the simplifying assumption that $\Omega \simeq 1$, eqs. (IV.3) to (IV.5) can be combined to obtain

$$\bar{K}_{13} = \frac{2}{3} \bar{v} \, \alpha \, R \qquad \text{(IV.6)}$$

and by using the theory developed elsewhere (Radjy (1974)), α is given by ($\Omega \simeq 1$):

$$\alpha = (1 + \frac{1}{\beta}) \frac{h_R}{\Delta h_{13}} \qquad \text{(IV.7)}$$

where $\beta = L^g/L^l$ - refer to fig. (IV.2), is given by:

$$\beta = \frac{16 \eta^l \bar{v} \, P_s^g}{3} (\frac{v^l}{RT})^2 \cdot \frac{1}{R} \cdot \frac{h_R}{\ln(h_1/h_R)} \qquad \text{(IV.8)}$$

where η^l is the viscosity of the capillary condensate, P_s^g the saturation vapour pressure, h_1 the upstream relative vapour pressure, and the other parameters have already been defined.

The amplification factor can range from unity (no capillary condensation) to order of over one thousand when the surface factor is unity (cf. fig. IV.3).

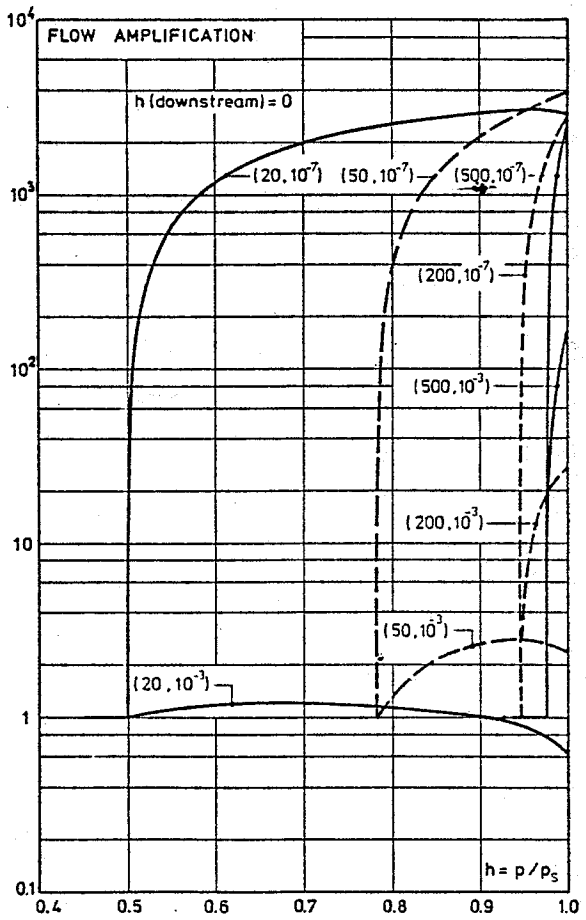

Fig. IV.3. Flow amplification factor as a function of the upstream relative vapour pressure. In parantheses: pore radius in Å, surface diffusion coefficient in cm^2/sec. (From Radjy (1974)).

IV.2. Flow through a distribution of pores

Having developed the basic relationships for flow through a single idealized pore next we consider parallel, non-interacting flow through a distribution of such idealized pores.

Consider a disc of thickness L and total cross-sectional area A_t exposed to flow. The total flow in mass units per second is given by (cf. eq. III.4 and III.7)

$$Q = A_t \frac{M}{\mathcal{R}T} \bar{K} \frac{\Delta P_{13} g}{L} \qquad \text{(IV.9)}$$

where $\bar{K}$ is the overall mean PV-permeability, and the subscripts 1 and 3 denote, respectively, the upstream and the downstream faces, as previously.

The flux, J_R, through a given pore of radius R and effective length L_e (tortuosity effect, L_e is greater than L if the pore is not straight) is given by

$$J_R = \frac{M}{\mathcal{R}T} \bar{K}_R \frac{\Delta P_{13} g}{L_e} \qquad \text{(IV.10)}$$

where $\bar{K}_R$ is the mean permeability for the pore in question.

The permeability $\bar{K}_R$ is identical with $\bar{K}_{13}$ of eq. IV.6.

Let G (R) be the pore volume cumulative distribution function (not normalized) per unit of total bulk volume. The cross-sectional area of pores in the size range from R to R +dR equals

$$LA_t \left(\frac{dG}{L_e} \right).$$

Hence, the total flow as a sum of the contributions by the individual pores is given by

$$Q = \int_{o}^{G_o} LA_t J_R dG/L_e \qquad \text{(IV.11)}$$

where G_o is the porosity. Eqs. (IV.9) to (IV.11) yield:

$$\bar{K} = \frac{1}{\kappa_t^2} \int_{o}^{G_o} \bar{K}_R dG \qquad \text{(IV.12)}$$

where $\kappa_t = L_e/L$ is the tortuosity factor.
By using eq. (IV.12) together with eq. (IV.6) and an appropriate pore size distribution function we are now in a position to compute $\bar{K}$. Generally the integral of eq. (IV.12) must be evaluated in two parts as:

$$\kappa_t^2 \cdot \bar{K} = \frac{2}{3} \bar{v} \int_{o}^{G^*} \alpha R \cdot dG + \frac{2}{3} \bar{v} \int_{G^*}^{G_o} R dG \qquad \text{(IV.13)}$$

where G^* is the pore volume with capillary condensate, and the second integral is the volume average pore size in the volume range from G^* to G_o. Prior to capillary condensation, therefore, the permeability is simply proportional to the volume average pore size.

IV.3. Analysis of results

In the previous section we arrived at an expression for computing the PV-permeability coefficient as a function of upstream humidity in a situation similar to that in the cup experiments, assuming a very simple model of the pore space.

In order to evaluate the permeability we need an appropriate pore volume distribution function. Pore size distributions obtained from sorption isotherms (fig. II.16) cover only pores of radii less than 1000Å and include only three specimen types. In addition, as was discussed earlier (section II.4.1.5) there is some uncertainty regarding the distribution curves at small radii. Consequently, the volume cumulative distribution functions obtained from mercury intrusion porosimetry were used in the computations.

Eq. (IV.13) together with eqs. (IV.7) and (IV.8) form the basis of the calculation. In the following the procedure for calculating the permeability at a given upstream humidity h_1 is illustrated.

First, the radius R^* at which the onset of capillary condensation occurs is calculated using the Kelvin equation (eq. II.5 with $\theta = 0$) with a "Kelvin radius" corrected for the adsorbed t-layer as obtained from fig. II.9, in a way similar to the procedure used in the pore structure analysis in section II.4.1.4 (cf. eqs. II.7 and II.8). The corresponding value of the distribution function is G^*. If h_1 has a value so that the calculated R^* is less than the smallest pore size included, G^* is set equal to zero. Once R^* and G^* is computed for the upstream humidity in question, the integrals in eq. IV.13 are easily evaluated numerically.

Such calculations were performed using the volume cumulative distribution functions in fig. II.18 including pore radii between 25Å and 30,000Å. The following values of the various constants appearing in the relevant equations were

$$
\begin{aligned}
T &= 298\ ^{o}K \\
\eta^{l} &= 8.904 \times 10^{-3}\ g/sec.\ cm \\
\mathcal{R} &= 8.314\ J/mole \cdot deg. \\
v^{l} &= 18\ cm^{3}/mole \\
p_s^{g} &= 23.76\ torr \\
\bar{v} &= 5.91 \times 10^{4}\ cm/sec. \\
M &= 18\ g/mole
\end{aligned}
$$

The computations yield values of $\kappa_t^2 \cdot \bar{K}$. From eq. III.7,

$$\nu = \frac{M}{\mathcal{R}T} K$$

Hence,

$$\kappa_t^2 \bar{\nu}\ (g/m \cdot h \cdot torr) = 0.350\ \kappa_t^2 \bar{K}\ (cm^2/sec.)$$

The results are shown in fig. IV.4 as plots of computed values of $\kappa_t^2 \bar{\nu}$ versus upstream humidity, together with the experimental results reproduced from fig. III.17 and a set of curves to which we will return later.

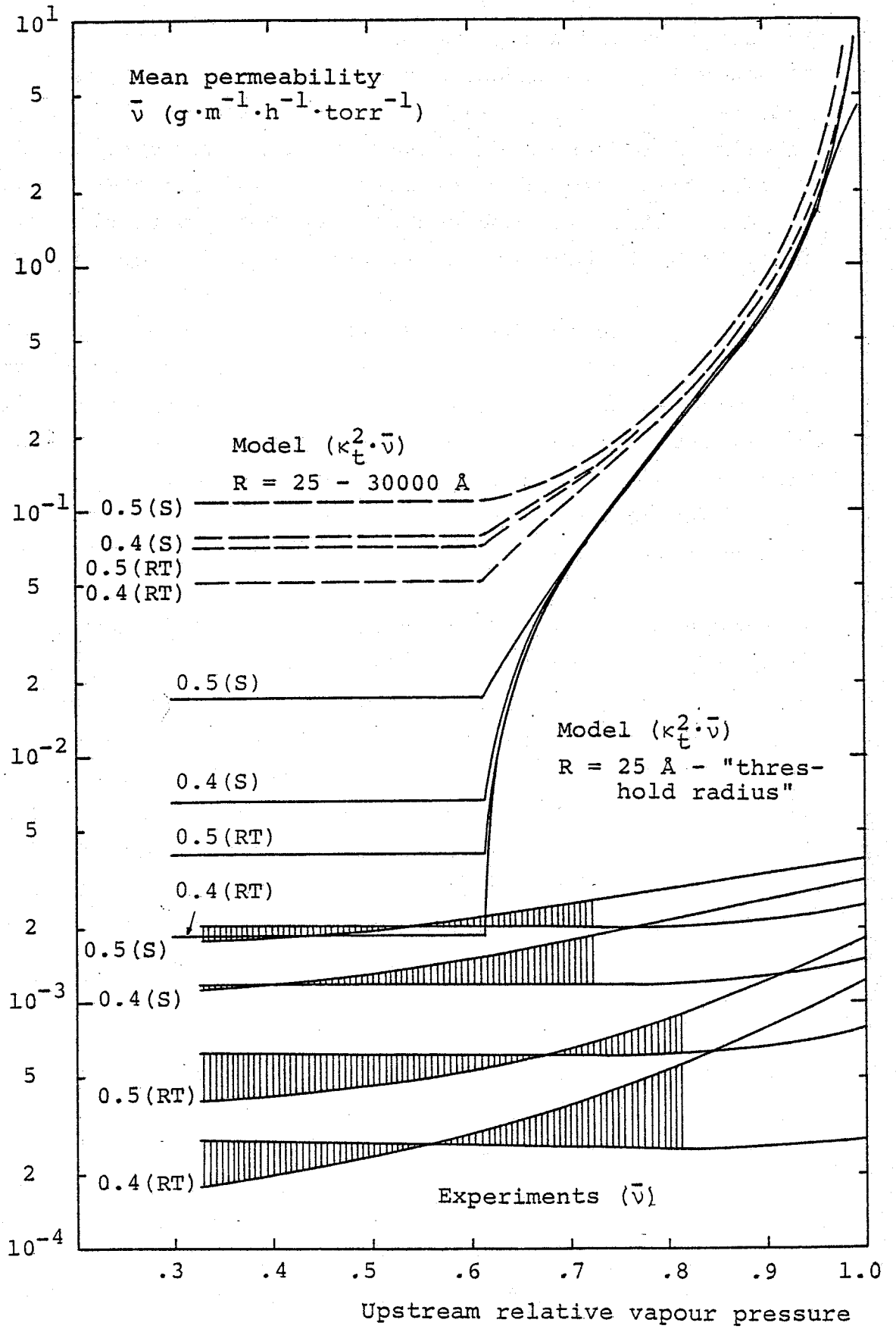

Fig. IV.4. "Model" and experimental permeability coefficients versus upstream humidity.

IV.4. Discussion and conclusion

The calculated mean permeabilities for the four specimen types, calculated by including the entire range of pore radii from the MIP analysis as continuous pores in the model, appear as the upper set of curves in fig. IV.4. As a matter of fact, the requirement for Knudsen flow that the pore diameter is less than the mean free path of water molecules (of the order 1000Å at 25°C and 1 atm.) is violated for the major part of the pore space. We will, however, ignore that for the time being.

At lower humidities the curves are characterized by a constant $\bar{\nu}$ value. At about h = 0.60 Kelvin capillary condensation(KCC) is assumed to occur in the smallest pores encountered (R = 25 - 30Å), giving rise to a considerable increase in the transport coefficient. The effect of capillary condensation is progressively increased with upstream humidity as condensation occurs in pores of still larger radii.

A comparison between the calculated "model" permeabilities, and the experimental ones shows that the two sets of curves share some qualitative features. The experimental adsorption permeabilities, when interpreted by reference to the theory outlined in section IV.1, suggest that capillary flow does not become active until an upstream humidity of about 0.80. The experimental desorption curves indicate that capillary flow takes place at lower relative humidities. However, the model predicts permeabilities some orders of magnitude higher than those found experimentally. This discrepancy will be discussed in the following.

One of our assumptions in deriving the expression for flow in a single capillary was that prior to KCC the flow contribution from surface diffusion is just balanced by the partial pore blocking effect of the adsorbed surface layer. Consequently, flow in pores empty of capillary condensate is calculated as if Knudsen flow were solely responsible for flow in the unblocked pore. As we have noted in section IV.2 the permeability in the absence of KCC is thus proportional to the volume average pore size. Hence, by reference to the cumulative distribution curves in fig. II.18 it is evident that the computed Knudsen $\bar{\nu}$ values are dominated by contributions from the largest pores.

The enhancement of flow due to KCC, however, largely depends on the amount of small pores: at $h_1 = 0.95$ only pores with radii less than about 200Å contain capillary condensate. If we assume that only the finer pores are continuous, and consequently use only the first portion of the distribution functions, the model would predict lower Knudsen permeability, whereas enhancement due to KCC remains largely unchanged. We will persue this point a little further.

The mercury intrusion data provide some information about the size of continuous pores. As discussed previously (section II.4.2.5) a "threshold radius" is displayed, below which a comparatively great portion of mercury intrusion commences. Winslow and Diamond (1970) interpreted the threshold radius as representing the minimum radius of pores which are geometrically continuous throughout all regions of the hydrated cement paste, and presented various pieces of evidence in favour of this interpretation (cf. section II.4.2.5). Thus, it seems justifiable to base the calculations on pores of radius less than the threshold radius.

Only the 0.4 (RT) specimen type shows a relatively well defined threshold radius. For the other specimen types the threshold radii were estimated from the point of intersection between straight lines drawn to touch the curves at each side of the knee. This yields for the four specimen types 0.5 (S), 0.4 (S), 0.5 (RT), and 0.4 (RT) about 2000Å, 800Å, 450Å, and 300Å, respectively. A new computation, using the previous model and including only pores of radii less than the threshold radius, yields the result shown in fig. IV.3 as the set of dotted curves.

As we would expect, the Knudsen permeabilities are signigicantly lower than those found in the first computation, whereas the excess flow due to KCC is nearly unchanged. Also, the size of pores involved in this computation is less than or at least comparable to the mean free path of water vapour as required for Knudsen flow.

At lower humidities the model now predicts permeabilities about one order of magnitude above those found experimentally.

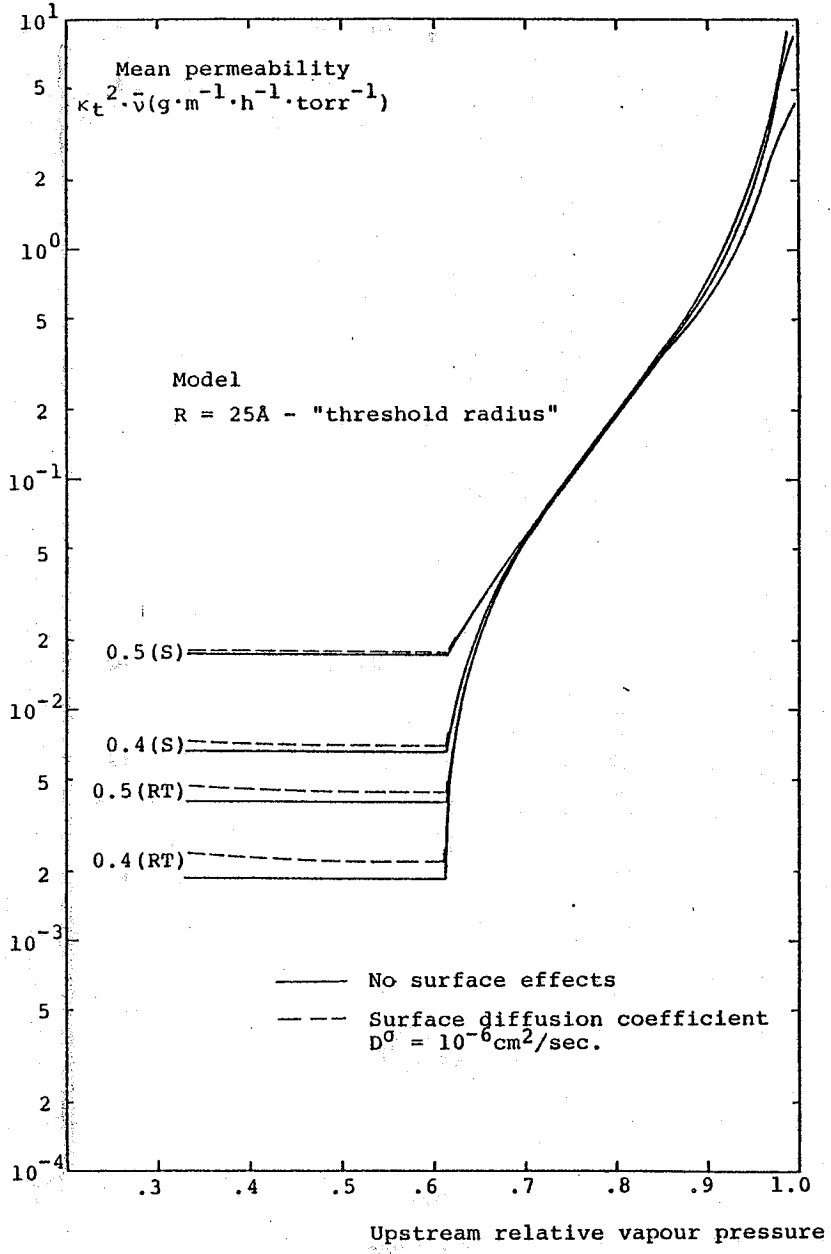

Fig. IV.5. "Model" permeability coefficients. Influence of surface effects.

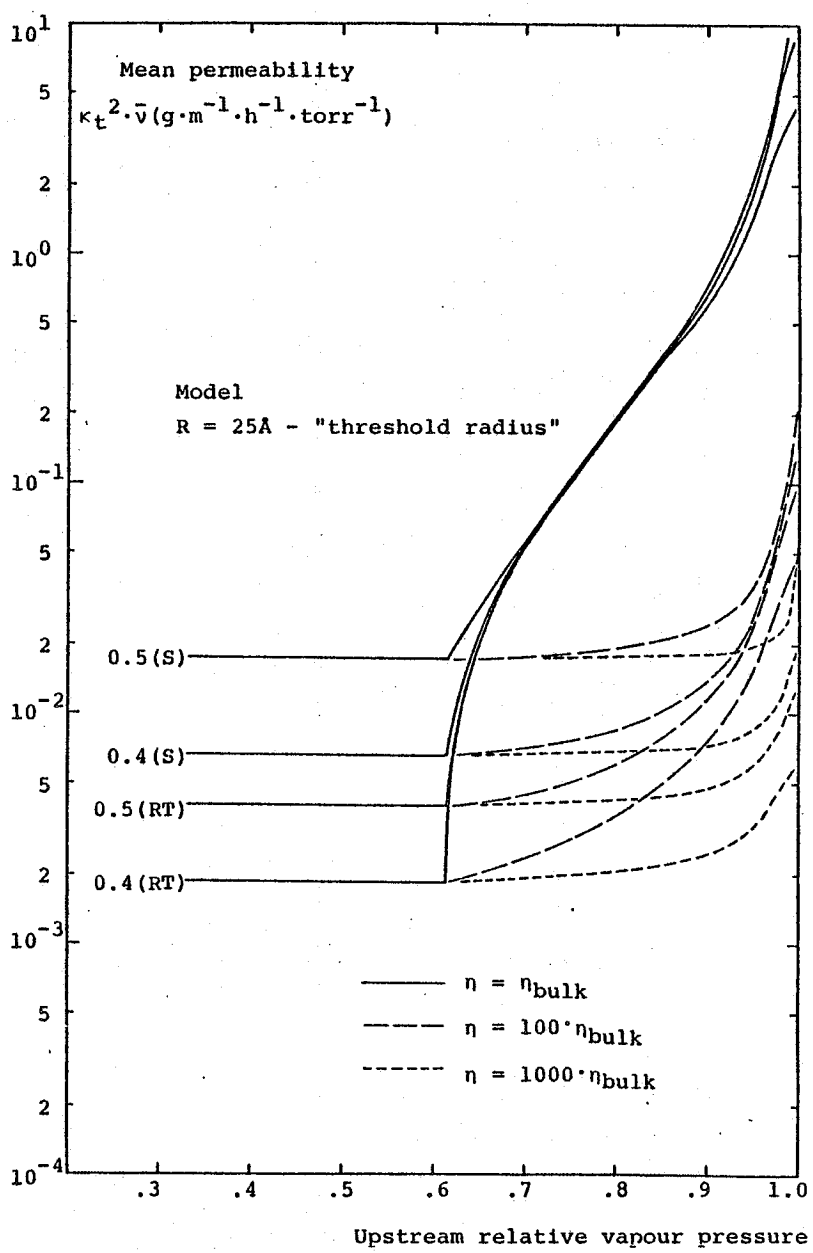

Fig. IV.6. "Model" permeability coefficients. Effect of water viscosity.

derived from the MIP distribution curve, is assumed to reside in straight, continuous parallel pores lined up in the direction of flow. If the pores are not straight throughout the specimen thickness L, but follow a tortuous path of length L_e, the model should lead to an overestimation of the permeability. This overestimate is compensated for by multiplying the permeability, calculated according to the straight pore model, by $(1/\kappa_t)^2 = (L/L_e)^2$, as shown previously. In the Knudsen range, tortuosity factors $\kappa_t = (L_e/L)$ about 3 are required in order to make the calculated and experimental permeabilities coincide. In the KCC range, the required tortuosity factors are even higher. Although tortuosity values of 3 and above have been reported for consolidated media (Carman (1956)), it is difficult to visualize paths of lengths several times the specimen thickness. Anyhow, tortuosity alone is not believed to be responsible for the observed discrepancies.

The model pore system is derived from mercury intrusion data. "Blind" pores are penetrated by mercury and are consequently part of the model pore system, but such pores do not contribute to flow. The "model" permeabilities are therefore overestimates. Furthermore, the MIP data were obtained from powders. As we discussed in section II.4.2.5, this procedure results in distribution curves with higher concentrations of large pores than tests seen on bulk samples.

Summarizing, we are in general forced to conclude that our simple pore model is inadequate to explain the permeability behaviour of a system as complicated as the system hcp-water. However, the model seems to be able to provide some qualitative information. The model predicts an enhancement of flow in the capillary condensation range, although far beyond that observed experimentally. At lower humidities, however, calculated permeabilities are "only" about one order of magnitude higher than experimental values for all specimen types when pores included in the computation are limited by an upper size determined from mercury intrusion data. This, together with the observation that calculated and experimental permeabilities at low humidities occur in the same order of sequence among the four specimen types suggests that the MIP pore size distributions is an indicator of water vapour permeability of hcp.

RESUMÉ

Det centrale formål med nærværende projekt har været at etablere systematiske vanddamppermeabilitetsdata for veldefinerede prøver af hærdnet cementpasta, samt ved anvendelse af generelle principper for fugttransport i porøse materialer at tilstræbe en forklaring af resultaterne på baggrund af materialets porestruktur.

De anvendte prøver af hærdnet cementpasta omfatter fire typer, beskrevet ved to vand-cement forhold - 0.40 og 0.50, og to hærdeprocesser - vandlagring ved stuetemperatur og damphærdning ved 97°C.

For karakterisering af de fire prøvetyper er der gennemført porestrukturanalyser baseret på såvel sorptionsisotermer som kviksølvpenetrationsporøsimetri.

De hærdnede pastaers vanddamppermeabiliteter er opnået gennem måling af stationær fugttransport ved den såkaldte "skålmetode". Hver måling resulterer i en middelværdi for permeabiliteten over det aktuelle fugtighedsområde. Det vises, hvorledes en serie af enkeltforsøg dækkende hele området af fugtigheder fra 0 til 1 danner grundlaget for udledning af de grundlæggende, fugtighedsafhængige permeabiliteter. For de fire prøvetyper er der etableret permeabilitetsdata af denne art. Forsøgene omfattede både prøver i oprindelig udtørret tilstand (adsorption) og prøver, som var i en oprindelig vandmættet tilstand (desorption).

Vanddamppermeabiliteten fandtes generelt at afhænge både af fugtigheden og af prøvens oprindelige fugttilstand. For alle prøvetypernes vedkommende var adsorptions-permeabiliteterne bemærkelsesværdigt konstante indtil en fugtighed på omkring 0.7, medens desorptions-permeabiliteterne udviste en jævn stigning med fugtigheden. Idet yderligere desorptions-permeabiliteterne fandtes at være betydeligt større end adsorptionsværdierne, udviser prøverne "permeabilitets-hysterese". Den absolutte størrelse af permeabiliteterne strækker sig over et område af cirka 2 størrelsesordener, fra 10^{-4} til 10^{-2} g · m^{-1} · h^{-1} · torr^{-1}. De fundne resultater er diskuteret i relation til litteraturstudier ved-

rørende såvel diffusions- som permeabilitetsmålinger.

Endelig er der gennemført en analyse af resultaterne i relation til materialets porestruktur ved at anvende generelle principper for fugttransport på en simpel model baseret på kviksølvpenetrationsdata. Skønt det viser sig, at denne model ikke er tilstrækkelig til at beskrive permeabilitetsopførslen i et så kompliceret system som hærdnet cementpasta-vand, giver modellen dog værdifuld kvalitativ information.

REFERENCES

ASTM
1974a "Water vapor transmission of materials in sheet form". ASTM Designation E 96-66, Annual Book of ASTM Standards

ASTM
1974a "Test for water vapor transmission of thick materials". ASTM Designation C 355, Annual Book of ASTM Standards

Auskern, A., and Horn W.
1973 "Capillary porosity in hardened cement paste". Journal of Testing and Evaluation, vol. 1 no. 1, pp. 74-79

Bager, D.H., and E.J. Sellevold
1975 "Mercury porosimetry of hardened Cement Paste: The influence of Particle size". Cement and Concrete Research, vol. 5, pp. 171-178

Barrer, R.M.
1967 "Surface and volume flow on porous media" In: "The solid-gas interface", E. Alison Flood (ed.), vol. II, pp. 557-609, Marcel Dekker, New York

Bazant, Z.P., and L.J. Najjar
1972 "Nonlinear water diffusion in nonsaturated concrete". Materiaux et Construction, vol. 5 no. 25, pp. 3-20

Bazant, Z.P., and L.J. Najjar
1972 "Drying of concrete as a nonlinear diffusion problem". Cement and Concrete Research, vol. I, pp. 461-473

Bray, W.H.
1969 "Diffusion of water in hardened portland cement paste". Ph. D. Thesis, Stanford University, Department of Civil Engineering, Stanford, California, Technical Report no. 112

Brunauer, S., P.H. Emmett, and E. Teller
1938 "Adsorption of gases in multimolecular Layers". Journal of American Chemical Society, vol. 60. p. 309

Brunauer, S., and S.A. Greenberg
1960 "The hydration of tricalcium silicate and β-dicalcium silicate at room temperature". Research Department Bulletin no. 152, Portland Cement Association, Chicago.

Brunauer, S., and L.E. Copeland
1963 "Physical adsorption of gases and vapors on solids". ASTM Special Technical Publication no. 340, pp. 59-79

Brunauer, S., I. Odler, and M. Yudenfreund
1970 "The new model of hardened Portland Cement Paste". Highway Research Record, no. 328, pp. 89-107

Carman, P.C.
1956 "Flow of gases through porous Media". Butterworths, London

Chang, S.-C., and N.B. Hutcheon
1956 "Dependence of water vapor permeability on temperature and humidity". American Society of Heating and Air-Conditioning Engineers, Transactions, vol. 62, pp. 437-450

Copeland, L.E., and J.C. Hayes
1953 "The determination of non-evaporable water in hardened portland cement paste". Research Department Bulletin no. 47, Portland Cement Association, Chicago

Copeland, L.E., and R.H. Bragg
1954 "The hydrates of magnesium perchlorate". Research Department Bulletin no. 50. Portland Cement Association, Chicago

Copeland, L.E., E. Bodor, T.N. Chang and C.H. Weise
1967 "Reactions of tobormorite gel with aluminates, ferrites, and sulfates". Research Department Bulletin no. 211, Portland Cement Association, Chicago.

Crank, J.
1967 "The mathematies of diffusion". 4. edition, Clarendon Press, Oxford

Diamond, S.
1971 "A critical comparison of mercury porosimetry and capillary condensation pore size distributions of portland cement paste". Cement and Concrete Research, vol. 1, pp. 531-445

Diamond, S.
1976 "Cement paste microstructure - an overview at several levels". Proceedings from the conference "Hydraulic cement pastes: their structure and properties", pp. 2-23. Cement and Concrete Association, Slough, U.K.

Everett, D.H.
1967 "Adsorption hysteresis". In: E. Alison Flood (ed.) "The solid-gas interface, vol. II, pp. 1055-1113. Marcel Dekker, New York

Feldman, R.F. and P.J. Sereda
1968 "A model for hydrated Portland cement paste as deduced from sorption-length change and mechanical properties". Materiaux et Constructions, vol. 1, no. 6, pp. 509-520

Feldman, R.F.
1972 "Density and porosity studies of hydrated Portland cement". Cement Technology, vol. 3, no. 1, pp. 5-14

Fisher, L.R., and P.D. Lark
1979 "An experimental study of the Washburn equation for liquid flow in very fine capillaries". Journal of Colloid and Interface Science, vol. 69, no. 3, pp. 486-492

Gregg, S.J., and K.S.W. Sing
1967 "Adsorption, surface area and porosity". Academic Press, New York

Hagymassy, J., S. Brunauer, and R.S. Mikhail
1969 "Pore structure analysis by water vapor adsorption. I t-curves for water vapor". Journal of Colloid and Interface Sceince, vol. 29, no. 3, pp. 485-491

Hagymassy, J., I. Odler, M. Yudenfreund, J. Skalny, S. Brunauer:
1972 "Pore structure analysis by water vapor adsorption. III. Analysis of hydrated calcium silicates and portland cements". Journal of Colloid and Interface Science, vol. 38, no. 1, pp. 20-34

Hancox, N.J.
1967 "A note of the form of the rate of drying curve for cement paste and its use in analysing the drying behavior of this material". Bulletin RILEM no. 36, September 1967, pp. 197-201

Hancox, N.J.
1968 "The rate of moisture diffusion in the drying of cement paste under the influence of temperature gradients". British Journal of Applied Physics, Ser. 2, vol. 1, pp. 1769-1777

Hansen, T.C., F. Radjy, and E.J. Sellevold
1973 "Cement paste and concrete". In: R.A. Huggins (ed.): Annual Review of Materials Science, vol. 3, pp. 233-268, Annual Reviews Inc., California

Hastrup, K.
1976 "Polymerimprægnering af porøse materialer. Porestruktur, molekylvægt og mekaniske egenskaber". Danmarks tekniske Højskole, Laboratoriet for Bygningsmaterialer. Available from the Library of the Danish Atomic Energy Commission, Risø, Roskilde, Denmark

Helmuth, R.A. and D.H. Turk
1967 "The reversible and irreversible drying shrinkage of hardened portland cement and tricalcium silicate pastes". Journal of the PCA Research and Development laboratories, May 1967, pp. 8-21

Hughes, B.P., I.R.G. Lowe, and J. Walker
1966 "The diffusion of water in concrete and temperatures between 50 and 95°C". British Journal of Applied Physics, vol. 17, pp. 1545-1552

Jain, K.K., and C.E. Kesler
1964 "Moisture exchange behavior in concrete and mortar". Department of Theoretical and Applied Mechanics, University of Illinois, T. & A.M. Report No. 646

Joy, F.A., and A.G. Wilson
1966 "Standardization of the dish method for measuring water vapor transmission". National Research Council, Division of Building Research, Ottawa, Canada, Research Paper no. 279. Also: International Symposium on Humidity and Moisture, Proceedings, Washington, D.C., 1963, vol. 4, chapter 31, pp. 259-270

Litvan, G.G.
1976 "Variability of the nitrogen surface area of hydrated cement paste". Cement and Concrete Research, vol. 6, pp. 139-144

Lowe, I.R.G., B.P. Hughes, and J. Walker
1971 "The diffusion of water in concrete at 30°C". Cement and Concrete Research, vol. 1, pp. 547-557

Mikhail, R.S. and S.A. Selim
1966 "Adsorption of organic vapors in relation to the pore structure of hardened portland cement pastes". Symposium on structure of portland cement paste and concrete, pp. 123-134. Sepcial Report 90, Highway Research Board, Washington D.C.

Newns, A.C.
1950 "The methods of determining the water vapour permeability of laminae. A review of the literature". Journal of the Textile Institute, Transactions, August 1950, pp. T269-T308

Nilsson, L.-O.
1977 "Fuktproblem vid betonggulv". (Moisture problems at concrete floors). Division of Building Materials, Lund Institute of Technology/University of Lund, Lund, Sweden. Report TVBM-3002

Odler, I.
1976 "Die Eigenschaften und Struktur des Warmbehandelten Portland-zementes". Tonindustrie-Zeitung, vol. 100, no. 1, pp. 29-33

Pihlajavaara, S.E.
1963 "Notes on the drying of concrete". The State Institute for Technical Research, Helsinki, Finland

Pihlajavaara, S.E.
1965 "On the main features and methods of investigation of drying and related phenomena in concrete". The State Institute for Technical Research, Helsinki, Finland

Powers, T.C., and T.L. Brownyard
1948 "Studies of the physical properties of hardened portland cement paste". Research Department Bulletin no. 22, Portland Cement Association, Chicago

Powers, T.C., L.E. Copeland, J.C. Hayes, and H.M. Mann
1955 "Permeability of portland cement paste". Research Department Bulletin no. 53, Portland Cement Association, Chicago

Powers, T.C., L.E. Copeland, and H.M. Mann
1959 "Capillary continuty or discontinuity in cement paste". Research Department Bulletin no. 110, Portland Cement Association, Chicago

Powers, T.C., H.M. Mann, and L.E. Copeland
1959 "The flow of water in hardened portland cement paste". Research Department Bulletin no. 106, Portland Cement Association, Chicago

Powers, T.C.
1960 "Physical properties of cement paste". Research Department Bulletin no. 154, Portland Cement Association, Skokie, Illinois.

Radjy, F.
1974 "Moisture transport in microporous substances. Part 1. The interaction of molecular streaming, surface diffusion and capillary suction". Journal of Materials Science, vol. 9, pp. 742-752

Radjy, F., and E.J. Sellevold
1972 "A phenomenological theory for the t-method of pore structure analysis. I. Slit-shaped pores". Journal of Colloid and Interface Science, vol. 39, no. 2, pp. 367-378

Rockland, L.B.
1960 "Saturated salt solutions for static control of relative humidity between 5° and 40°C". Analytical Chemistry, vol. 32, no. 10, pp. 1375-76

Ruettgers, A., E.N. Vidal and S.P. Wing
1934/35 "An investigation of the permeability of mass concrete with particular reference to Boulder Dam". Journal of the American Concrete Institute, vol. 6 pp. 382-416

Ruettgers, A., E.N. Vidal and S.P. Wing
1935/36 Discussion of the paper "An investigation of the permeability of mass concrete with particular reference to Boulder Dam". Author's closure. Journal of the American Concrete Institute, vol. 7, pp. 378-389

Scholten, J.J.F.
1967 "Mercury porosimetry and allied techniques". In: R.L. Boud (ed.) "Porous Carbon Solids", pp.225-249. Academic Press, New York

Sellevold, E.J.
1969 "Anelastic behavior of hardened portland cement paste". Ph.D. Thesis, Department of Civil Engineering, Stanford University, Technical Report no. 113

Sellevold, E.J., and F. Radjy
1972 "A phenomenological theory for the t-method of pore structure analysis. II. Circularly cylindrical pores". Journal of Colloid and Interface Science, vol. 39, no. 2, pp. 379-388

Sellevold, E.J.
1975 "Mercury porosimetry of hardened cement paste cured or stored at 97°C". Cement and Concrete Research, vol. 4, pp. 399-404

Stokes, R.H. and R.A. Robinson
1949 "Standard solutions for humidity control at 25°C". Ind. Eng. Chem., vol. 41, p. 2013

Taylor, H.F.W.
1964 "The steam curing of portland cement products". In: H.F.W. Taylor (ed.): "The chemistry of cements", vol. I, pp. 417-432. Academic Press, London

Tveit, A.
1966 "Measurements of moisture sorption and moisture permeability of porous materials". Norwegian Building Research Institute, Oslo, Norway

Verbeck, G.J.
1958 "Carbonation of hydrated Portland Cement". Portland Cement Association, Research Department, Bulletin 87. Also: ASTM Special Technical Publication no. 205, pp. 17-36

Wexler, A. and S. Hasegawa
1954 "Relative humidity-temperature relationships of some saturated salt solutions in the temperature range 0° to 50°C". Journal of Research of the NBS, vol. 53, no. 1, pp. 19-26

Wierig, H.-J.
1965 "Die Wasserdampfdurchlässigkeit von Zementmörtel und Beton". (The permeability of cement mortar and concrete to water vapor). Zement-Kalk-Gips, vol. 18, no. 9, pp. 471-482

Winslow, D.N., and S. Diamond
1970 "A mercury porosimetry study of the porosity in portland cement". Journal of Materials, JMLSA, vol. 5, no. 3, pp. 564-585

Winslow, D.N., and S. Diamond
1974 "Specific surface of hardened portland cement paste as determined by small-angle x-ray scattering". Journal of the American Ceramic Society, vol. 57, no. 5, pp. 193-197